Aston University

Some pages of this thesis may have been removed for copyright restrictions.

If you have discovered material in Aston Research Explorer which is unlawful e.g. breaches copyright, (either yours or that of a third party) or any other law, including but not limited to those relating to patent, trademark, confidentiality, data protection, obscenity, defamation, libel, then please read our Takedown policy and contact the service immediately (openaccess@aston.ac.uk)

A STUDY OF FIELD EMISSION FROM SEMICONDUCTORS

A THESIS SUBMITTED FOR THE DEGREE OF PHILOSOPHIAE DOCTOR IN THE UNIVERSITY OF ASTON IN BIRMINGHAM

David Edmund Sykes, B.Sc., M.Sc.

4 APR 1978

Department of Physics

March 1975.

ABSTRACT

In an attempt to clarify the behaviour of semi-conductor field emitters the properties of a narrow band gap material were investigated. A retarding potential analyser was built and tested using a tungsten emitter. The energy distribution of electrons emitted from single crystals of lead telluride (band gap 0.3 eV) and gallium phosphide (band gap 2.26 eV) were measured. The halfwidths of the distributions are discussed with respect to the relevant parameters for the materials. Methods of tip preparation had to be developed.

The halfwidth of the energy distribution of electrons field emitted from carbon fibres was measured to be 0.21 ± 0.01 eV. A mechanism explaining the long lifetime of the emitters in poor vacuua is proposed.

INDEX

Chapter 3 The Carbon Fibre Field Emitter

Chapter 4 Experimental Techniques

Chapter 5 Presentation of Results

CHAPTER 1

INTRODUCTION

1.1 PROLOGUE

Field emission is the process of emission of electrons from a conductor, through the potential barrier at the surface of the conductor, under the action of an electric field. The effect is an example of quantum mechanical tunnelling as the electrons on leaving the cathode pass through the classically forbidden barrier with no loss of energy. For the field emission current to be significant the barrier width has to be of the order of 10 Å corresponding to a field strength of about 10^7 volts cm^{-1}. These high field values can be achieved in two ways : either the specimen is in the form of a flat plate on which is deposited a very thin layer of insulating material, then another electrode and a voltage applied across the insulator (thin film tunnelling), or the specimen is etched to a very sharp point, typically 1000 Å radius, and using the fact that the field at the surface of a sphere is equal to the applied voltage divided by the radius, suitable fields can be achieved by the application of a few kilovolts (the field emission cathode). This discussion will be concerned only with the latter case.

The field emission cathode is of interest in several ways. Technologically as an electron source, it is a high brightness coherent point source capable of delivering current densities as high as 10^6 amps cm^{-2} (1). Experimentally as a means of investigating clean metal and semiconductor surfaces to determine band structure effects, work functions, thermal effects and surface states (2). The theory of field emission

from metals is reasonably well understood in so much as experimental current-voltage characterisitics and energy distributions hardly differ from those predicted by theory and relatively sophisticated techniques have to be employed to bring out the differences. In the case of semiconductors, however, the situation is very different. Only recently has any qualitative agreement, between theory and experiment, been found and then only in the specific case of germanium. In general, the agreement between theory and experiment is poor, to say the least.

1.2 FIELD EMISSION FROM METALS

The first theory of field emission was proposed in 1928 by Fowler and Nordheim (3) who used the then new quantum mechanics to estimate the emitted current density as a function of applied field. They assumed a triangular barrier and by solving the Schrödinger equation found the escape probability of an electron with a given energy. Using the Somerfeld theory of metals they deduced the number of electrons arriving at the barrier within a given energy range. Integration of these quantities over all energies produced an expression for the total emitted current density of the form

$$j = \frac{4\sqrt{\mu\phi}}{\mu+\phi}\,\frac{e^3}{8\pi h\phi}\,F^2 \exp\left(\frac{-8\pi\sqrt{2m}}{3he}\,\frac{\phi^{3/2}}{F}\right)$$

where μ and ϕ are the emitter Fermi energy and work-function respectively, m is the electron mass and h Plank's constant. Nordheim (4) modified the expression to include the effect of the image force. Fig. (1.1) The Fowler-Nordheim equation, as the

Fig. 1.1

(a) Basic potential barrier

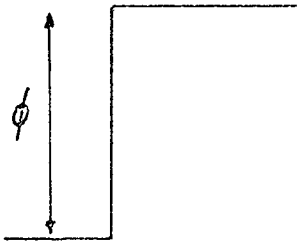

(b) Application of field

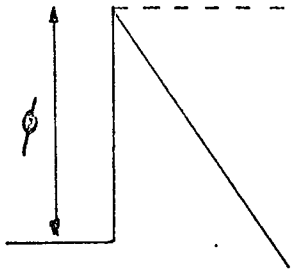

(c) With image force correction

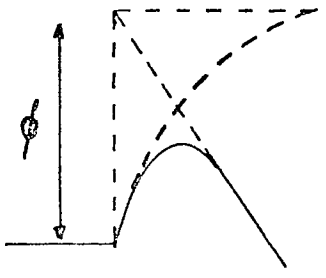

expression has become known, shows that the emission originates from the region of the Fermi level, further a plot of log j/F^2 vs $1/F$, the Fowler-Nordheim plot, should have a gradient proportional to the work-function of the emitter.

Experimentally field emission became a very useful technique by the invention of the field emission microscope (5). Muller realised that if he produced a hemispherical, smooth,clean emitter he could project a greatly enlarged image of the emission distribution onto a fluorescent screen. The image produced is almost a stereographic projection of the emitter, the darker regions corresponding to areas of low emission, due to high work-function or low field, and the brighter regions to areas of low work-function or high field. This technique allows the direct observation of adsorbate or contaminant on the emitter surface and changes in the surface structure under changing fields and temperatures.

The next major step came in 1959 when Young and Muller (6) used a retarding potential analyser to measure the total energy distribution of electrons field emitted from tungsten and Young (7) derived a theoretical expression for the toal energy distribution. Although earlier workers had been trying to measure energy distributions (8) (9) they thought they were measuring the normal energy distribution and their instruments did not have sufficient resolution to show otherwise. In the Fowler-Nordheim equation the parameter which determines the tunnelling probability is the "normal component" of energy, that which is directed towards the surface, hence one would expect that in field emission the energy distribution would be the

normal distribution. This is true for the plane parallel case but in the spherical geometry of the more usual field emission cathode situation the "transverse component" of the energy, which is conserved in the tunnelling process, is rapidly transferred to the direction of motion once the electron has left the tip, hence the total energy of the electron is measured and not the normal energy.

Recently with the development of a new generation of energy analysers (10) the electrostatic deflection analysers, having a much higher resolution than the retarding potential type it has become possible to investigate the effect of surface states in the emission from metals. These developments have been reviewed by Gadzuk and Plummer (2) and will not be considered further as the present work is primarily concerned with field emission from semiconductors.

1.3 FIELD EMISSION FROM SEMICONDUCTORS

Field emission studies on semiconducting materials are a logical development from work on metals but it was not until the 1950's that much work was done. This was probably a result of the difficulty in producing the materials and making suitable emitters. Apker and Taft (11) drew field emission currents from single crystals of cadmium sulphide "sharpened" by electron bombardment. They suggested that their sharpening process occurred by preferential evaporation but found that they were unable to produce smooth tips. Their work showed that the emission current was sensitive to illumination but only when the emitting area was illuminated, also they realised that the high resistance of the specimen could produce a loss of field at the tip.

The subject received an incentive when in 1955 Stratton (12) published his first paper on the theory of field emission from semiconductors. He used a Fowler-Nordheim type barrier and modified the transmission probability to include the effect of the dielectric constant of the material. He applied this barrier to different models of a semiconductor surface,with and without field penetration and with and without surface states. He showed that at low fields the presence of surface states should give low currents until the field is high enough to reduce the internal barrier and allow field penetration. This should lower the conduction band edge eventually causing degeneracy and metal like emission. The plot of log i vs 1/F for such an emitter should consist of two straight line sections of equal gradient connected by a curve of greater gradient.

The experimental work following Stratton's paper was directed towards investigations of the Fowler-Nordheim characteristics to find departures from linearity. Perry (13) and Elison and Vasiliev (14) found non-linear plots for germanium but field emission patterns taken at the time suggest the surfaces were contaminated, Perry (15), so the results cannot be reliably attributed to germanium. Allen (16) was able to produce clean reproducible emission patterns from silicon tips. He found that, over the range investigated, plots of log i vs 1/V were linear and the emission was independent of temperature (up to 1200^{o}K) and illumination. He concluded that the surface must be degenerate n-type or surface states present in densities exceeding 10^{13} cm^{-2} eV Perry (15) also working on silicon, but over a wider range of currents, found two types of plot, one linear and the other two linear sections of equal gradient joined by a third of less

gradient (not in agreement with Stratton's predictions). He hoped to interpret the linear plots as due to p-type material and the other to n-type but found the reverse, with the n-type specimens having strongly p-type surfaces which he attributed to boron contamination from the vacuum system deposited during bakeout.

Klimin (17) et al investigating germanium emitters prepared by cleavage, electron bombardment and heat treatment found current-voltage characteristics over a range of temperatures. They used Stratton's model of a semiconductor with no surface states to interpret their results and found good agreement. These results, however, are extremely unlikely to be representative of a clean surface as symmetrical images were not obtained and the experiment conducted in vacuum of the order of 10^{-7}torr.

In 1962 Stratton (18) published another paper on the theory of field emission from semiconductors which overcame some of the shortcomings of his previous work. Using a Fowler-Nordheim barrier, as in the earlier work, he produced expressions for the emitted current density from both the valence band and conduction band containing effective mass corrections allowing for variations in band shapes. He also considered the effect of surface states in more detail but did not allow for the possibility of emission from such states. Applying his expressions to germanium for different surface state models he found there should be a change in slope of the Fowler-Nordheim plot at flat band conduction, and that valence band emission predominates unless there is field penetration. Stratton compared his predictions with the experimental work of Allen (19) and concluded the

emission characteristics were consistent with emission from the conduction band, indicating that field penetration had occurred.

Savage (20) successfully produced emission from gallium arsenide but was unable to produce a clean symmetrical image. Current voltage measurements revealed two distinct regions in the Fowler-Nordheim plots, a flat portion at low fields (attributed to leakage currents between electrodes) and a straight line section at higher fields.

A quantitative approach to the problem was made possible by the work of Arthur (21) by the ingenious use of field ion and field emission techniques. Previous workers had experienced difficulty in estimating the field at the emitter surface and used voltage rather than field in their Fowler-Nordheim plots. Arthur's method of finding an absolute value of the field voltage ratio was to assume that the ionization field for hydrogen was the same over tungsten and germanium, thus, knowing the value of the "best image" field for tungsten, the voltage producing the "best image" for germanium should correspond to that value of field. Unfortunately calculations using this method produced work function values that were 30% too large. His Fowler-Nordheim plots, however, were linear but with different slopes for field evaporated and annealed surfaces which indicates build up of ridges during the annealing process.

In a later work Arthur (22) found linear Fowler-Nordheim plots for n-type germanium specimens but with p-type specimens the plots exhibited a linear region at low fields followed by a saturation region then a region where the emission increased very rapidly with field. The position of the saturation region was found to move to

higher current values with increase in temperature and also to be dependent on illumination. Ernst (23) used Arthur's (21) method for estimating the field at the tip in comparing his results for n-type germanium with Stratton's theory. His results, although linear, gave work-functions considerably greater than the accepted value and the emitted current density for a given field was less than expected from Stratton's theory. He did point out the over-simplification in Stratton's theory, that the energy bands centred on k = 0, and that if the band is centred elsewhere the field emission work-function exceeds its true value by an amount

$$\phi_0 = \frac{\hbar^2}{2m} k_0'^2$$

where $\hbar$ is Plank's constant, m the electronic mass and k_0' the component, normal to the emission direction, of the vector joining the band centre to k = 0 in the Brillouin zone.

Marien et al (25), in a study of the emission characteristics of undoped zinc oxide, found two types of Fowler-Nordheim plot. For the $(0\ 0\ 0\ \bar{1})$ orientation the plots were linear over the range investigated whilst the (0 0 0 1) orientation produced a plateau region, between two linear sections, with increasing voltage over the same range, moreover a plot with decreasing voltage, from above the plateau region, was linear. They showed that over the range of their plots field penetration did occur but the surface did not become degenerate. They suggested that a set of surface states, initially empty, trapped charge thus producing the plateau region and that, as the work was carried out at nitrogen temperature, once

filled the states would stay filled as not enough thermal energy was available to empty them. This implied that subsequent plots with increasing voltage should be linear, which fact they observed, moreover, heating the tip to room temperature for a few seconds reproduced the plateau structure. In a later work (26) they conclude that the conduction band does become degenerate and that the plateau structure is not only due to trapping of charge in surface states but also to a change in electron affinity.

Marien and Loosveldt (26) also used Arthur's (21) method in their work on cadmium sulphide and found reasonable agreement between their estimated value of electron affinity and the accepted value. In determining this value they used their low field Fowler-Nordheim plots which were linear, however at high fields their plots showed a change of slope and in some cases a hysteresis effect.

The work reviewed above shows, to some extent, the inadequacy of the Stratton theory in explaining experimental results. The earlier works, however, should be treated with caution as experimental techniques, e.g. tip preparation and cleaning, vacuum conditions, were not sufficiently developed to produce results attributable to clean, well characterised surfaces. The recent work, on the other hand, utilising u.h.v. techniques and refined methods of sample cleaning is more reliable and indicates a need for a more sophisticated explanation of current-voltage characteristics for semiconductors.

This need was fulfilled in 1971 by Baskin, Lvov and Fursey (27). They did not confine their argument to a constant Fermi level situation, as did Stratton, but developed a theory without the use of a zero current approximation. By this means they were able to

show that for p-type specimens a depletion layer is formed just behind the surface which will exert a limiting effect on the rate of arrival of carriers at the surface, thus giving a saturation region in the emission characteristic. In n-type specimens, however, this depletion layer is not formed but a similar saturation region may be observed if the specimen is unable to generate enough carriers, in the bulk, to constitute the emission current. Numerical calculations based on their expressions showed qualitative agreement with observed effects although the saturation currents were smaller than experimental values which they attributed to the one-dimensional nature of their model.

1.4 ENERGY DISTRIBUTIONS OF ELECTRONS FIELD EMITTED FROM SEMICONDUCTORS

Russel (28) realised that more information about the electronic structure of semiconductor field emitters could be obtained by retarding potential measurements than the more usual, at that time, current voltage characteristics. He was able to show, by critical bias measurements, that the emission from a silicon tip originated less than half the band gap below the Fermi level. Later (29), using an energy analyser, similar to that of Young and Muller (6), he reported metal like energy distributions from silicon, attributed to emission from a p-type surface layer.

Then, following a fortuitous fracture of his specimen, he observed two peaks separated by an amount equal to the band gap, the obvious interpretation is conduction and valence band emission. His results, however, should be treated with scepticism as his measurement of the half width of the tungsten distribution was three times the accepted value.

Scherbakov and Skol'skaya (30), in their work on cadmium sulphide, used a similar type of analyser first calibrating it with tungsten. Although the shape of the distribution differed from that of Young and Muller (6) the half-width was of a comparable value. They obtained half-widths for the cadmium sulphide distribution ranging from 0.6 eV to almost 2eV. However, due to the finite resistance of their specimens, they were unable to locate their distributions with respect to the Fermi level. It should be pointed out that their specimens contained several microneedles which could lead to confusion in interpretation of their results.

A measurement of 0.1 eV to 0.2 eV for the half-width of the energy distribution from germanium was reported by Kagan et al(31). They report the shape of the distribution to be characteristic of semiconductors but quote no references, also, as they made no attempt to clean their specimens, their results should be treated with caution.

Stratton (32) produced theoretical expressions for the energy distributions of electrons emitted from the conduction band and valence band of a semiconductor. A previous attempt had been made by Fischer (33) (34) but his expression for the valence band emission was based upon an earlier derivation by Stratton (18) which was incorrect. Stratton was able to show that his expression for the conduction band emission reduced to the same form as Fischer's. Numerical analysis of his results predicted conduction band half-widths between 2kT and 7kT and valence band half-widths between 3kT and 12kT for all degeneracies over a typical range of fields. Unfortunately, these

values are narrower than experimental results.

The first reliable measurement of the energy distribution of electrons emitted from germanium was due to Arthur (35) who investigated a range of germanium crystals in a Young and Muller (6) type analyser. He found distributions of approximate gaussian shape immediately below the Fermi level with a width about twice that obtained for tungsten, with the distribution narrowing as the surface was annealed. Occasionally a second peak 0.15 eV below the main one was observed that was sensitive to tip positioning and could be removed by field evaporation. No difference was observed between specimens of different conductivities of either n- or p- type materials. Arthur interprets his results as emission from a degenerate conduction band with a very low density of surface states but questions his decision as the distribution from the field evaporated surface narrows with annealing. Interpretation of the subsidiary peak as surface state emission must, he concludes, be dismissed as the density consistent with a degenerate conduction band could not supply sufficient current.

Hughes and White (36) working on gallium arsenide produced results similar to Arthur but with the subsidiary peak appearing on the high energy side of the distribution. Critical bias measurements suggested to them that their main peak was valence band emission and the subsidiary peak, which was sensitive to tip positioning and surface condition, surface state emission as it was found immediately below the Fermi level. Using Stratton's (32) theory they calculated the theoretical half width to be 0.3 eV whilst their measured values were of the order of 0.7 eV. Salmon and Braun (37) using a similar analyser have measured half widths between 0.6 eV and 1.6 eV for cadmium sulphide and have observed a second

peak on the low energy side of the distribution which could be removed by field evaporation. This extra peak was attributed to emission from surface states due to contamination. The distributions with the larger half widths were thought to be artefacts resulting from anomalous broadening of the energy distribution at the relatively high currents used or due to poor resolution as a result of a slight misalignment. A comparison with Stratton's prediction for emission from a degenerate conduction band again showed the experimental half width to be several times greater than the theoretical one.

Shepherd and Peria (38) used an electrostatic deflection analyser to investigate emission from (100) oriented germanium. This type of analyser has a better resolution and signal to noise ratio than a retarding potential analyser, and, they claim, can discriminate against electrons with high transverse momenta in the specimen.

Their analyser can discriminate against electrons arriving at the collector with high transverse momenta but these do not necessarily correspond to electrons with high transverse momenta in the bulk. As will be shown in a subsequent chapter the transverse momentum component of an electron within the crystal is rapidly transferred to the direction of motion of the electron once it has left the tip in the spherical geometry of the field emission system. In using the transverse momentum component of a conduction band electron within the crystal to show that such an electron cannot be collected by their analyser Shepherd and Peria have overlooked the fundamental difference between normal and total energy distributions.

Their results showed two peaks, a dominant higher energy peak 0.6 eV to 0.7 eV below the Fermi level (half width about 0.2 eV) and

a lesser peak of lower energy. The positions of the peaks moved to lower energies with increasing fields. In interpreting their results they attribute the high energy peak to surface states and the lower energy one to the valence band. Although the Fermi level was found to lie in the conduction band they did not observe conduction band emission due to the peculiar transmission properties of their analyser and the reduced tunnelling probability of conduction band electrons in the (100) direction.

In an attempt to quantify their results they followed a method similar to Stratton (32) in deriving an expression for the theoretical valence band distribution. This was then multiplied by an arbitrary factor with until agreement was obtained with the observed valence band peak. By this method the field voltage ratio was obtained and used to compare theoretical valence band Fowler-Nordheim plots with total current and probe hole measurements. Each plot though linear, showed a different slope. In obtaining the density of surface states from their results the peak and onset voltages were plotted against field, as these showed a rapid movement to lower energies at high fields they were corrected, by an unspecified method, for a resistive drop to produce a straight line. The density of surface states obtained by this method was $6.3\ 10^{12}\ cm^{-2}$ which is at least an order of magnitude lower than other estimates.

The inability of Stratton's (32) theory to adequately explain the experimental results is obvious and the need for a theory including emission from surface states apparent. Modinos (39) has recently proposed such a theory. Concisely Modinos took Stratton's (32) expression for conduction and valence band emission and included the

effect of surface state emission, by deriving an expression for tunnelling from surface states and equating this with the replenishment of the surface states by carriers from the valence and conduction bands. Numerical analysis of his results for germanium are very similar to the results of Shepherd and Peria. There is a dominant high energy surface state peak (half width 0.1 eV to 0.2 eV) with a lesser low energy valence band peak which shift to lower energy with increase in field. The major difference between experiment and theory is that Modinos predicts the surface state peak to be immediately below the Fermi level, except at high fields, whilst Shepherd and Peria do not find this to be so, however this difference could be attributed to experimental error as Shepherd and Peria only investigated one emitter (40).

The work reviewed above shows the need for further work on semiconductors, although Modinos has produced a theory almost consistent with experimental results for germanium, other materials should be investigated. Lead telluride was chosen for this investigation as it has a small band gap and the bands are centred on the origin of the Brillouin zone. For a comparison some preliminary results were obtained from a large band gap material, gallium phosphide.

CHAPTER 2

THEORY OF FIELD EMISSION

PART A : METALS

2.1 THE FOWLER-NORDHEIM EQUATION

The first formulation of a theory of field emission in terms of quantum mechanics was due to Fowler and Nordheim (3), and Nordheim (4), who derived an expression relating the emitted current density to the applied field, the Fowler-Nordheim equation. They investigated the possibility of an electron escaping from a metal through the surface potential barrier, when deformed by an applied electric field and the image force Fig.(2.1), by considering a free electron incident upon the barrier. In order to find the transmission probability of an electron with an energy "component" E_x normal to the barrier a Schroedinger equation of the form

$$\frac{\partial^2 \psi}{\partial x^2} + \left(\frac{2m}{\hbar^2} \right) \left(E_x + \frac{e^2}{4x^2} + eFx \right) \psi = 0$$

must be solved, where $\hbar$ is Plank's constant, m the electronic mass, e the electronic charge and F the applied field. This has been done rigorously by Nordheim (4) and using the W.K.B. approximation by Good and Muller (41). The transmission probability $D(E_x)$ is

$$D(E_x) = \exp\left(\frac{-4\sqrt{2m|E_x|^3}}{3\hbar e F} v(y) \right)$$

where v(y) is a slowly varying function tabulated in (41)

Fig. 2.1

Potential barrier with applied field and image force.

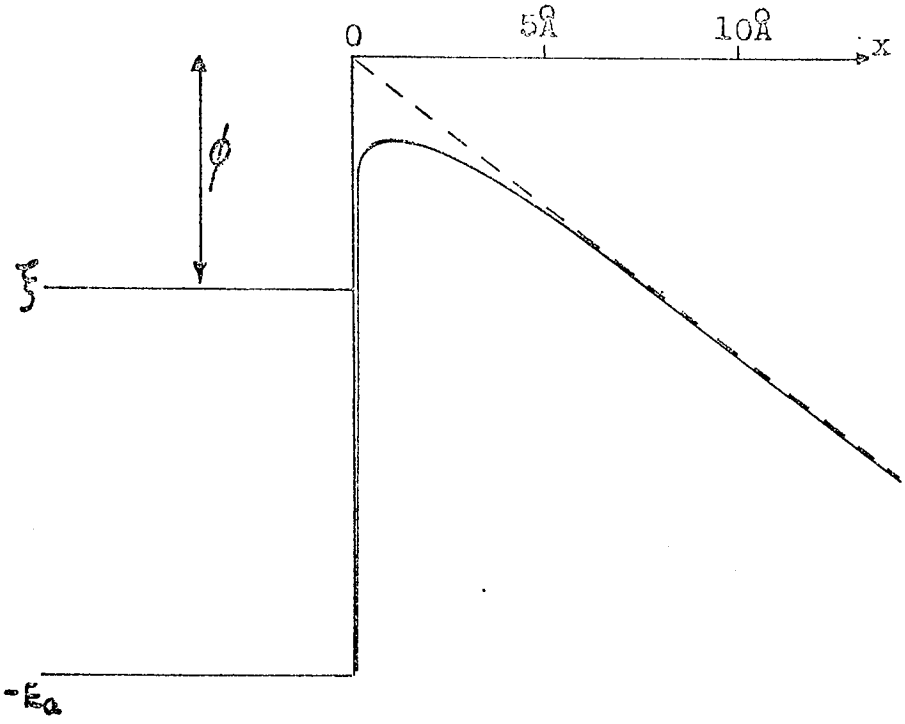

Potential energy $= -eFx - \frac{e^2}{4x^2}$ for $x>0$

The next factor governing the emission of electrons is the supply of electrons to the surface barrier. The number of electrons moving towards the surface barrier with normal momenta between p_x and $p_x + dp_x$ per second per unit area is given by :

$$dn_x = \int_{p_y=-\infty}^{\infty} \int_{p_z=-\infty}^{\infty} \frac{p_x}{m} \frac{2}{h^3} dp_x\, dp_y\, dp_z\, F(E)$$

where F(E) is the Fermi distribution function.

$$F(E) = \left[\exp\left(\frac{E - \xi}{kT} \right) + 1 \right]^{-1}$$

where ξ is the Fermi energy, k is Boltzman's constant and T the absolute temperature. From the above expression the number of electrons incident on the barrier with normal "component" of energy in the range E_x to $E_x + dE_x$ per unit area per unit time can be obtained, this is

$$N(E_x)\, dE_x = \frac{4\pi m k T}{h^3} \log \left[1 + \exp -\left(\frac{E_x - \xi}{kT} \right) \right]$$

The number of electrons penetrating the barrier per unit area per unit time within dE_x is

$$P(E_x)\, dE_x = N(E_x)\, D(E_x)\, dE_x$$

and integration of this quantity over E_x gives the total emitted current density

$$I = \int_{-E_a}^{\infty} N(E_x)\, D(E_x)\, dE_x$$

Thus

$$P(E_x)\,dE_x = \frac{4\pi m kT}{h^3}\exp\left[\frac{-4\sqrt{2m|E_x|^3}}{3\hbar eF}\,v\left(\sqrt{\frac{e^3F}{|E_x|}}\right)\right]\log\left[1+\exp-\left(\frac{E_x-\xi}{kT}\right)\right]dE_x$$

For electrons near the Fermi level the exponent of the transmission probability can be approximated by the first two terms of a power series :

$$\frac{-4\sqrt{2m|E_x|^3}}{3\hbar eF}\,v\left(\frac{\sqrt{e^3F}}{|E_x|}\right) = -c + \frac{E_x-\xi}{d}$$

where

$$c = \frac{4\sqrt{2m\phi}}{3\hbar eF}\,v\left(\frac{\sqrt{e^3F}}{\phi}\right)$$

$$d = \frac{\hbar eF}{2\sqrt{2m\phi}\;t\left(\sqrt{\frac{e^3F}{\phi}}\right)}$$

$$t(y) = v(y) - \frac{2}{3}y\frac{dv(y)}{dy}$$

$\phi = -\xi$ is the work function.

Finally

$$P(E_x)\,dE_x = \frac{4\pi m kT}{h^3}\exp\left[-c+\frac{E_x-\xi}{d}\right]\log\left[1+\exp-\left(\frac{E_x-\xi}{d}\right)\right]dE_x$$

At low temperatures

$$kT\log\left[1+\exp-\left(\frac{E_x-\xi}{d}\right)\right] = 0 \quad \text{for } E_x > \xi$$

and

$$= \xi - E_x \text{ for } E_x < \xi$$

Substituting into the above expression

$$P(E_x)\,dE_x = 0 \qquad \text{for } E_x > \xi$$

$$= \frac{4\pi m}{h^3}\left[\exp -c+\frac{E_x-\xi}{d}\right](\xi - E_x) \quad \text{for } E_x < \xi$$

As there are no electrons above ξ the upper limit of the integral can be changed from ∞ to ξ and as no electrons are emitted from well

below ξ the lower limit can be changed from $-E_a$ to $-\infty$.

The total emitted current density can now be written

$$I = \frac{4\pi me}{h^3} \int_{-\infty}^{\xi} \exp\left[-c + \frac{E_x - \xi}{d}\right] (\xi - E_x)\, dE_x$$

or performing the integration

$$I = e^3 F^2 \left[8\pi h \phi t^2\left(\frac{\sqrt{e^3F}}{\phi}\right)\right]^{-1} \exp\left[\frac{-4\sqrt{2m}\,\phi^{3/2}}{3\hbar eF}\right] v\left(\frac{\sqrt{e^3F}}{\phi}\right)$$

the Fowler-Nordheim equation. From a plot of log I/F^2 against $1/F$, the Fowler-Nordheim plot, the work-function, ϕ , of the emitter can be obtained from the gradient of the straight line.

2.2 THE ENERGY DISTRIBUTION

2.2 a THE NORMAL ENERGY DISTRIBUTION

The normal energy distribution P(Ex) is the number of electrons leaving the emitter with a given "component" of energy normal to the barrier. This is the quantity determined in the previous section as the Fowler-Nordheim equation depends on the "component" of energy normal to the barrier.

$$P(E_x) = \frac{4\pi m kT}{h^3} \exp\left[-c + \frac{E_x - \xi}{d}\right] \log\left[1 + \exp -\left(\frac{E_x - \xi}{kT}\right)\right]$$

2.2 b THE TOTAL ENERGY DISTRIBUTION

The total energy distribution P(E) is the number of electrons leaving the emitter with a given total energy. The derivation of the total energy distribution is discussed by Gadzuk and Plummer(2) with consideration given to the different approximations used, a general result only will be given.

$$P(E) = \frac{4\pi m d}{h^3}\left[\exp\left(-C - \frac{\zeta}{d}\right)\right]\frac{\exp\left(\frac{E}{d}\right)}{\exp\left(\frac{E-\zeta}{kT}+1\right)}$$

2.2 c THE NORMAL AND TOTAL ENERGY DISTRIBUTIONS

The normal energy distribution cannot be measured in a conventional field emission system as once the electrons leave the emitter they are acted upon by the electric field and their energy "components" redistributed. Consider a field emitted electron in the spherically symmetric emission geometry shown in Fig. 2.2. The particle moves in a central force field in which angular momentum is conserved (2). If the particle has an initial transverse velocity $V_T(r_o)$ and energy $E_T(r_o)$ it can be shown that

$$V_T(r) = V_T(r_o)\,\frac{r_o}{r}$$

and

$$E_T(r) = E_T(r_o)\left(\frac{r_o}{r}\right)^2$$

It is easy to see, from these equations, that any transverse energy of the electron is rapidly converted to radial energy; hence a field emission system measures total energy and not normal energy.

2.3 THE MEASURED DISTRIBUTION

Gadzuk and Plummer (2) define two total energy distributions, the one that is normally calculated and the one that, in fact, is measured. They define a function $P(\hat{n}_o, \hat{n}_1, E)$ as the number of electrons entering the probe hole with energy E originating from unit area at the intersection of $\hat{n}_1$ with the emitter surface, see Fig. (2.2) The collected total energy distribution, per unit solid angle of the probe hole in the

Fig. 2.2

Spherically symetric geometry of a field emission system.

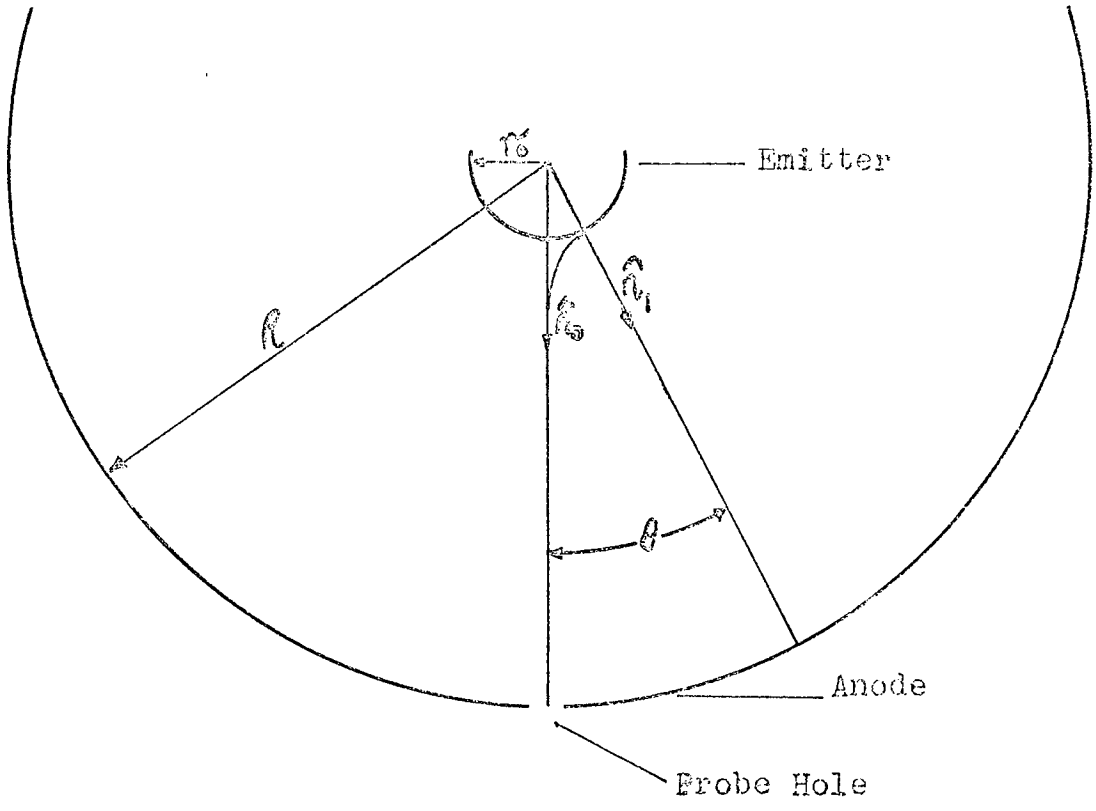

$\hat{n}_o$ direction, (the measured quantity) is found by integrating the function over the emitter surface :

$$P(\hat{n}_o, E) = \int_0^{\pi} \int_0^{2\pi} P(\hat{n}_o, \hat{n}_1, E)\, r_o^2 \sin\theta \, d\theta \, d\phi$$

The emitted total energy distribution from unit area denoted by $\hat{n}_1$ (the calculated quantity) is found by integrating over all directions of the probe hole $\hat{n}_o$:

$$P(\hat{n}_1, E) = \int_0^{\pi} \int_0^{2\pi} P(\hat{n}_o, \hat{n}_1, E) \frac{r_o^2}{1} \sin\theta \, d\theta \, d\phi$$

If $P(\hat{n}_o, \hat{n}_1, E)$ is a function only of θ and not dependent on the direction of $\hat{n}_1$ or $\hat{n}_o$ the two expressions are equivalent. For free electron-like metals and spherical geometry they are identical.

PART B : SEMICONDUCTORS

2.4 THE TOTAL EMITTED CURRENT DENSITY

In this section the theories describing the total emitted current density will only be discussed qualitatively as the quantative treatment can be obtained from the energy distribution which will be discussed more fully in a later section. The emitted current density, j, is related to the energy distribution, P(E), by :

$$j = \int_{E_0}^{\infty} P(E)\, dE$$

An attempt to formulate a theory of field emission from semiconductors was made by Stratton (12) in 1955 who calculated the emission current from the conduction band for a surface in several idealised situations. He developed this theory later (18) to include an effective mass correction and the effect of valence band emission. Generally, his results showed that a plot of log. j vs 1/F should be composed of two parallel linear

sections of negative slope at high and low currents joined by a section of greater negative slope. He found his results to be in agreement with experimental evidence existing at that time (19), however, later work has shown markedly different results (22),(24),(25). This led Baskin, Lvov and Fursei (27) to consider the problem in more detail and explain the saturation region observed in the mid-current range where Stratton had predicted a pronounced increase in current. By considering a situation where the Fermi level was not constant throughout the specimen. They showed that for a p-type specimen a depletion layer is formed just behind the surface which limits the rate of arrival of carriers to the surface. In n-type specimens the carrier concentration in the bulk limits the current. Beyond this saturation region they attribute the increase in current to avalanche breakdown.

2.5 THE ENERGY DISTRIBUTION

The major work on the energy distribution of electrons field emitted from semiconductors was again due to Stratton (32). He derived expressions for the total and normal energy distributions of electrons emitted from the conduction and valence bands. This work has recently been extended by Modinos(39) who has used Stratton's results and included the effect of surface state emission for the specific case of germanium. The argument, however, is sufficiently general to be applicable to most narrow band gap semiconductors, provided that the surface is non-degenerate and that the current is below the saturation level as defined in (27). The model of a semiconductor surface, without surface states, used in this discussion is shown in Fig. 2.3.

Fig. 2.3

Model of a semiconductor surface without surface states.

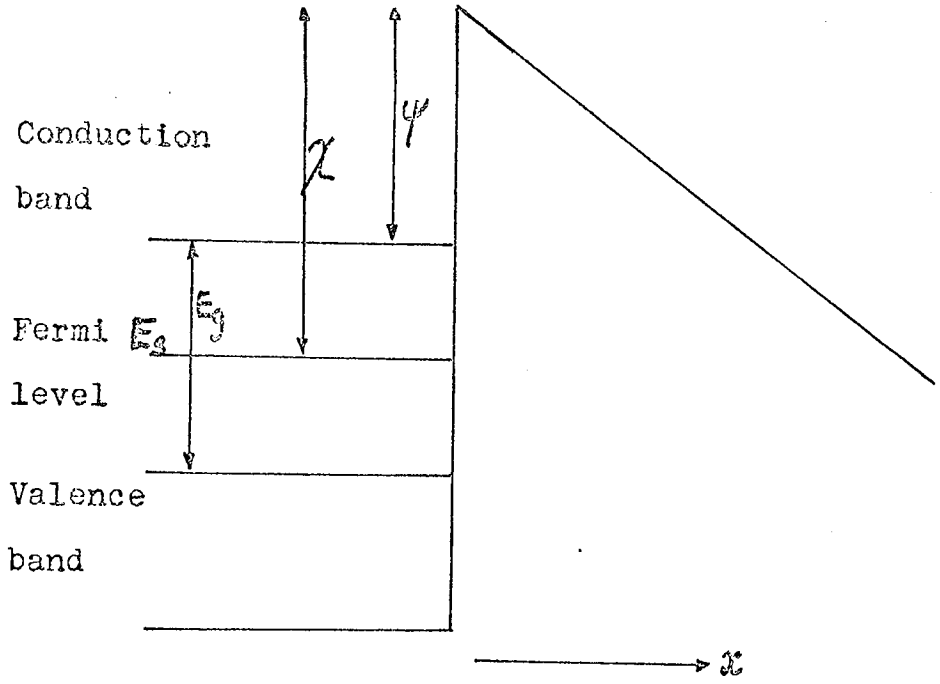

2.5 a Basic Equations, Conduction Band Emission

The energy distribution of the emitted electrons is found by considering the product of several terms :

i) the Fermi distribution function $f(E)$ which determines the occupancy of the states within the material

ii) a probability function $D(E_x)$ the probability that a particle incident upon the barrier will be transmitted.

iii) a velocity V_x, the velocity of a particle towards the barrier

iv) a volume element.

Formally, the total energy distribution $P(E)$ can be written

$$P(E)\,dE = \frac{2e}{h^3} f(E) \int D(E-E_\perp)\, v_x\, dp_x\, dp_y\, dp_z$$

where e is the charge on an electron

and h is Plank's constant

$$D(E_x) = D(E-E_\perp)$$

$$E_\perp = \frac{p_\perp^2}{2m} = \frac{p_y^2 + p_z^2}{2m}$$

The electron velocity V_x can be written as

$$v_x = \frac{\partial E}{\partial p_x}$$

Thus

$$P(E)dE = \frac{2e}{h^3} f(E) \int_E^{E+dE} D(E-E_\perp) \frac{\partial E}{\partial p_x}\, dp_x\, dp_y\, dp_z$$

or

$$P(E) = \frac{2e}{h^3} f(E) \int D(E-E_\perp)\, dp_y\, dp_z$$

Transferring to polar coordinates

$$P(E) = \frac{2em}{h^3} f(E \int_0^{2\pi} d\phi \int_0^{E_M(E,\phi)} D(E - E_\perp)\, dE_\perp$$

where $E_m(E,\phi)$ is the maximum value of $E_\perp = {}^{P_\perp^2}/_{2m}$ for a particular ϕ.

This can be re-written in the form

$$P(E) = \frac{4\pi em}{h^3} f(E) \int_0^{E} D(E_x)\, dE_x - \frac{1}{2\pi} \int_0^{2\pi} d\phi \int_0^{E-E_M} D(E_x) dE_x$$

or

$$P(E) = K f(E) \int_0^{E} D(E_x) dE_x - \frac{1}{2\pi} \int_0^{2\pi} d\phi \int_0^{E-E_M} D(E_x)\, dE_x$$

where

$$K = \frac{4\pi me}{h^3}$$

2.5 b <u>The Transmission Probability.</u>

By using the W.K.B. approximation it has been shown (42) that the transmission probability has the form :

$$D(E_x) = \exp(-B(E_x))$$

where

$$B(E_x) = 2\left[\frac{(2m)^{1/2}}{\hbar}\right] \int_{x_1}^{x_2} (\varphi(x) - E_x)^{1/2}\, dx$$

φ (x) is the barrier potential measured with respect to the conduction band edge.

To facilitate calculations $B(E_x)$ is expanded in a Taylor series about a convenient value of energy $\mathcal{E}$

Thus

$$B(E_x) = b(\varepsilon) - (E_x - \varepsilon)c(\varepsilon) + (E_x - \varepsilon)^2 a(\varepsilon)$$

where $b(\varepsilon) = B(\varepsilon)$

$c(\varepsilon) = -B'(\varepsilon)$

$a(\varepsilon) = B''(\varepsilon)/2$

The coefficients have been derived (43) including an image for a correction and are :

$$a = 2{\cdot}56 \left[\theta^{1/2} \left(\frac{F}{10^7} \right) \left\{ 1 - \left(\frac{\psi_i}{\theta} \right)^2 \right\} \right]^{-1} \nu \left(\frac{\psi_i}{\theta} \right) \quad eV^{-2}$$

$$b = 6{\cdot}38\, \theta^{3/2} \left(\frac{10^7}{F} \right) \nu \left(\frac{\psi_i}{\theta} \right)$$

$$c = 10{\cdot}25\, \theta^{1/2} \left(\frac{10^7}{F} \right) t \left(\frac{\psi_i}{\theta} \right) \quad eV^{-1}$$

where $\theta = \psi - \varepsilon$

ψ is the electron affinity and ν , t are tabulated functions (44) of the order of unity

ψ_i is the depression of the barrier due to the image force

$$\psi_i = 1{\cdot}2 \left(\frac{F}{10^7} \right)^{1/2} (k-1)^{1/2} (k+1)^{-1/2}$$

k is the dielectric constant.

2.5 c <u>The Total Energy Distribution.</u>

The total energy distribution of electrons emitted from the conduction band is obtained by inserting the expression for the tunnelling probability, $D(E_x)$, into the equation for the energy distribution, P(E) :

$$P(E) = K f(E) \frac{e^{-b}}{2\pi} \int_0^{2\pi} d\phi \int_{E-E_M}^{E} \exp\left[c(E_x - \varepsilon)\right] dE_x$$

ignoring quadratic and higher terms in the expansion.

As the major part of the integral is due to values of E_x near to E, ε can be made equal to E, then after integration we have

$$P(E) = K f(E) \frac{e^{-b(E)}}{c(E)} \left[1 - \frac{1}{2\pi} \int_0^{2\pi} e^{-c(E)E_M} d\phi\right]$$

When the conduction band is degenerate, the Fermi energy is positive, it is more convenient to make the expansion about the Fermi energy E_S.

Thus
$$P(E) = \frac{K f(E)}{c(E_S)} e^{-\left[b(E_S) + c(E_S)E_S\right]} e^{c(E_S)E} \left[1 - e^{-r_c c(E_S)E}\right]$$

where
$$r_c = \frac{m}{m_c}$$

Mc is the effective mass of an electron in the conduction band. Similarly for a non-degenerate band, negative Fermi energy, the expansion is made about the bottom of the conduction band.

$$P(E) = \frac{K f(E)}{c(0)} e^{-b(0)} e^{c(0)E} \left[1 - e^{-r_c c(0)E}\right]$$

2.5 d Valence Band Emission.

By a derivation similar to that for conduction band emission the total energy distribution of electrons emitted from the valence band is

$$P(E_v) = \frac{K}{cv_1} f_v(E_v)\, e^{-[bv_1 + cv_1 \xi_v] - cv_1 E_v} \left[1 - e^{-\Gamma_v cv_1 E_v}\right]$$

for a degenerate band

and for a non-degenerate band

$$P(E_v) = \frac{K}{cv_0} f_v(E_v)\, e^{-bv_0 - cv_0 E_v} \left[1 - e^{-\Gamma_v cv_0 E_v}\right]$$

$$bv_0 \equiv b_v(0)\,, \quad bv_1 \equiv b_v(\xi_v)$$

the coefficients are as defined for the conduction band but with α redefined as $\alpha_v = \psi + E_g + \epsilon_v$

and $\psi_i = \psi_i + E_g$

2.5 e Band Structure Effects.

In evaluating the integral :

$$P(E) = \frac{2e}{h^3} f(E) \int D(E - E_\perp)\, dp_y\, dp_z$$

the integrations are performed over values of dp_y, dp_z which lie in the shadow of the energy surface, E, on the plane normal to the x-direction, or, in polar co-ordinates over values of $p_\perp$ and ϕ defining the shadow Fig. 2.4. If the energy surface is spherical and centred on p =(0,0,0), the centre of the Brillouin zone, the limits on the integrals will run from 0 to 2 and 0 to $p_\perp$ max (this is the case considered in the previous section). If, however, the energy surface is centred off p = (0,0,0) the limits will run from ϕ_1 to ϕ_2 and from $p_\perp$ min to $p_\perp$ max. In this case the expression for the tunnelling probability $D(E_x) = D(E-E_\perp)$ will never reach its maximum value, D(E), as it would for a band centred on p = (0,0,0), but only $D(E-E_\perp min)$. The tunnelling probability, therefore, for a band centred off p = (0,0,0) is reduced compared with a band centred on p = (0,0,0).

Fig. 2.4

(a) Band centred on $p = (0,0,0)$

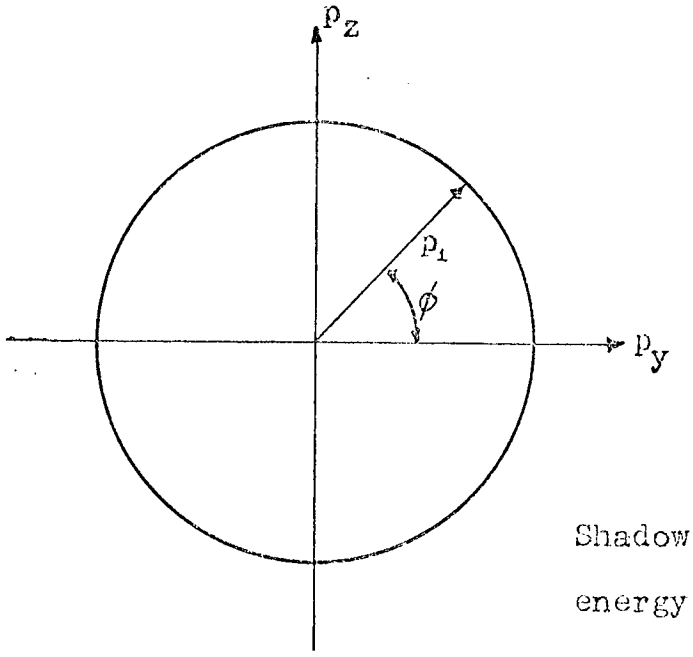

Shadow of constant energy surface

(b) Band not centred on $p = (0,0,0)$

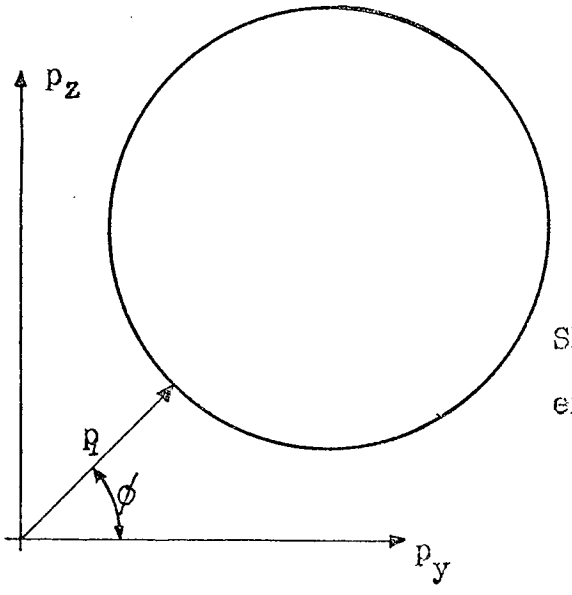

Shadow of constant energy surface

The argument presented above is, to some extent, an over-simplification of the true situation; it indicates, however, the inadequacy of considering the field emission process in terms of idealised conditions.

2.6 SURFACE STATE MODEL

The surface state model used in this section is shown schematically in Fig. 2.5. This model was originally proposed by Handler (45) for Ge. There are two bands of states, one of donor levels S_1 neutral when occupied, and one of acceptor levels S_2 negative when occupied. The S_1 band lies well below the top of the valence band and its contribution to the emission process can be neglected. The S_2 band is assumed to be two dimensional and circular with a density of states per $cm^2 eV$ given by

$$N_0 = \frac{4\pi m^*}{h^2}$$

where m* is an effective mass.

The bottom edge of the band is at E_o below the top of the valence band edge at the surface and the total width of the band Γ is larger than the band gap Eg and is taken to be

$$\Gamma = E_g + 2|E_o|$$

but this is not important as the band is only partly occupied.

Under the application of an electric field to a semiconductor surface the energy bands will bend down as the field lines terminate on surface charges or on excess electrons in the space charge region. The amount of bending can be calculated exactly for a given model of surface states

Fig. 2.5

Surface state model for Germanium.

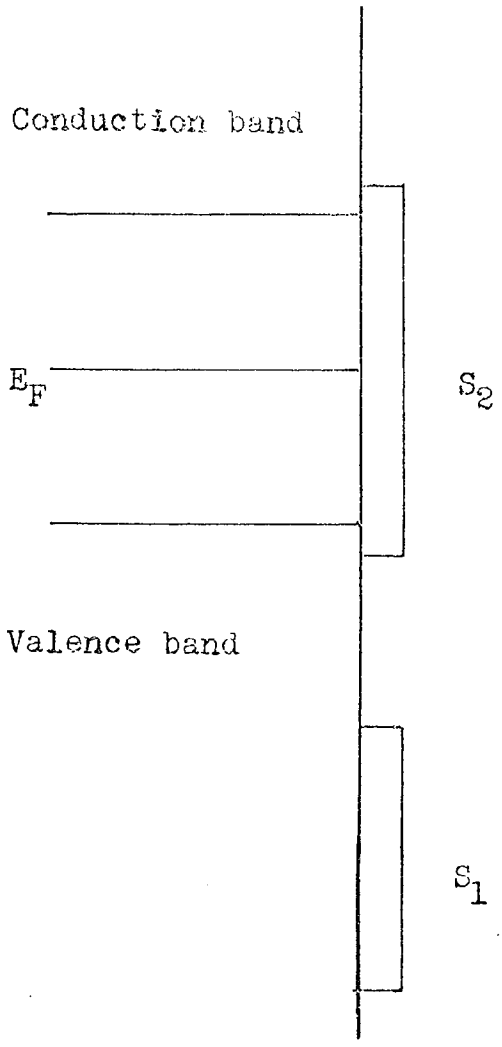

and donor (or acceptor) concentration for a given field. When no field is applied the energy bands will be bent upwards due to the presence of acceptor surface states. It will be assumed that neither the conduction band nor the valence band is degenerate either in the bulk or in the space charge region. Also the Fermi level will be assumed constant throughout the material, i.e. the resistive drop can be ignored.

The concentrations of electrons and holes in the bulk of the semiconductor are given by (39)

$$n = n_i \exp\left(\frac{e\phi_b}{kT}\right) \quad , \quad p = n_i \exp\left(\frac{-e\phi_b}{kT}\right)$$

where n_i is the intrinsic concentration and $u_b \equiv \frac{e\phi_b}{kT}$ is a parameter determining the position of the Fermi level relative to its intrinsic value.

The shift V_s of the electrostatic potential at the surface relative to its bulk value is found by solving Poissons equation (46)

$$-F + \frac{eN_s}{\varepsilon_0} = \left[\frac{kT\varepsilon}{eL_D}\right] 2^{1/2} \left[(u_b - u_s)\sinh u_b - \cosh u_b + \cosh u_s\right]^{1/2} \qquad (1)$$

F is the applied field and U_s is related to V_s by

$$V_s = \frac{kT}{e}(u_s - u_b)$$

ε_0 is the permitivity of free space, ε is the dielectric constant and

$$L_D \equiv \left[\frac{\varepsilon\varepsilon_0 kT}{2e^2 n_i}\right]^{1/2}$$

N_s is the number of electrons in the surface states and is given by

$$N_s = N_0 kT \log\left[1 + \exp\left(\frac{F_t - E_0 + eV_s}{kT}\right)\right]$$

where F_t is an effective Fermi level for the surface states and is different from the Fermi level in the bulk and is measured from the top of the bulk value of the valence band. If the left hand side of equation (1) is positive then $U_s < U_b$ and if negative $U_s > U_b$, the sign of the square root is taken accordingly.

2.7 REPLENISHMENT OF SURFACE STATES

If significant field emission currents are to be drawn from the surface states the states must be capable of being refilled with electrons which must come from the valence and conduction bands. Under steady state conditions the current density emitted from the states must be equal to the total current density supplied to the states.

$$I_{ss} = I_{v,c \rightarrow ss}$$

$$I_{v,c \rightarrow ss} = I_{v \rightarrow ss} + I_{c \rightarrow ss}$$

$I_{v \rightarrow ss}$ is the current density flowing into the surface states from the valence band and $I_{c \rightarrow ss}$ the current density from the conduction band.

Consider first the electrons flowing into the surface states from the valence band, or equivalently the flow of holes from the surface states to the valence band. The flow of holes from the valence band

to the surface states in the energy interval E to E + dE is given by :

$$V_p S p_s N_o f(E) dE$$

where N_o is the density of states and $f(E)$ is the probability of the state being occupied.

$$f(E) = \left[1 + \exp\left(\frac{E - F_t}{kT}\right)\right]^{-1}$$

where F_T is the effective fermi level as defined in the previous section. This assumes that the electrons in the surface states are in thermal equilibrium with themselves though not with the bulk electrons. This is justified if the relaxation time is less than the lifetime of an electron in a state.

p_s is the hole concentration at the surface of the valence band and for a non-degenerate surface is related to the bulk concentration by

$$p_s = p \exp\left(-\frac{eV_s}{kT}\right) = n_i \exp\left(-U_b - \frac{eV_s}{kT}\right)$$

Vp is a velocity which when multiplied by p_s gives the flux of holes crossing unit area from one direction

$$V_p = \left(\frac{kT}{2\pi M_v}\right)^{1/2}$$

Mv is the hole effective mass

finally S denotes an average recombination cross section

There will also be a flow of holes in the reverse direction and this is given by

$$g_t v_p S N_0 f'(E)\, dE$$

where

$$f'(E) = 1 - f(E) = f(E) \exp\left(\frac{E - F_t}{kT}\right)$$

g_t is determined by the fact that in thermal equilibrium

$F_t = E_F$

and the net current is zero

hence

$$g_t = p_s \exp\left(\frac{E - F_t}{kT}\right)$$

The net flow of holes from the valence band to the surface states is given by the algebraic sum of these two expressions, hence the net current density is given by

$$I_{v \to ss} = e v_p S n_i \exp\left(-U_b - \frac{eV_s}{kT}\right) N_0 kT \log\left[1 + \exp\left(\frac{F_t - E_0 + eV_s}{kT}\right)\right] \times \left[\exp\left(\frac{E_F - F_t}{kT}\right) - 1\right]$$

Similarly the net current density from the conduction band is given by

$$I_{c \to ss} = e v_n S n_i \exp\left(U_b + \frac{eV_s}{kT}\right)\left\{N - N_0 kT \log\left[1 + \exp\left(\frac{F_t - E_0 + eV_s}{kT}\right)\right]\right\} \times \left[1 - \exp\left(\frac{F_t - E_F}{kT}\right)\right]$$

where $v_n = \left(\frac{kT}{2\pi m_c}\right)^{1/2}$

m_c is the effective mass for conduction band electrons.

2.8 TUNNELLING FROM THE SURFACE STATES

The current tunnelling from a surface state can be expressed as a product of an attempt frequency ν and the penetration probability T

$$j_{ss} = \nu T$$

ν is strongly dependent on the localisation of the surface state wave function and will be large for a localised wave function and smaller for a less localised wave function. The localisation can be characterised by a parameter t which is the distance of the centre of gravity of the surface state charge from the surface

Then ν is given by

$$\nu = \left(\frac{\hbar k_t}{m} \right) q$$

where $q = \frac{1}{2t}$

and $\frac{\hbar k_t}{m}$ is a characteristic velocity of the order of 1 Å^{-1}

q acquires its maximum value near the middle of the energy gap and goes to zero at the edges, it can be parametrized as

$$q = \lambda \left[1/4\,\Gamma^2 - (E - E_0 + eV_s - 1/2\,\Gamma)^2 \right]^{3/4} \left(\frac{2m}{\hbar^2} \right)^{1/2}$$

the energy E is measured from the top of the valence band q acquires its maximum value at the centre of the band which corresponds to the centre of the energy gap

$$q_{max} = \lambda \left(\frac{m\Gamma}{\hbar^2} \right)^{1/2}$$

This has been estimated for Si to be = 0.15Å^{-1} corresponding to a localisation of 8 Å. The case for Ge is assumed similar and hence

The tunnelling probability is given by

$$T = A \exp \left[-6.83 \left(\psi + E_g - eV_s - E \right)^{3/2} \left(\frac{10^7}{F} \right) \nu \left(\frac{\psi_i}{\psi + E_g - eV_s - E} \right) \right]$$

which is similar to the expression for the conduction and valence bands except that E is measured from the top of the valence band.

The pre exponential term A is generally assumed to be of the order of unity and is most likely to be in the range $0.1 < A < 1$

The total energy distribution emitted from the surface states is then given by

$$j_{ss}(E) = \theta e N_0 \left(\frac{2}{m}\right)^{1/2} \left[1 + \exp\left(\frac{E - F_t}{kT}\right)\right]^{-1} \left[\frac{1}{4}\Gamma^2 - \left(E - E_0 + eV_s - \frac{1}{2}\Gamma\right)^2\right]^{1/4}$$
$$\times \exp\left[-6.83\left\{\psi + E_g - eV_s - E + \frac{m^*}{m}(E + eV_s - E_0)\right\}^{3/2}\left(\frac{10^7}{F}\right)\right.$$
$$\left.\times\, w\left(\frac{\psi_i}{\psi + E_g - eV_s - E}\right)\right]$$

with θ given by $\theta \equiv \lambda A k_r$ thus combining the three unknowns to give effectively one parameter.

The corresponding emitted current density is given by

$$I_{ss} = \int_{E_0 - eV_s}^{E_0 - eV_s + \Gamma} j_{ss}(E)\, dE$$

The current density emitted from the surface states can now be written explicitly as

$$e v_p S n_i \exp\left(-U_b - \frac{eV_s}{kT}\right) N_0 kT \log\left[1 + \exp\left(\frac{F_t - E_0 + eV_s}{kT}\right)\right]$$
$$\times \left[\exp\left(\frac{E_F - F_t}{kT}\right) - 1\right] + e v_n S n_i \exp\left(U_b + \frac{eV_s}{kT}\right) \qquad (2)$$
$$\times \left\{N - N_0 kT \log\left[1 + \exp\left(\frac{F_t - E_0 + eV_s}{kT}\right)\right]\right\}\left[1 - \exp\left(\frac{F_t - E_F}{kT}\right)\right]$$

$$= \theta e \left(\frac{2}{m}\right)^{1/2} N_0 \int_{E_0 - eV_s}^{E_0 - eV_s + \Gamma} \left[1 + \exp\left(\frac{E - F_t}{kT}\right)\right]^{-1} \left[\tfrac{1}{4}\Gamma^2 - (E - E_0 + eV_s - \tfrac{1}{2}\Gamma)^2\right]^{1/4}$$

$$\times \exp\left\{-6.83 \left[\psi + E_g - eV_s - E + \frac{M^*}{m}(E + eV_s - E_0)\right]^{3/2} \left(\frac{10^7}{F}\right) \nu\right\} dE$$

2.9 APPLICATIONS

In order to calculate the emitted current density from the valence, conduction and surface bands it is first necessary to determine Vs and Ft for given values of applied field F. This is achieved by solving equations 1 and 2 simultaneously to give self-consistent solutions for Vs and Ft. Modinos (39) has calculated the energy distributions of electrons field emitted from germanium with values of U_b = -4,0, +4 corresponding to p-type, intrinsic and n-type specimens. Fig. 2.6 shows his result for $U_b = 0$, the curves for $U_b = \pm 4$ are identical except for a displacement along the energy axis corresponding to different values of E_F. The result resembles the experimental observations of Shepherd and Peria (38) except that experimentally the energy distribution is always well below the Fermi level. It has been shown (47), however, that a slight change of the parameter S in the theoretical expression reproduces the experimental results.

Modinos has also calculated the energy distribution for cadmium sulphide (47) by including the parameters pertainant to cadmium sulphide in the above expressions, see Table 2.1.

Fig. 2.6

Theoretical energy distribution of electrons field emitted from germanium according to Modinos.

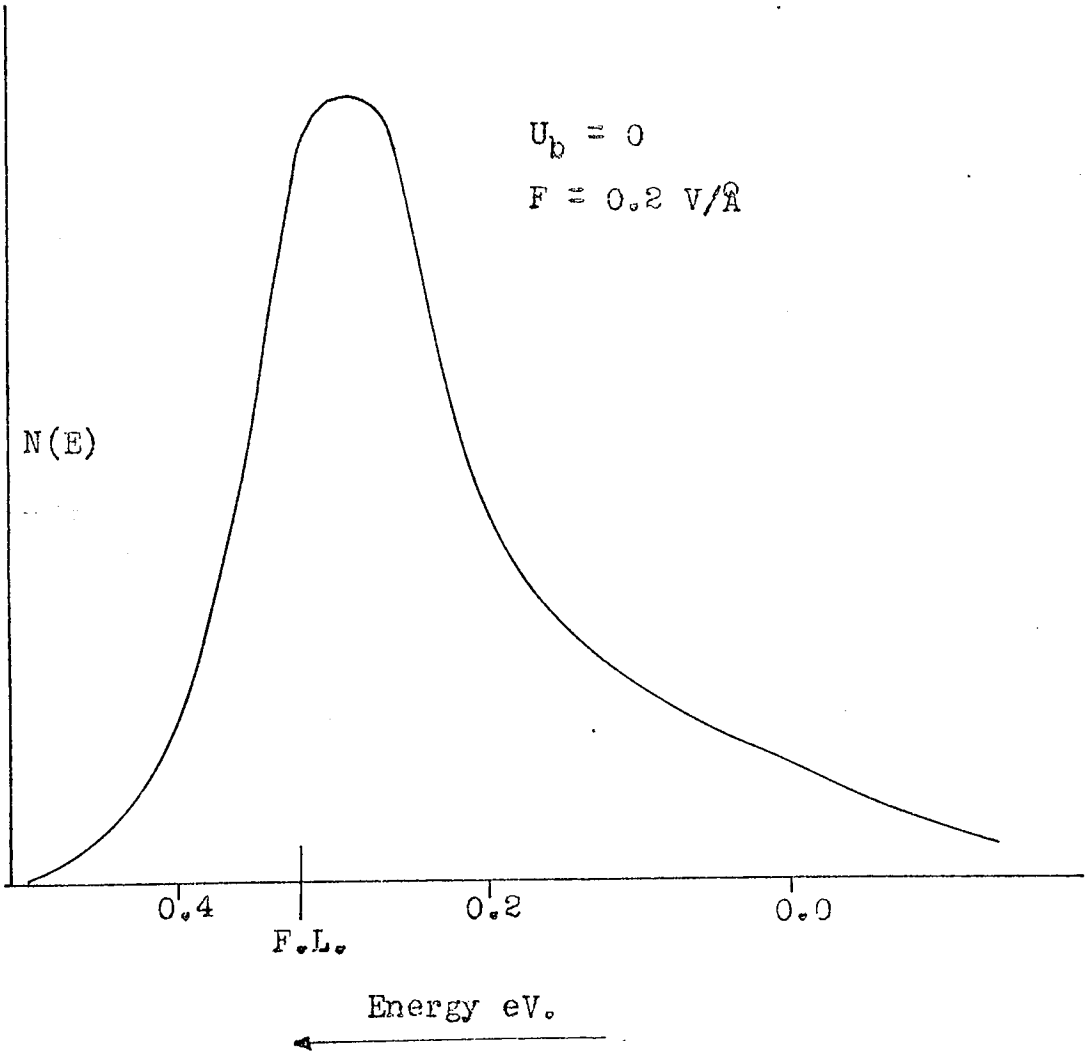

Table 2.1

Parameters for Cadmium Sulphide

	Bulk			Surface	
M_c	.20 m	(48)	N_o	1.6×10^{13} eV^{-1} cm^{-2}	(49)
M_v	5 m‖and .7 m⊥	(48)	E_o	+ 1.5 ± 1.5 eV	(49)
n_i	6×10^{-3} cm^{-3}	(48)	S	1×10^{-16}	(50)
ε	9.3	(48)			
E_g	2.4 eV	(48)			
ψ	4.8 eV	(49)			

The result is shown in Fig. 2.7 a, unfortunately the distribution is much narrower than those measured experimentally (51), but when the applied field is about 0.4 V A^{-1} the conduction band becomes degenerate and the theory as proposed is unsuitable. Modinos is of the opinion, however, that when the theory is improved to incorporate degeneracy the result will be as shown in Fig. 2.7 b and if the condition of thermal equilibrium is relaxed the result will resemble Fig. 2.7c tending to a limit Fig. 2.7 d which is more representative of the experimental result. An electron supplied to the surface state band from the conduction band must loose some energy before it reaches equilibrium, the maximum energy it can loose per event is of the order of kT so in a wide band gap material the electron has to undergo many events before reaching equilibrium. If the time taken for emission is less than the time required to reach equilibrium the electron has a high probability of being emitted from a non-equilibrium state, thus broadening the distribution.

Fig. 2.7

Predicted energy distribution for cadmium sulphide according to Modinos.

(a)

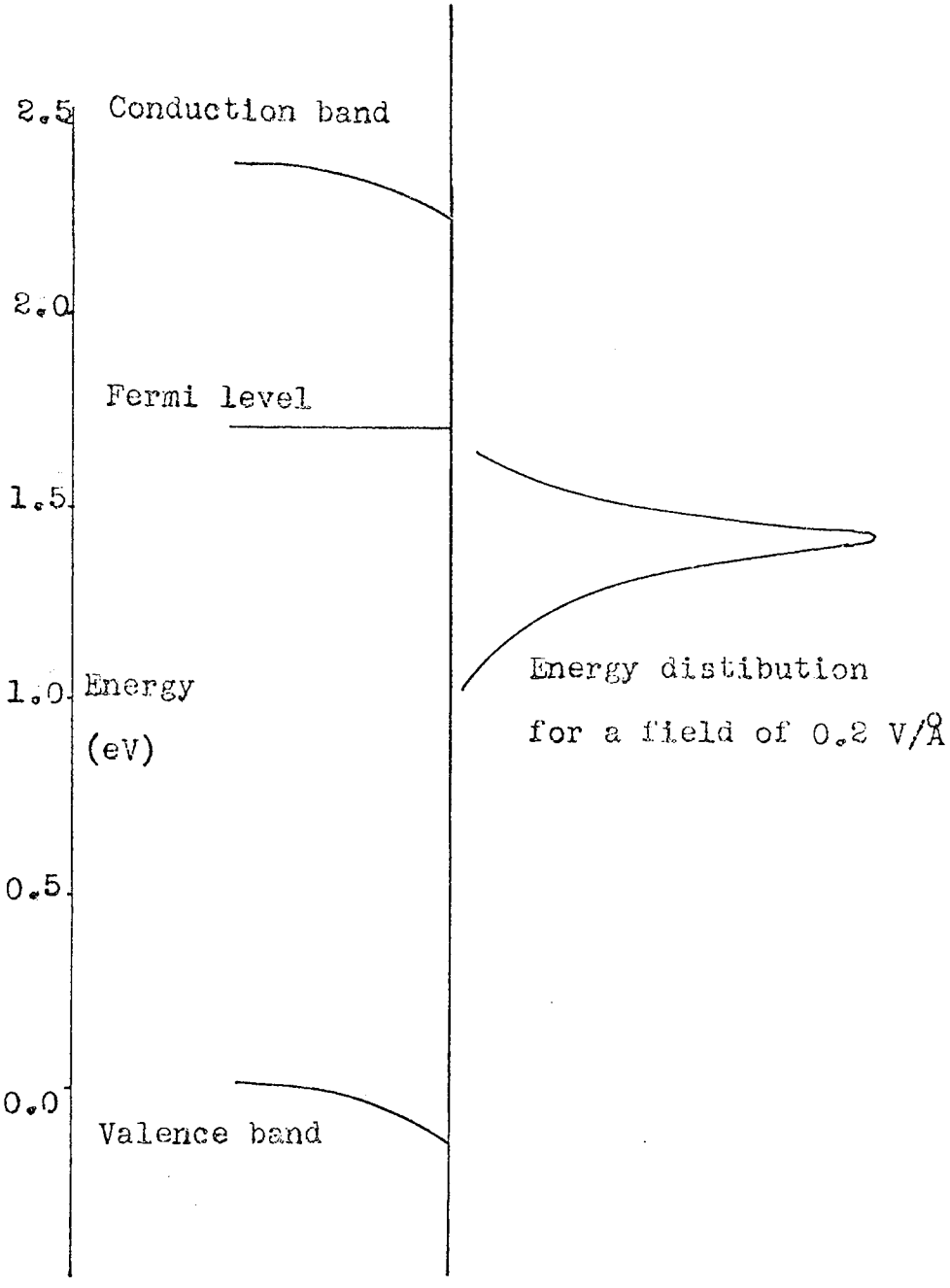

(b)

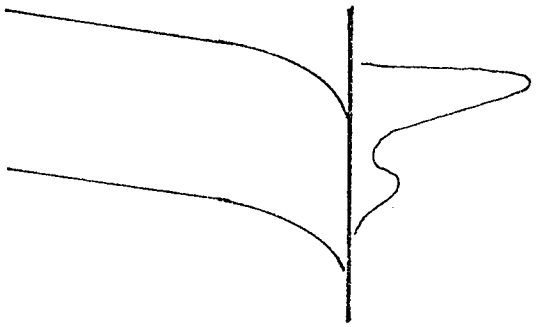

(c)

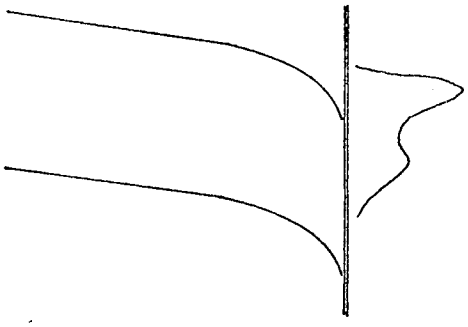

(d)

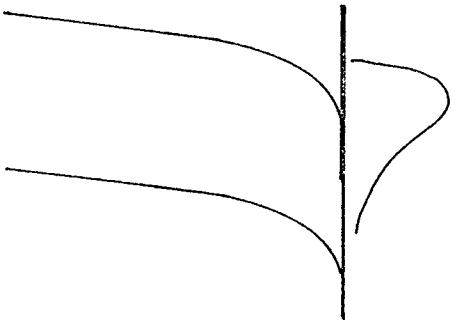

CHAPTER 3

THE CARBON FIBRE FIELD EMITTER

3.1 INTRODUCTION

Field emission electron sources, for use in electron optical devices, are superior to conventional sources utilising hot filaments as they are physically smaller and have a much higher brightness (52). Refractory metals are usually used in field emission electron guns as they can withstand the high stresses imposed by the field, however, they are very susceptible to contamination and consequently require ultra-high vacuum conditions for successful operation. Electron optical instruments are normally unbaked systems reaching base pressures in the 10^{-6} to 10^{-7} torr range and are therefore incompatible with the requirements of a field emission system. This has led to the development of sophisticated differentially pumped systems (53)(54), to overcome this limitation. An alternative approach to the problem is to find a material which will emit a stable current in poor vacuum conditions but will not be destroyed by the high field. There is some evidence that carbon fibres should be able to meet the high stress requirement, and, as the contamination in unbaked systems is often of an organic nature, contamination effects should not be as great as with metallic emitters.

3.2 MANUFACTURE, STRUCTURE AND ELECTRICAL PROPERTIES

Carbon fibres are produced by heating a synthetic fibre yarn, the precursor, to temperatures between 1000°C and 3000°C in various atmospheres(55). Otani et al. (56) report producing carbon fibres by heat treatment of filaments spun from P.V.C., coal tar pitch and

petroleum asphelt at 1000°C for twenty minutes in a nitrogen atmosphere. More usual precursors are polyacrylonitrile (P.A.N.) and rayon (57). Moreton, Watt and Johnson (58) have shown that heating the precursor to about 2500°C produces a fibre with a high modulus of elasticity, if, however, a high tensile strength and breaking strain only are required it is only necessary to heat to 1500°C.

Johnson and Watt (59) have used transmission electron microscopy to investigate the structure of high modulus carbon fibres produced from polyacrylonitrile by heat treatment at 3000° C. They cut thin sections from the fibres and found the internal structure to be composed of long narrow units, about 100 Å across but of undetermined length, lying parallel to the fibre axis. Some of their specimens ruptured to form a network of fibrils 800 Å to 1000 Å across and apparently running the whole length of the specimen. Badami et al (60) have used x-ray diffraction techniques and have shown P.A.N. based fibres are composed of graphite crystallites about 60 Å in size with their basal planes highly oriented along the fibre axis. They also used transmission electron microscopy of sections, replicas and cut ends to substantiate their x-ray measurements. The cut ends of the fibres showed them to be composed of fibrils 250 Å to 1000 Å in diameter, and the replicas showed fibrils lying parallel to the fibre axis. Dark field images of the sections confirmed the x-ray measurements of crystallite size throughout the specimen, the crystallites becoming aligned towards the edges of the specimen and joining together to form chains along the fibre axis.

Later work by Johnson and Tyson (61) has suggested that the fibrillar nature of the fibres indicated by earlier workers had been overstressed. They used x-ray techniques and electron microscopy to show that the fibres are composed of turbstratic graphite crystals about 65 Å long, (the carbon atoms form two dimensionally ordered basal layers randomly stacked along the c-axis). They also found three dimensionally ordered flakes of graphite distributed throughout the fibres. This structure is quite different from that of any of the precursor fibres. Wicks (62) has studied flame polished fibres in the electron microscope and also found them to be composed of turbostratic graphite. The preferred orientation of the basal planes was found to be parallel to the fibre axis and the degree of orientation increased progressively with the temperature of graphitization. He also found the crystallites formed into parallel ribbons enclosing a network of pores, the ribbons getting longer as the temperature of graphitization increased. The platelets of graphite found by Johnson and Tyson (61) were also observed.

Bacon and Silvaggi (57) investigating the structure of rayon based fibres found a structure similar to that reported by Johnson and Watt (58) and Badami et.al. (60). Electron microscopy of sections cut from fibres showed a honeycomb structure of pores oriented along the fibre axis, the pores being about 60 Å apart separated by ribbons of turbostratic graphite. On a larger scale they found the fibres to be composed of bundles of fibrils about 500 Å in diameter.

Raman spectroscopy has been used by Tunistra and Koenig (63) in an investigation of the surface of carbon and graphite fibres. They found that in most graphite fibres in the surface layer the crystallites were

oriented with the graphite planes parallel to the surface and that the crystallite size is greater near the surface than in the interior.

Owston (64) has studied the electrical properties, under stress, of batches of carbon fibres from several sources and considers conduction mechanisms which could explain his results. Resistance measurements of the different fibres showed them to have resistivities in the range 150 $k\Omega m^{-1}$ to 700 $k\Omega m^{-1}$, this is ten to one hundred times larger than would be expected for basal plane conduction in pure graphite of the same dimensions. He also found that the spread of resistances in a batch of fibres was greater than the spread in cross sectional areas. Analysis of the noise generated in the fibres showed it to be of the form that is found in carbon composition resistors (due to variations in contact resistance between granules) rather than of thermal origin. The fractional change in resistance was measured as a function of strain, results differed markedly from fibre to fibre, generally showing an increase, becoming linear at high strains but in some cases he reports observing a decrease. The characteristics of most of the fibres examined were time independent but some showed a variation of resistance over a period of minutes whilst subjected to a constant load. These properties are discussed in relation to the structures proposed by Johnson and Watt (59) and Johnson and Tyson (61) and found them to be compatible with either, as, in both models, the fibres are composed of conducting particles bonded at some points and conducting but not bonded at others. The time dependent phenomena can be attributed to either local heating effects at contact points between particles or a movement of long fibrils within the fibre structure.

3.3 PREVIOUS WORK

Early work was done by Montet et.al.(65) on field emission from graphite knife edges. Williams (66) has produced field ion images from cleaved graphite plates but found that the streaks in the image were at right angles to the basal planes due to distorted magnification resulting from the two dimensional nature of the specimen. He also observed that, under vacuum conditions which produced stable images with metals, the graphite image was unstable due to impurity gases attacking the surface. As the previous work suggests that graphite planes cannot be suitably observed if the (0001) planes are parallel to the viewing direction, Hughes and Montague-Pollock (67) deposited carbon films on platinum emitters by the pyrolysis of acetylene. They obtained field emission and field ion images and found the carbon to be partly graphitic and partly amorphous.

This early work was primarily concerned with imaging carbon and so was carried out under ultra high vacuum conditions. The importance of carbon fibres as stable field emitters in poor vacuum was first demonstrated by Baker et. al.(68) and in this laboratory by Smith (69). Baker et.al.(68) were specifically looking for field emitters for use in poor vacuum and after unsuccessful work on silicon whiskers turned to carbon fibres. They prepared their emitters by controlled corona discharge in air and mounted them with 'Aquadag'. In the pressure range 10^{-7} torr to 10^{-8} torr their fibres were found to emit well with lifetimes in excess of 2400 hours at nominal emission currents of 10 μA although an emission current of 100 μA reduced the lifetime to 500 hours. They report the emission to be confined within a cone of angle 60° although

this could be reduced to 10^{o} by modifying the field in the region of the tip (this illustrates the dependence of the electron beam on electrode geometry in field emission systems). A scanning electron microscope with a resolution of 0.2 microns using a carbon fibre source is also reported.

English, Lea and Lilburn (70) have reported the use of a carbon fibre field emission electron gun. They coated their fibres with tungsten so that lengths of the coated fibre could be spot welded to a filament. The coating is then stripped off and the protruding fibre A.C. electropolished in sodium hydroxide with a current of 50μA. Once under vacuum small asperitives on the tip were removed by heating to 2500^{o}C in vacuum of 10^{-9} torr and larger ones by heating in oxygen a pressure of 10^{-5}torr. Tips produced in this way are reported to give single spot emission patterns but were not used at emission currents greater than 5μA. Before heat treatment, however, emission revealed a pattern of many small emission centres corresponding to asperitives on the tip surface as small as 50 Å in diameter.

Lea (71) reporting on the field emission characteristics of carbon fibre tips prepared as above has measured Fowler-Nordheim characteristics of the single spot emitters found a marked insensitivity of the work-function and emitting area to the vacuum conditions, the same results being obtained for emission in poor vacuum as after prolonged heating in ultra high vacuum. The angular distribution of the beam was measured to be approximately gaussian. Lea discusses the importance of the virtual size of the electron source in field emission gun systems and shows that his single spot emitters to be far superior to those reported by Baker.

3.4 PREPARATION OF EMITTERS

The carbon fibres used were supplied by Courtaulds Ltd. and were approximately eight microns in diameter. Despite their high strength individual carbon fibres can be easily damaged, so, to make them easier to handle, the fibres were first electroplated with copper. This was done by picking up a fibre about six inches long on a piece of sellotape and sticking it to a copper plate so the fibre could be hung from the plate with a small weight attached to the other end to steady it (the fibres were easily disturbed by slight draughts otherwise). The fibre was suspended in the centre of a cylindrical copper electrode and the vessel surrounding it filled with slightly acidic saturated copper sulphate solution, Fig. 3.1. A current of a few tens of milliamps flowing for a few hours was found to produce a suitable covering of copper. The plated fibre was cut into suitable lengths and the copper stripped off the last 5 mm. of the fibre with concentrated nitric acid. The fibres were d.c. electropolished in normal sodium hydroxide with a current of about 50 μA, when the current fell to zero the fibre was removed and washed. Examination under the scanning electron microscope showed the tips to have a radius of about 1000 Å Fig. 3.2.

Tips produced in this way are more robust than those of Baker (68) and more simply produced than those reported by Lea (71). Unfortunately, the copper plating, although allowing the fibre to be spot welded to a filament, prohibits any attempt at heat treatment of the tip after the method of Lea (71), as at low temperatures the copper could contaminate the emitter and at temperatures sufficiently high to restructure the end-form the copper would evaporate.

Fig. 3.1

Cell for copper plating carbon fibres.

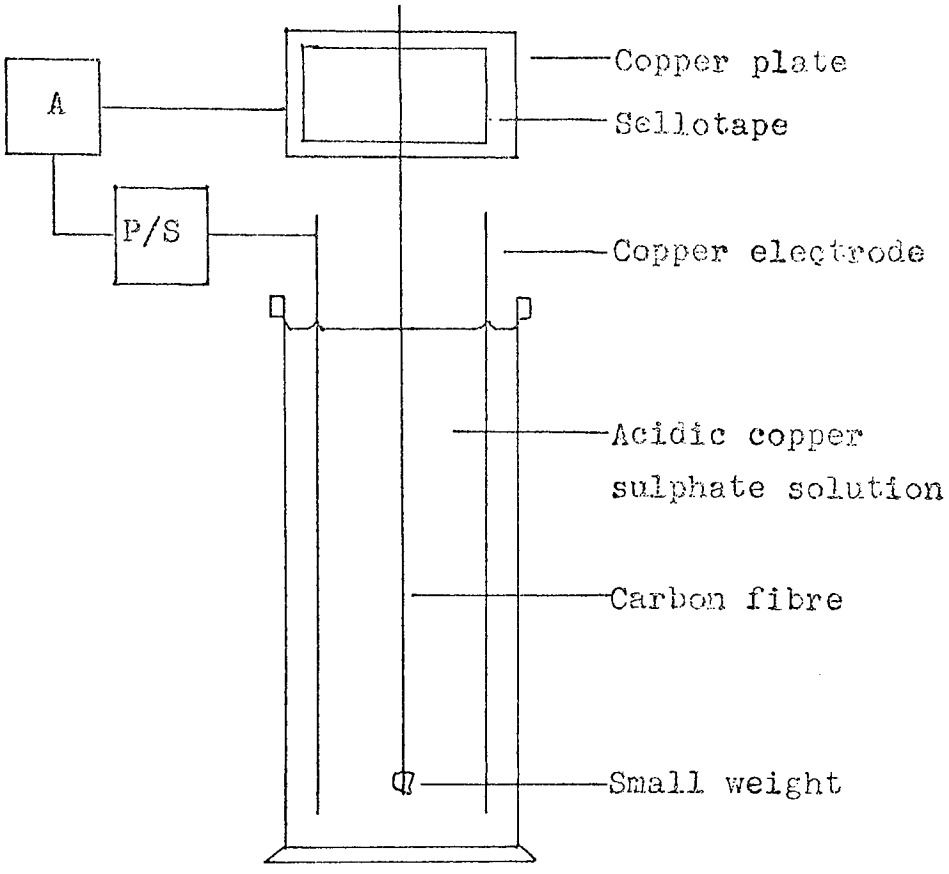

Fig. 3.2 A Typical Carbon Fibre Emitter.

Top x3300

Bottom x160

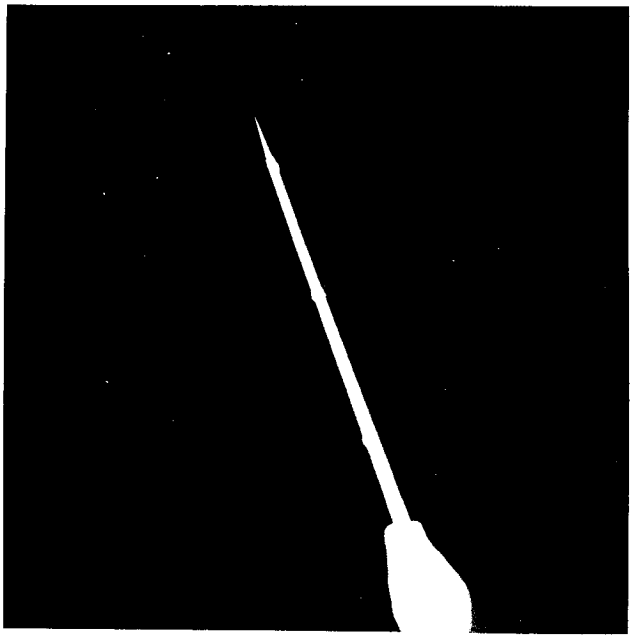

3.5 RESULTS

Tips used in this work produced emission patterns composed of many random spots with no obvious symmetry. It has been shown that (72) the stability of the emission current, in poor vacuum, is comparable with that reported by other workers (68),(71). Smith (69) has shown that, in a vacuum of 10^{-7} torr, for a nominal emission current of 10 μA the current remained within $\pm$ 3% over many hours and that the life-times of the emitters under such conditions are in excess of several hundred hours.

Fowler-Nordheim characteristics of several carbon fibre tips were measured using a simple field emission microscope, Fig. 3.3. Plots were found to be linear, Fig. 3.4, provided that the current was not allowed to exceed a few microamps as this presumably produced a change in end-form in the poor vacuum used.

Energy distributions were measured using the retarding potential analyser described by Salmon (57). The vacuum system was baked before making any measurements but the vapour trap on the diffusion pump was not filled, as a result the pressure in the analyser was in the 10^{-8} torr to 10^{-9} torr range. As the fibres were only 8 microns in diameter it was not possible to see them once they were mounted in the analyser, so it was not possible to set the tip to the position of optimum resolution. To get the tip to the optimum position a spot in the emission pattern was positioned over the probe hole and the applied voltage reduced until the maximum collected current was between 1 and 5 x 10^{-11} A. The tip was then moved progressively towards, or away from, the screen, the collected current being maximised at each step and the energy distribution

Fig. 3.3

The simple field emission microscope.

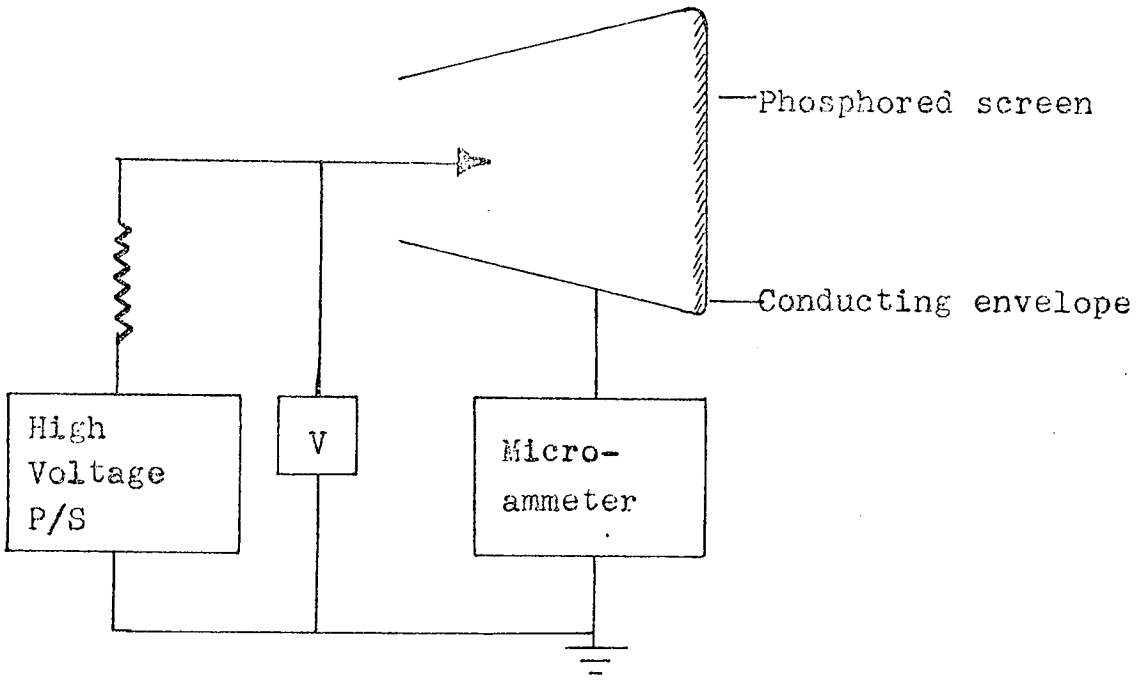

Fig. 3.4

Carbon fibre 3

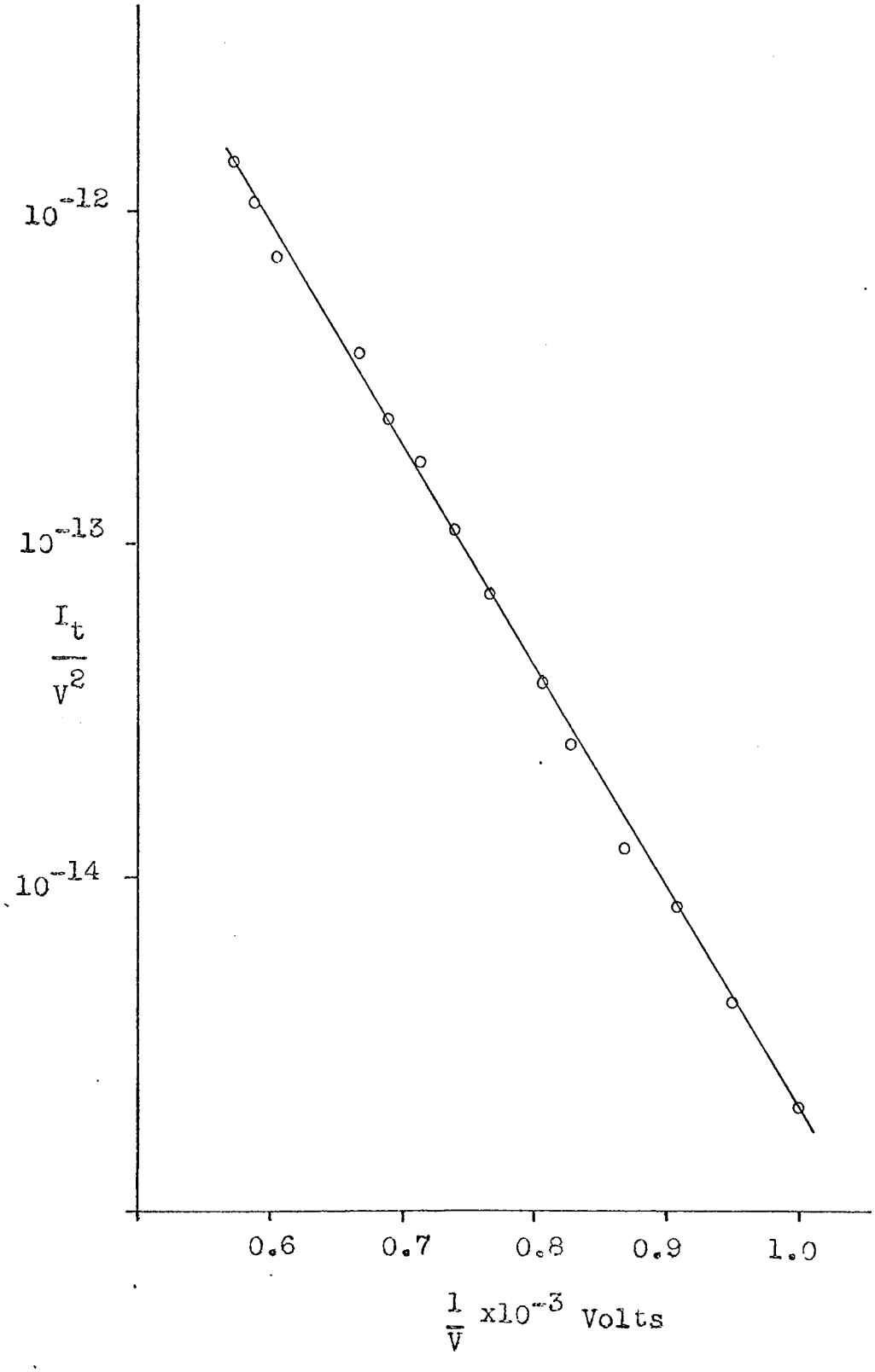

measured. If the half width of the distribution showed no distinct minimum another spot was selected and the procedure repeated until a well defined minimum could be obtained. The tip was then assumed to be at the optimum distance from the screen and on the axis. A typical run in which the emitter passes through the position of optimum resolution is shown in Fig. 3.5. The process was repeated with several tips to show the minimum value of the half-width was reproducible Fig. 3.6 .

With some tips it was observed that as the applied field was increased the spots in the emission pattern would elongate until they became a series of parallel lines. This could be attributed to a magnification effect due to the structure of the fibre, similar to the effect described by Williams (66) in graphite. Alternatively, the cause could be that as the field is increased the stressed fibre comes into resonance with the slight vibrations in the apparatus caused by the rotary pump. The latter explanation is more credible as this effect was only observed when the fibre extending beyond the copper coating was long, about 1 cm.

In some cases when measuring the energy distributions it was noticed that after increasing the applied voltage slightly the collected current increased slowly over a period of minutes whilst everything else remained constant. This could be similar to the time dependent resistance observed by Owston (64). If the emission in any particular spot can be assumed to originate from a particular component fibril, the change in collected current could be due to an effect peculiar to a fibril rather than to the whole fibre. The increase in

Fig. 3.5(a)

Carbon fibre 1

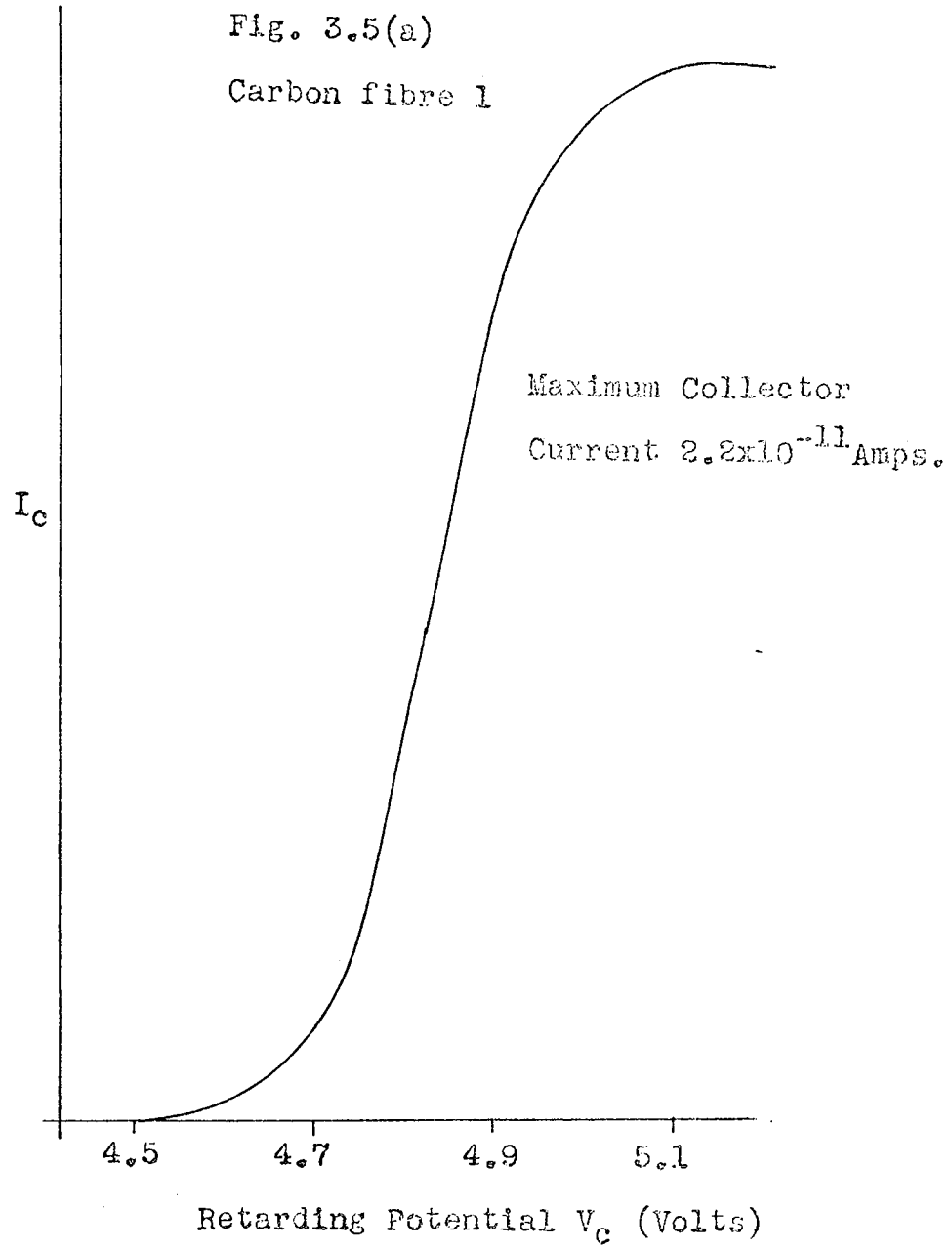

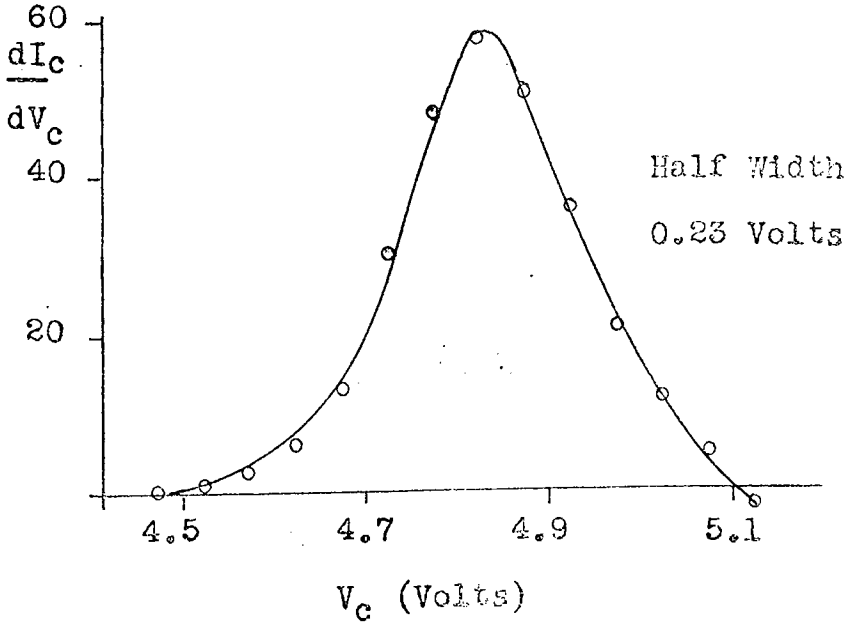

Fig. 3.5(b)

Carbon fibre 1

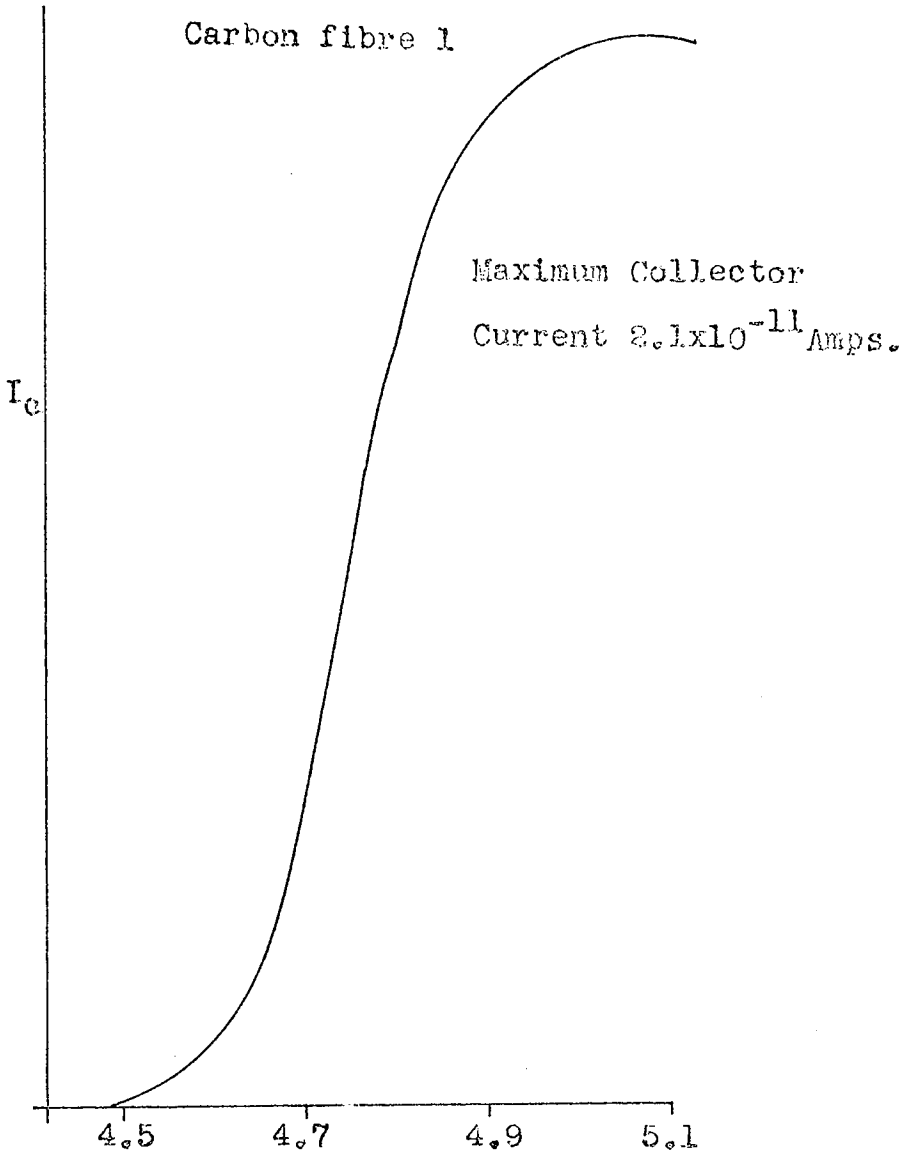

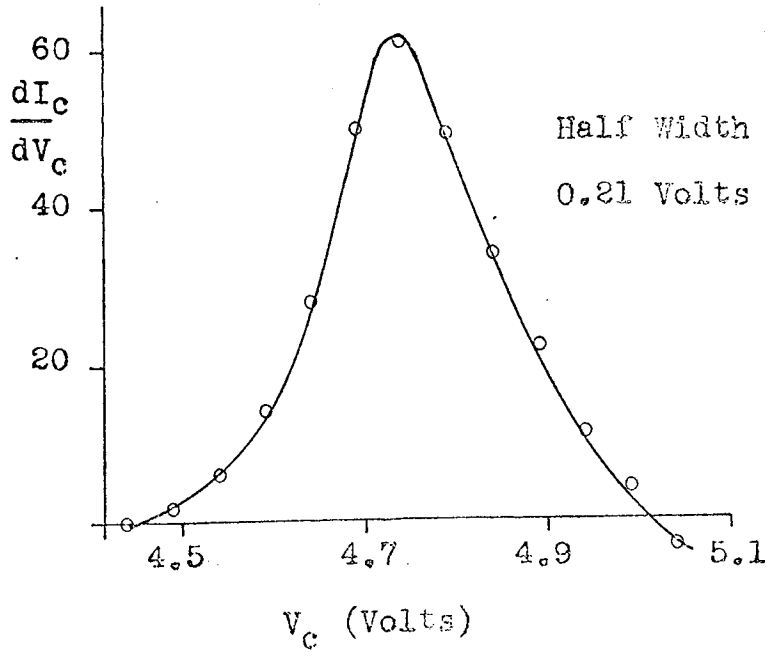

Fig. 3.5(c)

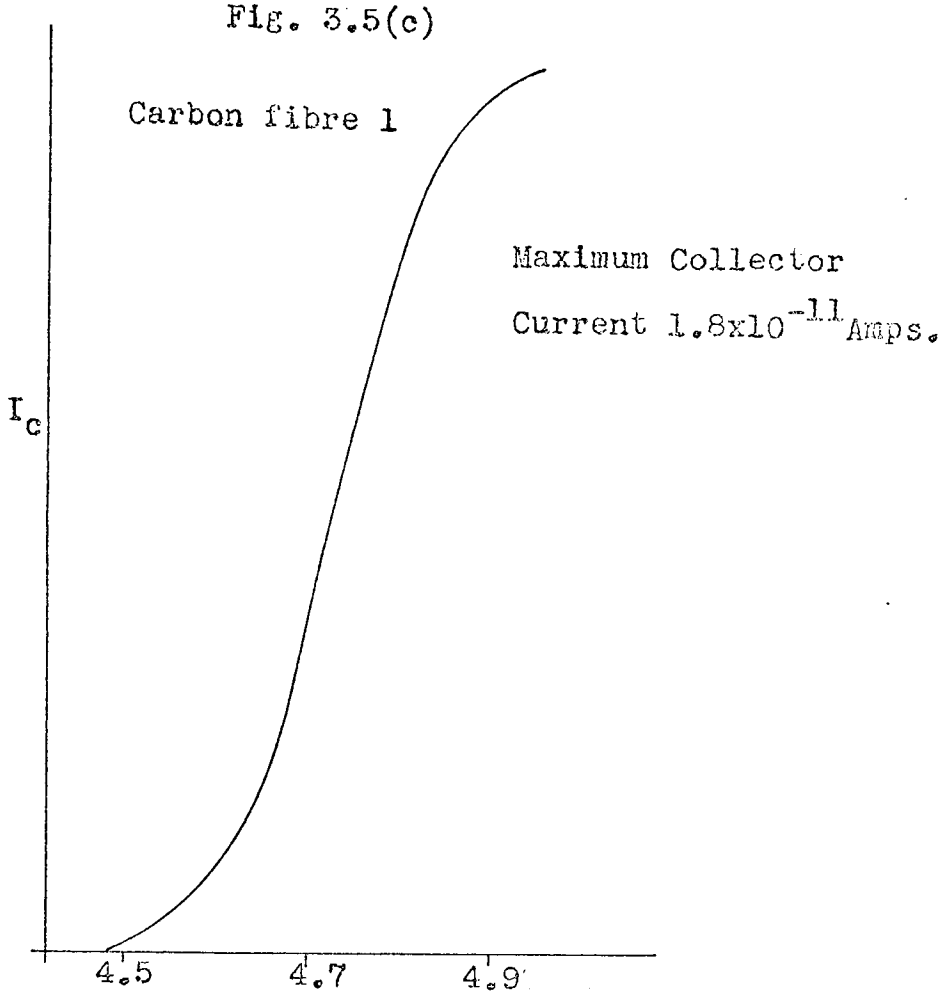
Carbon fibre 1
Maximum Collector
Current 1.8x10^{-11} Amps.
I_c
4.5
4.7
4.9
Retarding Potential V_c (Volts)

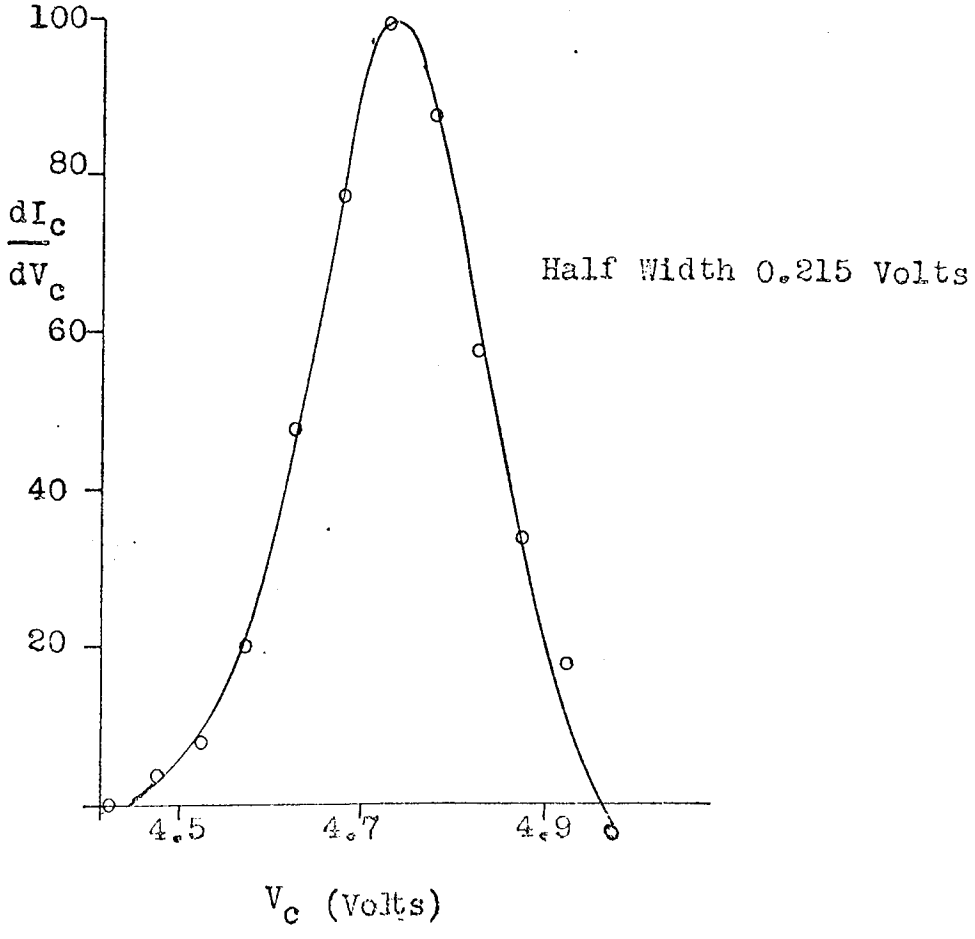
100
80
60
40
20
$\frac{dI_c}{dV_c}$
Half Width 0.215 Volts
4.5
4.7
4.9
V_c (Volts)

Fig. 3.5(d)

Carbon fibre 1

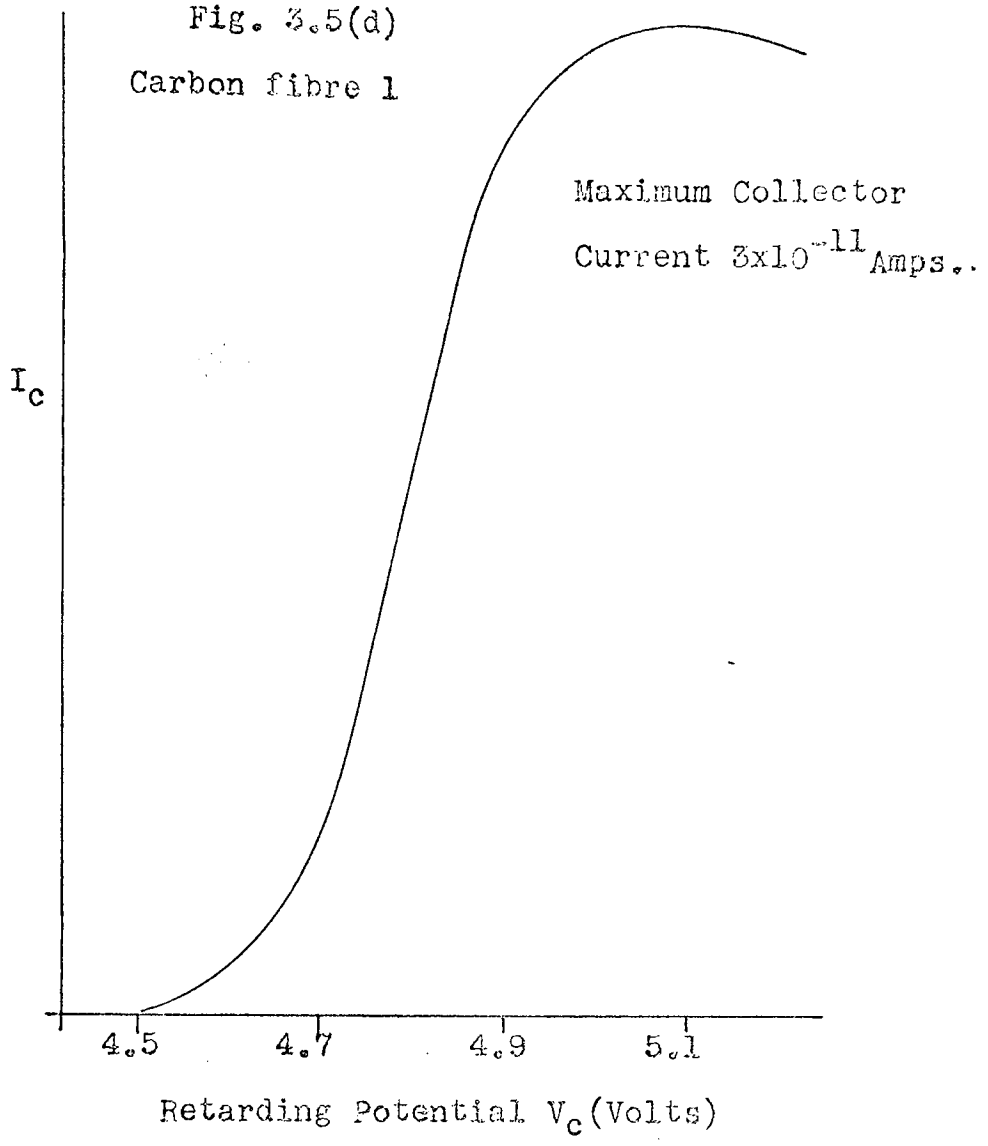

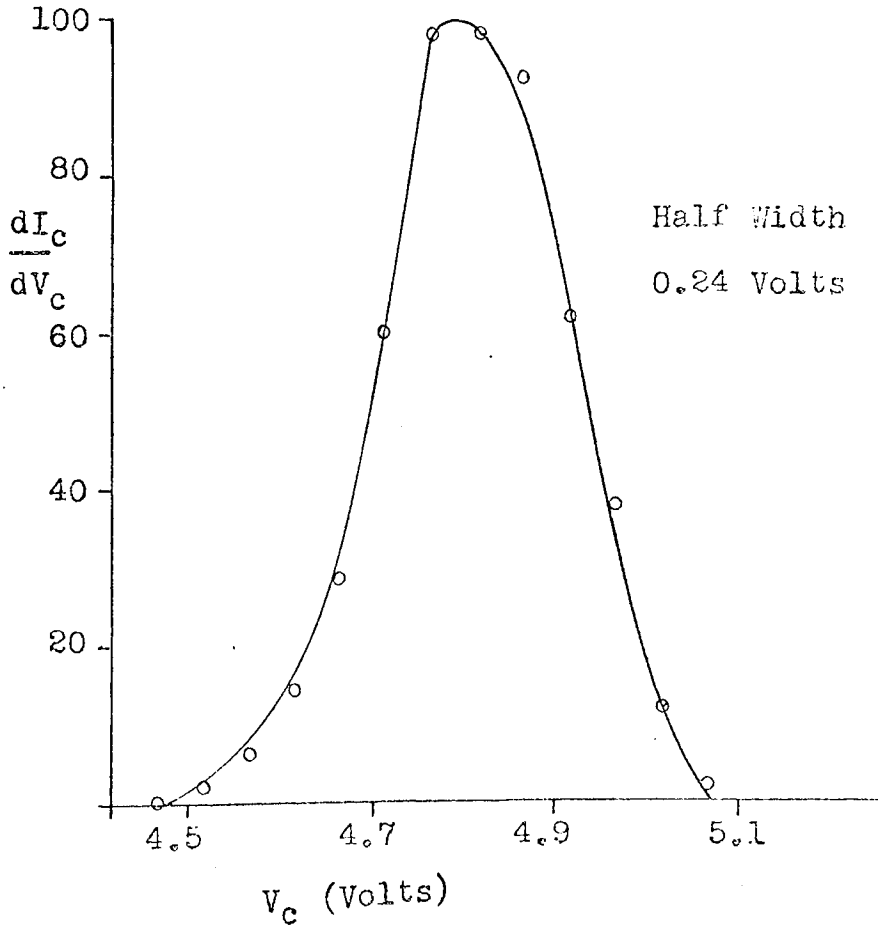

Fig. 3.6

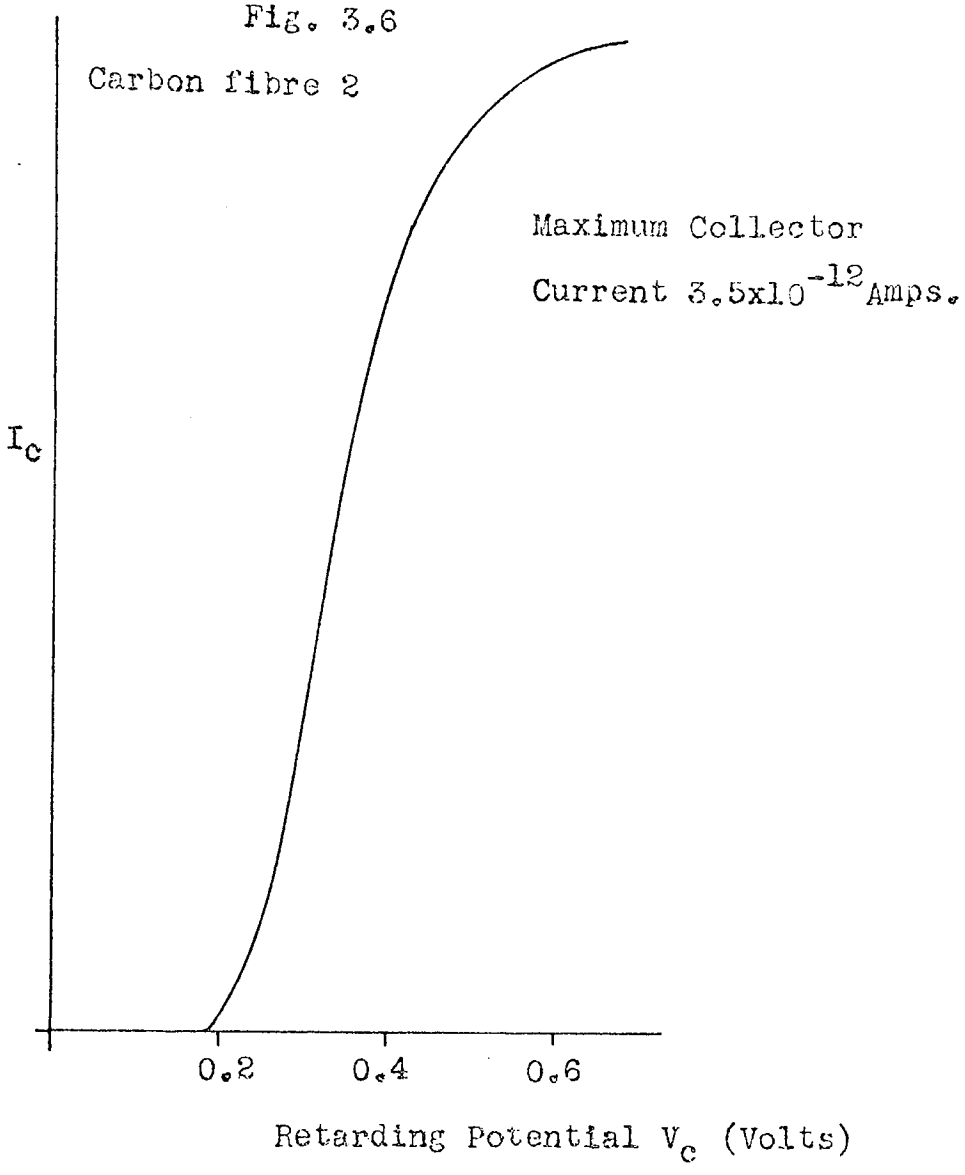
Carbon fibre 2
Maximum Collector
Current 3.5x10^{-12} Amps.
I_c
0.2
0.4
0.6
Retarding Potential V_c (Volts)

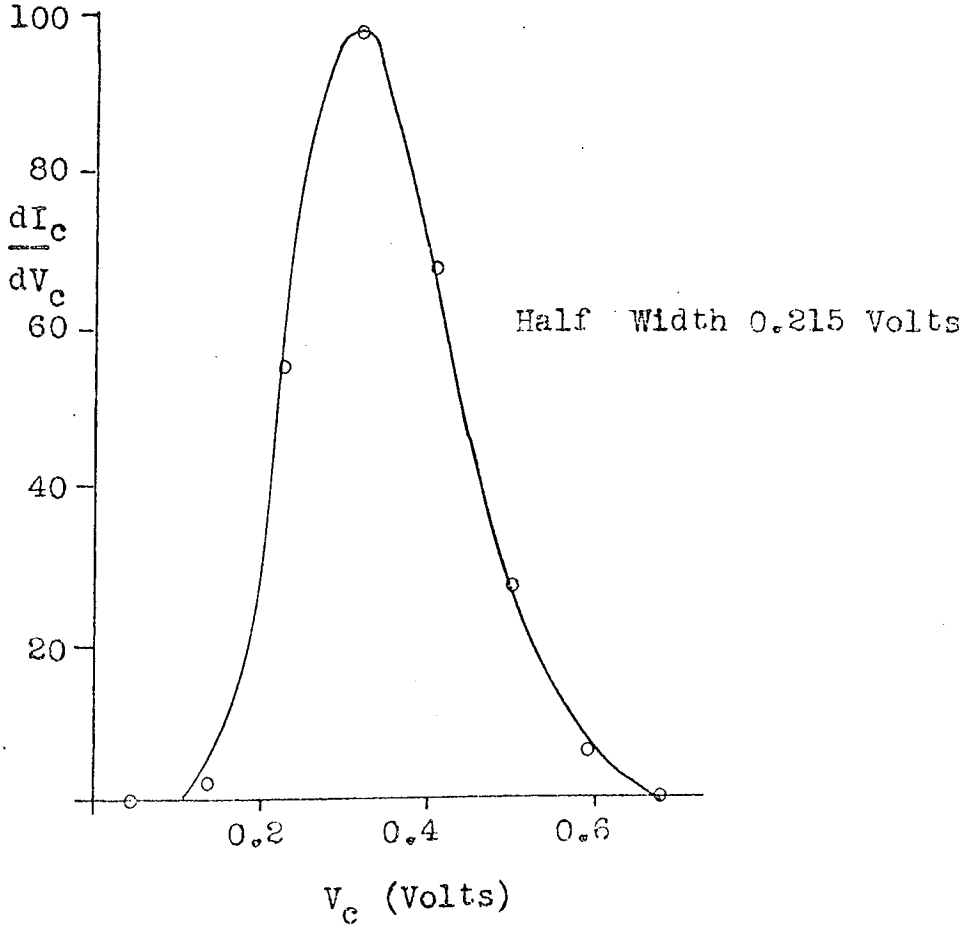
100
80
$\frac{dI_c}{dV_c}$
60
40
20
Half Width 0.215 Volts
0.2
0.4
0.6
V_c (Volts)

applied voltage will produce an increase in strain on the tip, this could cause movement of the fibrils pulling one out slightly into a region of higher field, hence causing an increase in local current. This is only a small change in a fraction of the total current and hence the effect is insignificant when emission from the whole fibre is considered.

3.6 DISCUSSION

The emission patterns of randomly placed spots resemble those reported by other workers (68), (71) for untreated tips and the patterns produced by Okuyama (73) in an attempt to image potassium chloride by field emission microscopy. The spots presumably correspond to emission from the ends of fibrils protruding from the emitter surface. Unfortunately, the history of the fibres used in this work is unknown and so the exact nature of the fibre structure is not known.

The energy distributions shown in the previous section are derived by differentiation of the collected current vs. retarding potential curves and no correction has been made for reflection effects (6), however Salmon (51) has shown that this does not affect the half-width of the distribution. The measured value of 0. 21 eV $\pm$ 0. 01 eV for the halfwidth compares very well with metallic emitters for use in electron guns. These distributions have been measured from part of a multi-spot emission pattern and not from the single spot type of emission reported by Lea (71), however, there is no reason to suppose that these would have a different halfwidth although the temperature to which the tips have been heated would be sufficient to produce a structural change in the fibre.

The reasons why carbon fibres emit so well in poor vacuum are probably two-fold. At low fields, low emission currents, the sputtering rate is probably low, contamination effects nowhere near as great as for metals as shown by Lea (71), and the strain produced by the field is not sufficient to produce movement of the fibrils within the fibre. As the field is increased the energy of the sputtering ions increases causing more damage and possibly penetrating the fibre down the voids between fibrils. The increased field could induce movement of the fibrils. This mechanism could continue to produce a supply of fibrils to the surface (each fibril is sufficiently small to produce field emission without being polished) whilst other fibrils are sputtered off thus maintaining the mean level of the emission current. This is consistent with the random spotty emission pattern where the main spots change in position over periods of hours.

The mechanism producing stable field emission in poor vacuua for carbon fibres is somewhat analagous to that reported by Utsumi and Dalman (74) who have produced a regenerative field emission cathode from a flat germanium surface by vacuum breakdown. The breakdown initially produces micron-sized emitting sites on the flat surface and they are maintained during operation by a regenerative process. Emission currents of up to 0.5 mA in vacuua of 10^{-7} torr are reported to be stable over periods of several days.

3.7 CONCLUSIONS

Carbon fibre field emitters are potentially superior to metallic emitters as electron sources in all situations, and are ideally suited to applications where power requirements make thermal sources undesirable

and vacuum conditions prohibit the use of conventional field emitters. The effect of different ambient atmospheres on the emission characteristics of carbon fibres justifies further examination, as do the changes in endform during emission to resolve whether the changes are produced by the effect of the field, local heating between fibrils, or sputtering.

CHAPTER 4

EXPERIMENTAL TECHNIQUES

4.1 RETARDING POTENTIAL MEASUREMENTS

Until the recent development of electrostatic deflection analysers, the major technique for measuring energy distributions of field emitted electrons has been the retarding potential analyser. The principle of operation of this system is shown schematically in Fig. 4.1 for a metallic emitter. If the emitter and collector are electrically connected, in equilibrium, they will have a common Fermi level. Electrons leaving the emitter from the Fermi level will be accelerated to the transparent anode and then decelerated towards the collector but will not quite reach it and return to the anode. By applying a positive voltage V to the collector, with respect to the emitter, the barrier at the collector, as seen by the electrons, will be reduced until, when $V = \phi_c$, the electrons, from the Fermi level in the emitter will be collected. If the retarding potential, V, is swept over a range in the region of ϕ_c the collected current will be the integral of the energy distribution of the emitted electrons. By differentiation of the collected current the energy distribution can be obtained Fig. 4.1c.

4.2 CRITIQUE OF SALMON'S ANALYSER

The work presented in Ch. 3 on carbon fibres and some preliminary investigations on lead telluride were carried out in a retarding potential analyser, similar to that of Young and Muller (6), designed and built by Salmon (51) but with slight modification to the measuring circuit Fig. 4.2. The instrument, although intrinsically of high resolution, needed considerable alignment with each specimen to

Fig. 4.1

The principle of retarding analysers.

(a) In equilibrium

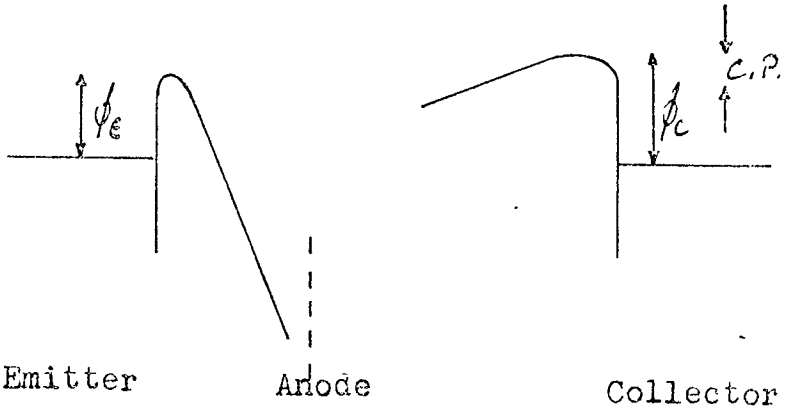

(b) Application of retarding potential

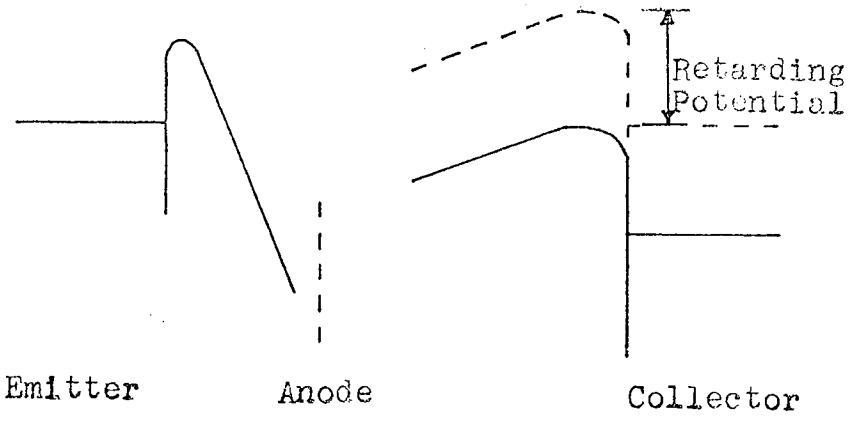

(c) Interpretation

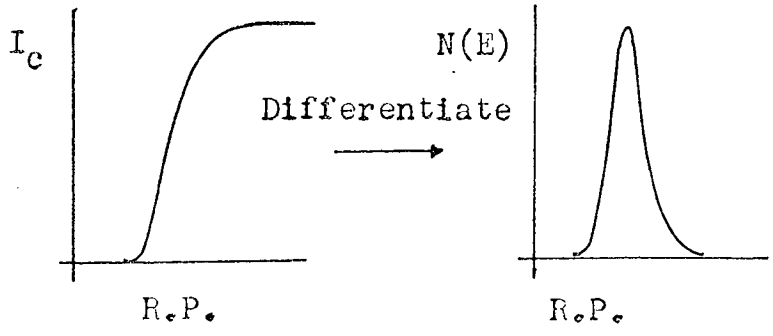

Fig. 4.2

The measuring circuit used with Salmon's analyser.

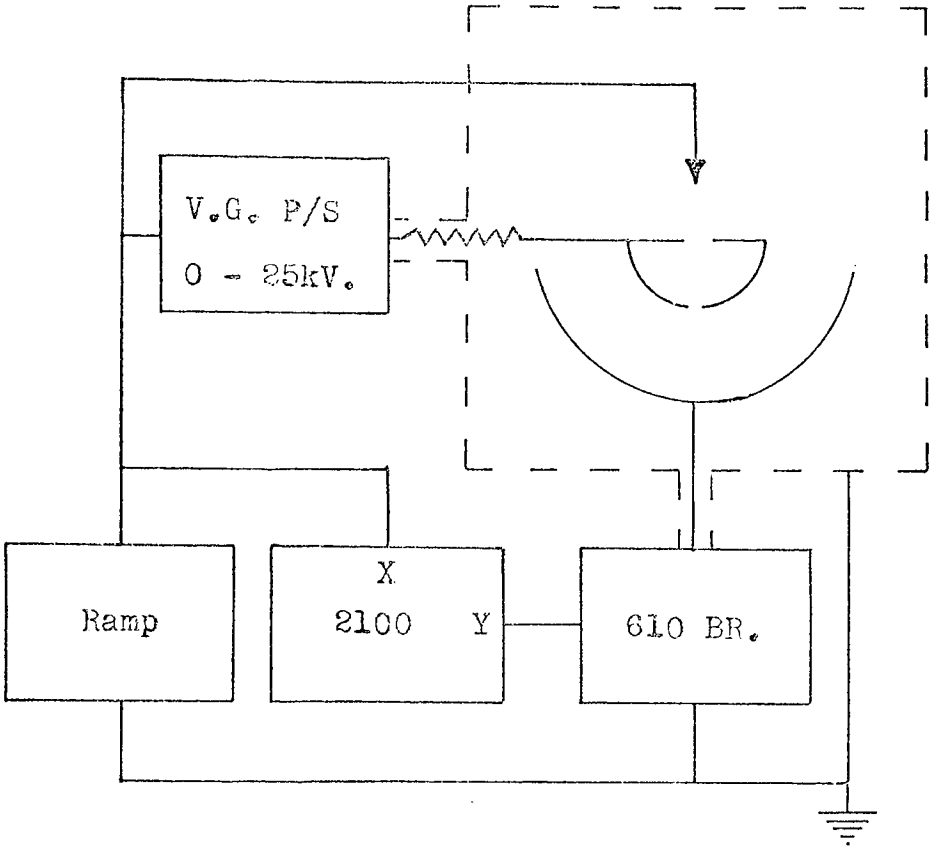

produce accurate results and it was all too easy to get energy distributions that were anomolously wide. For the resolution to be at its best the emitter had to be positioned at a point within a millimeter or so of the emitter axis and 33± 1 mm. from the fluorescent screen. To align the emitter with such accuracy was tedious and relied upon a part of the emission pattern covering the probe hole.

The analyser was equipped with a tip wheel mechanism which allowed observation of up to six emitters without letting the system up to air. Although this ingenious mechanism proved useful it did introduce problems. Because six emitters were present at once the five unwanted emitters had to be screened from the field, this was achieved by allowing the emitter under observation to protrude through a plate at the same potential as the emitters. This method successfully screened the other tips but also reduced the field at the emitter so unnecessarily high voltages had to be applied. The tip wheel mechanism was made entirely of metal and consequently was electrically connected to the vacuum system and pumps, so, to apply the retarding potential the whole vacuum system had to be floated to emitter potential. As all the emitters were mounted on the tip wheel it was not possible to heat the specimens.

The vacuum vessel was mainly a five litre glass flask which was joined to the specimen manipulator stage by a large glass-to-metal seal. This seal had outlived its guaranteed shelf life before this work was started. The presence of this seal meant that during bakeout the system had to be heated slowly and not above 200^{o}c, usually the bakeout cycle took several days.

The vacuum system was capable of producing pressures in the low 10^{-10} torr range but with the vacuum vessel and pipework used its capability was severely limited, the pressure in the chamber hardly bettering 1×10^{-9} torr. This was due in part to the high surface to volume ratio of the analyser and partly to the reduced pumping speed resulting from the tortuous pipework connecting the chamber to the pumps. The phosphor screen was a source of gas and had to be outgassed for some hours by electron bombardment before no pressure rise was generated by the emission.

In the course of the preliminary work on lead telluride electrical breakdown occurred many times within the vacuum system between the high voltage feedthrough and the collector and sometimes the tip wheel assembly. The collector structure had to be screened from electrical noise by enclosing the entire analyser in an earthed cage. For these reasons and those outlined above it was decided to abandon Salmon's analyser and replace it with a Van Oostrum type analyser (75) whilst maintaining the original pumping system.

4.3 THE ANALYSER

The analyser, based upon the design of Van Oostrum (75) modified slightly to make it compatible with a metal vacuum system is shown in Fig. 4.3 and schematically in Fig. 4.4. The drawings for the analyser were very kindly supplied by Mr. B. Singh of Salford University. The electrode structure consists of a phosphored anode, a lens electrode and a Faraday cage, the latter consisting of a shielding electrode containing a hemispherical collector. Electrons passing through the aperture in the anode are focused somewhere in the region of the centre

Fig. 4.3 The Analyser.

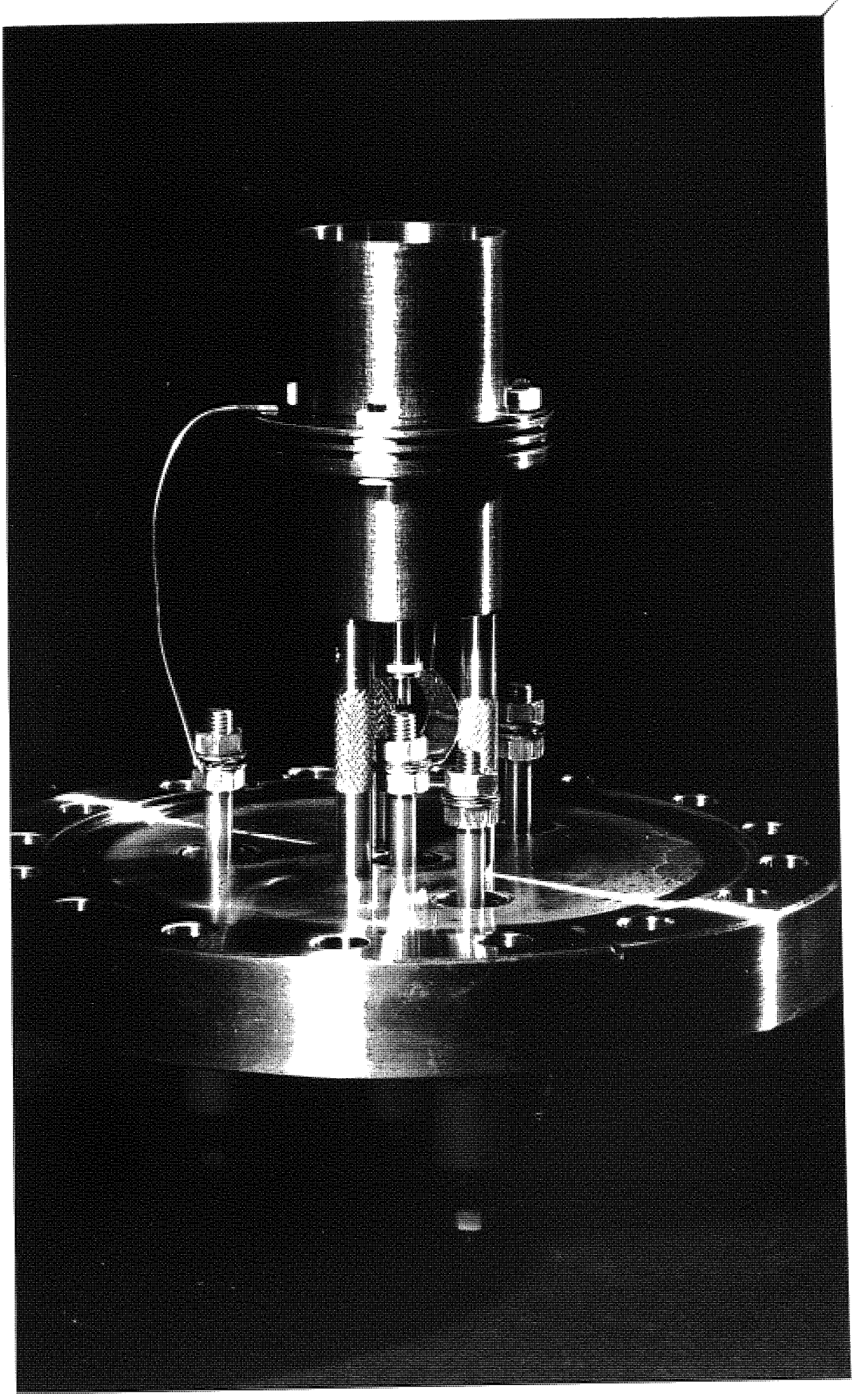

Fig. 4.4

Schematic diagram of the analyser.

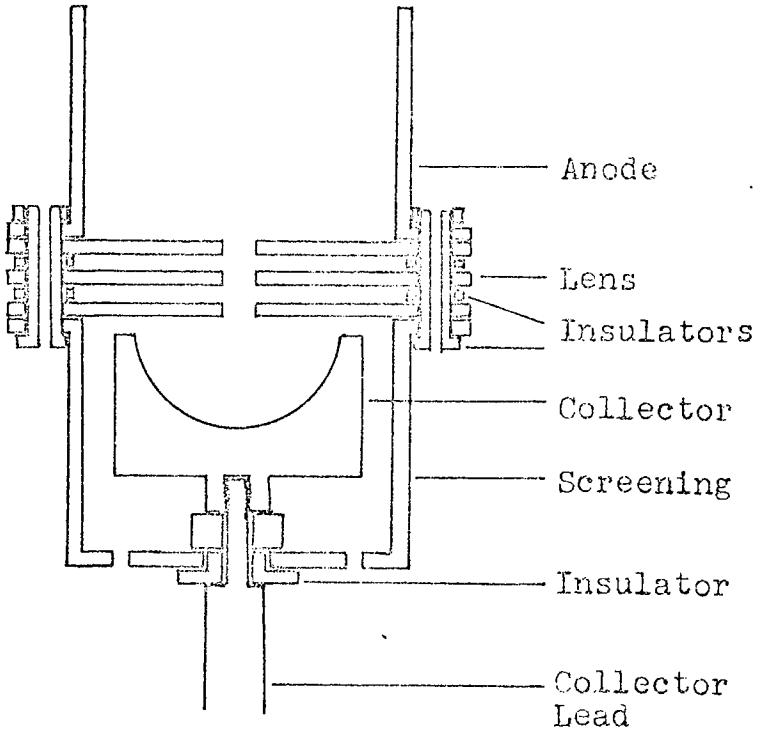

of the hemispherical collector. Electrons passing through this point will arrive perpendicularly at the collector surface. The focal length of the lens can be adjusted by varying the potential on the lens electrode.

The electrodes and support structure of the analyser were machined from high grade non-magnetic stainless steel and the insulators from

Prior to assembly all the metallic parts were cleaned by washing in hot detergent solution followed by a rinse in deionized water and then ultrasonic cleaning in iso-propyle alchohol for fifteen minutes and dried over the vapour. A thin phosphor screen was deposited on the anode plate from a suspension of blue fluorescent material in deionized water using potassium silicate as a binder. Electrical connections to the anode and lens were made by nickle wires spot welded to the electrodes. The Ceramtec insulators were fired to 1000^{o}C at a rate not exceeding 100^{o}C per hour and allowed to cool at the same rate. On removal from the furnace the insulators were put into the analyser assembly without further cleaning. The analyser assembly was mounted on a Vacuum Generators FC100 flange fitted with four electrical feedthroughs. The anular insulators between the anode, lens and collector used in the original design were replaced by washers of the same thickness to increase the pumping speed in the interior of the analyser, otherwise the pumping would have been through the lens apertures.

4.4 THE SPECIMEN MANIPULATOR

Originally it was intended to use the specimen manipulator outlined in Fig. 4.5. This consisted of a V.G. FC100 flange fitted with a bellows

Fig. 4.5

The original specimen stage

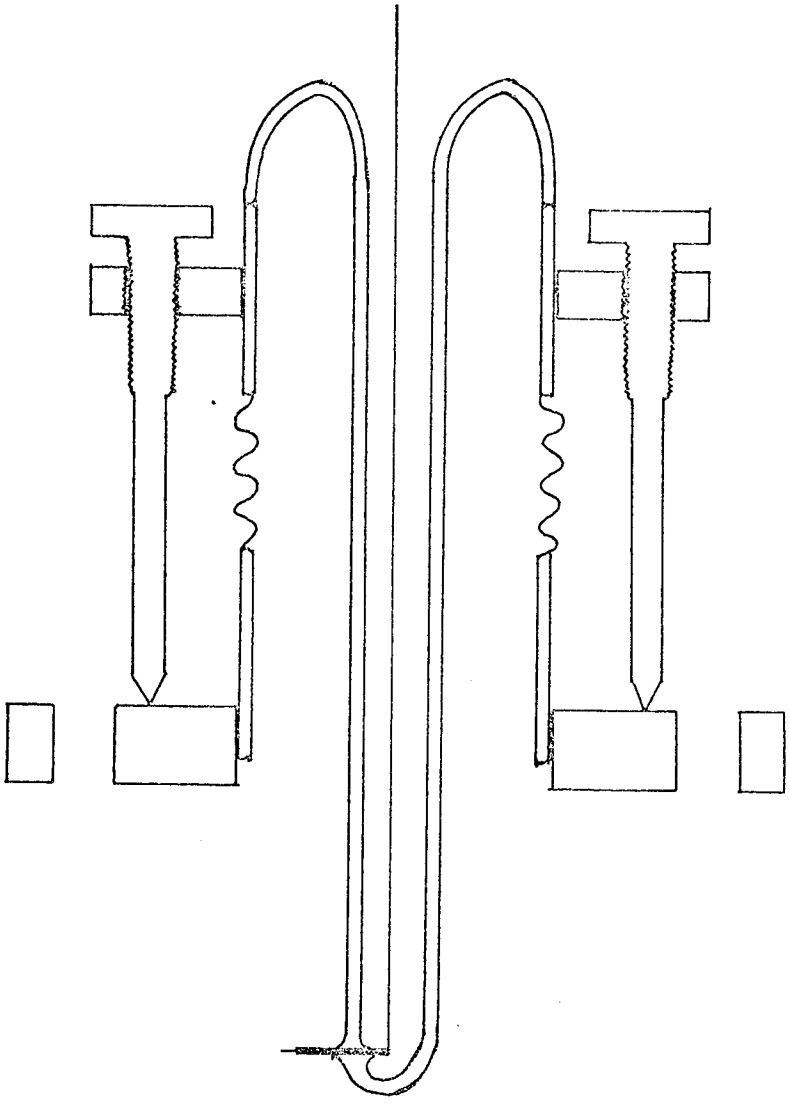

and pyrex adaptor with a re-entrant glass tube terminating in three tungsten leadthroughs pointing along the axis of the analyser system. Manipulation of the specimen was achieved by a yoke clamped around the metal above the bellows fitted with three threaded studs which acted against the face of the flange. This specimen stage was used for some of the initial work on tungsten but proved unsatisfactory for several reasons. Specimens had to be prepared on a jig and transferred to the holder after etching, this was a somewhat delicate task and could easily result in damage to the tip. The movement of the specimen was restricted by the diameter of the re-entrant tube passing through the 1½" diameter hole in the flange. Excessive movement of the tip could have fractured the glass with disasterous results. The movements produced by the three adjusting screws interacted and it was not possible to shift the tip in the plane normal to the analyser axis without introducing movement along the analyser axis (causing a change of field). The only advantage of this manipulator over the one which was to replace it was that the specimen could be cooled to some extent by filling the re-entrant tube with liquid nitrogen.

The majority of this work was carried out using the specimen manipulation system shown in Fig. 4.6 and Fig. 4.7. The manipulator consisted of eight electrical leadthroughs mounted around a central bellows assembly on an FC 100 flange, the bellows terminating in an FC 38 flange. Vertical movement was achieved by a large brass nut, which was screwed around a threaded yoke clamped to the pipework above the bellows, acting on a table supported on two pivots above the top of the leadthroughs. A micrometer screw was fixed between an arm extending from the table and the flange face to provide horizontal movement of the

Fig. 4.6 The Specimen Stage.

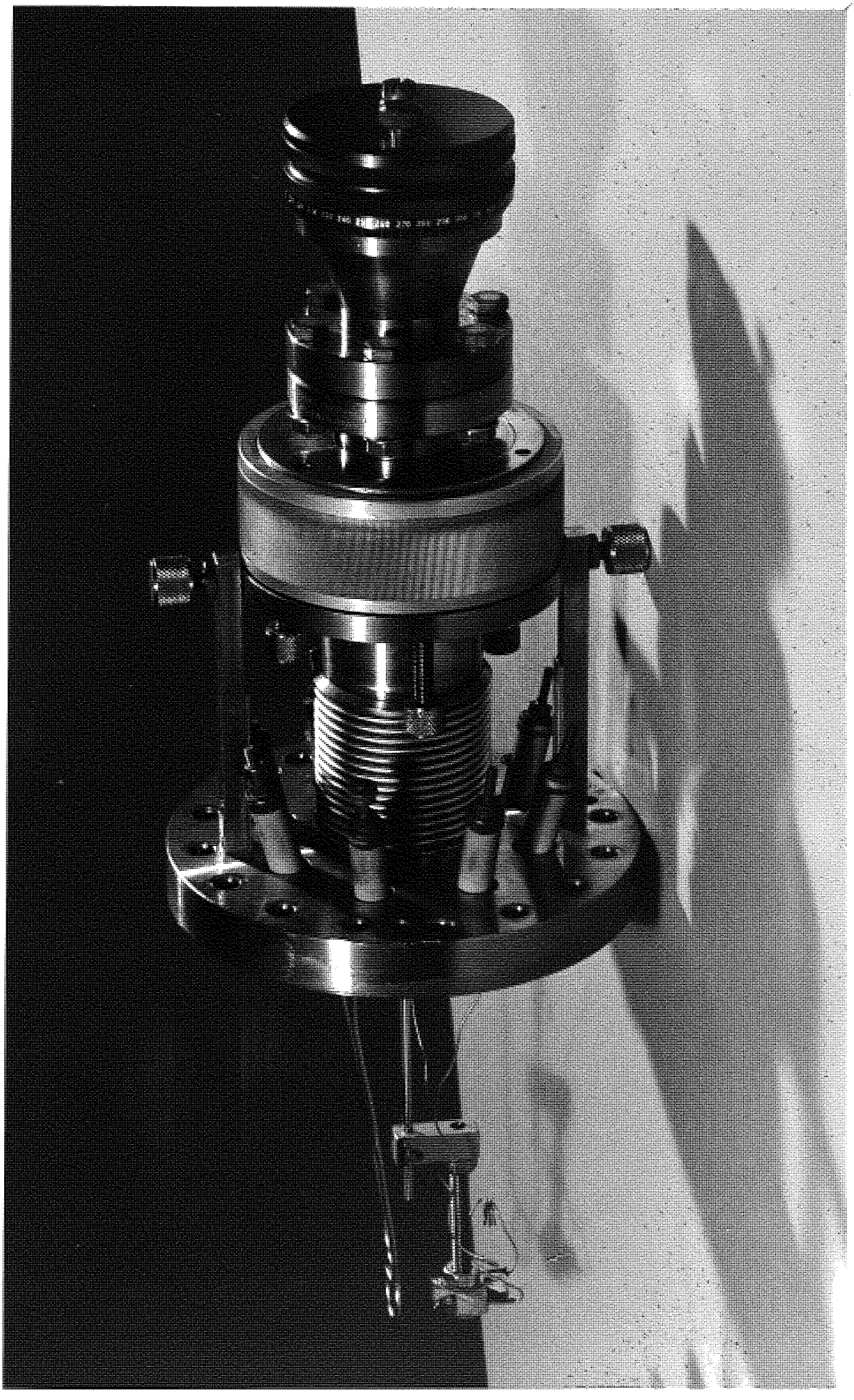

Fig. 4.7

The specimen stage.

(a) The specimen manipulator

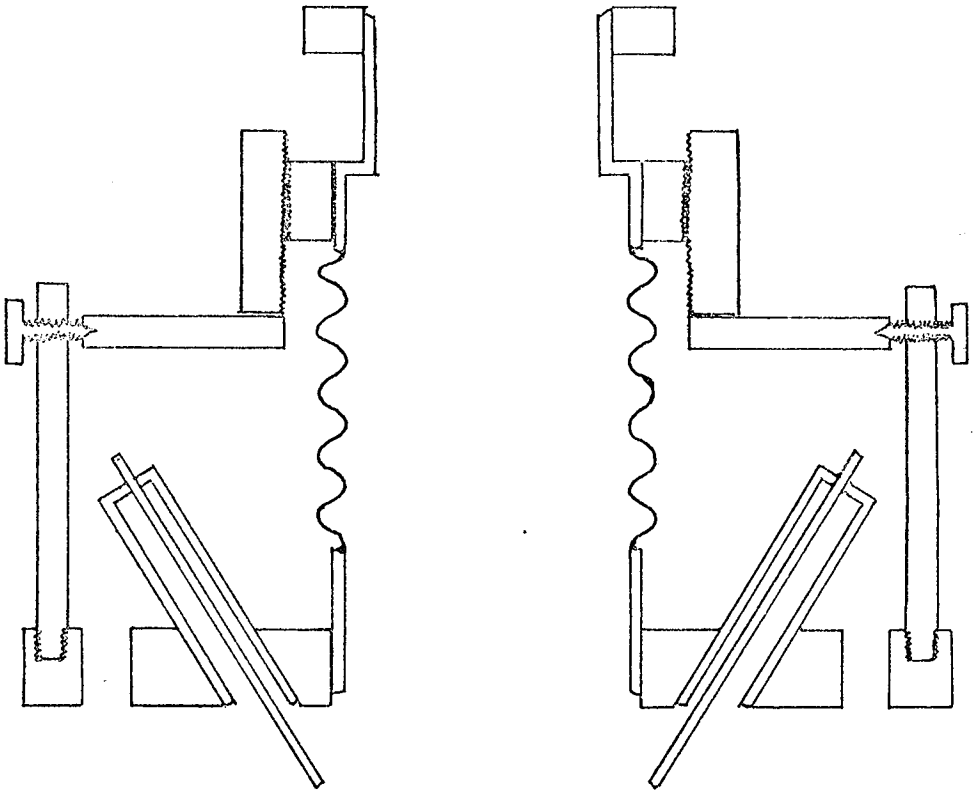

(b) The electrode assembly

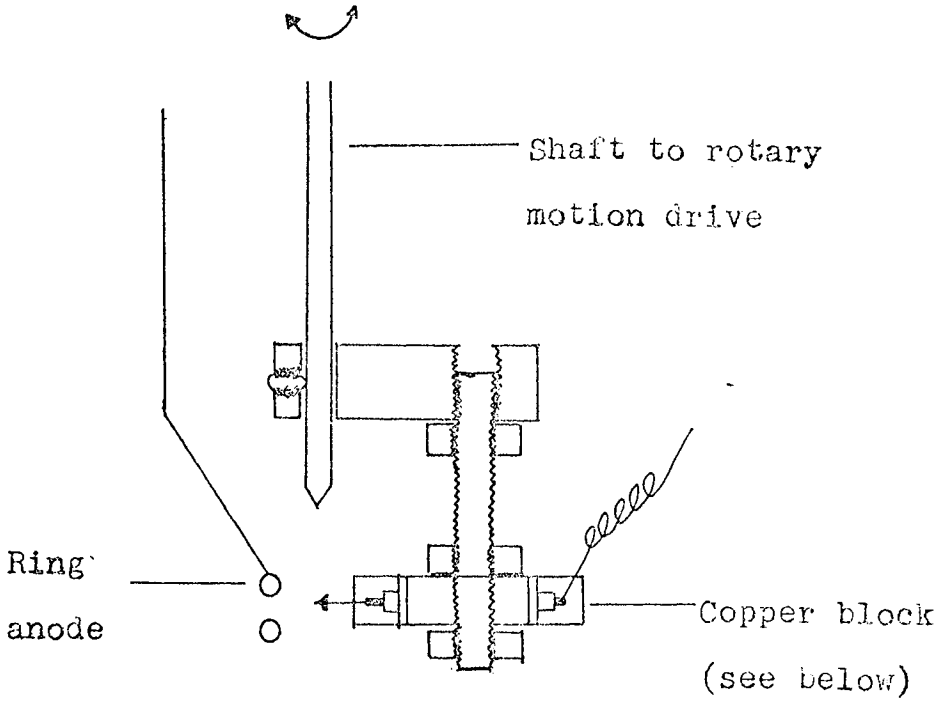

(c) The tip holder

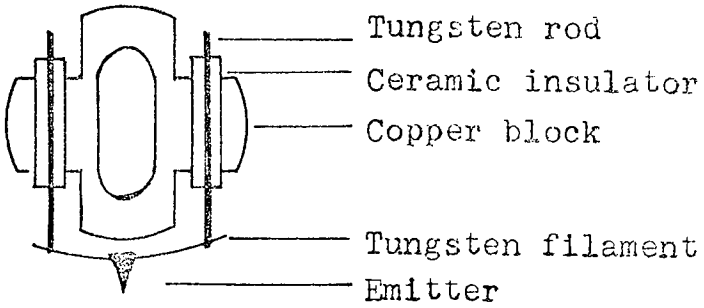

tip. Three threaded studs were mounted in the table to hold the manipulator in position when the large brass nut was removed for baking. A rotary motion drive was attached to the FC 38 flange at the top of the bellows assembly. A cranked assembly, Fig. 4.7 b, was attached to the bottom of the rotary drive, terminating in an O.F.H.C. copper block Fig. 4.7 c which was demountable. In fact two such blocks were made so that one could be in use in the system whilst a tip was mounted on the other one, thus considerably reducing the turn around time of the vacuum system. By careful adjustment of the manipulator, when mounting the tip, the specimen could be set with its tip on the axis of rotation of the rotary drive and on the axis of the analyser before insertion into the vacuum system. This arrangement allowed for heating the tip but not temperature measurement or cooling. Tungsten results were obtained at reasonable voltages, less than five kilovolts, from this configuration but for the semiconductor work a ring anode was included about 1 cm. in front of the tip in order to produce sufficient field at the same voltages.

4.5 THE VACUUM SYSTEM

The pumping system employed was that built by Salmon (51) which consisted of an Edwards ED50 rotary pump, a nitrogen cooled foreline trap and an Edwards E01 backing an Edwards E02 diffusion pump with a cherron baffle and nitrogen trap, this was followed by a 2½" bakeable valve from which point Salmon's analyser was removed. The vacuum chamber which replaced it was a 6" long elbow in 4"pipe terminating in FC100 flanges. Fitted to the elbow were an FC38 flange for an ion gauge and two FC64 flanges, one for a window and one for the pumping

line. The system is shown in Fig. 4.8. The port on which the ion gauge was fitted also contained a window to allow observation of the tip. A base pressure of 2×10^{-10} torr was readily attainable, after an overnight bake at 250°C, within twenty-four hours of letting the system up to air.

4.6 THE MEASURING CIRCUIT

The measuring circuit is shown schematically in Fig. 4.9. The high voltage was supplied by a Brandenburg alpha series 5kV supply via a resistor chain with a tapping for the lens element, except in the field evaporation mode when sometimes the voltage was applied directly to the ring anode from a Brandenburg 800 30kV supply. The collected current was measured by a Keithley 610 BR electrometer used in the fast mode. The three volt analogue output of the electrometer was used to drive the Y deflection of a Bryans 2100 X Y recorder whilst the X deflection was provided by a ramp generator which produced the retarding potential. The total current could be measured by a V.G. log. picoameter which floated on top of the retarding potential, however due to the vulnerable position of the picoameter, in event of electrical breakdown and the calibration of the instrument when supplied, it spent more time out of the circuit than in.

4.6 a The Potential Divider

Originally it was intended to use electrostatic deflector plates to sweep the emission pattern across the screen. This idea was not followed up as use of the rotary motion drive accomplished the same result (in one direction), however a resistor chain had been built which could

Fig. 4.8 General View Of The Analyser.

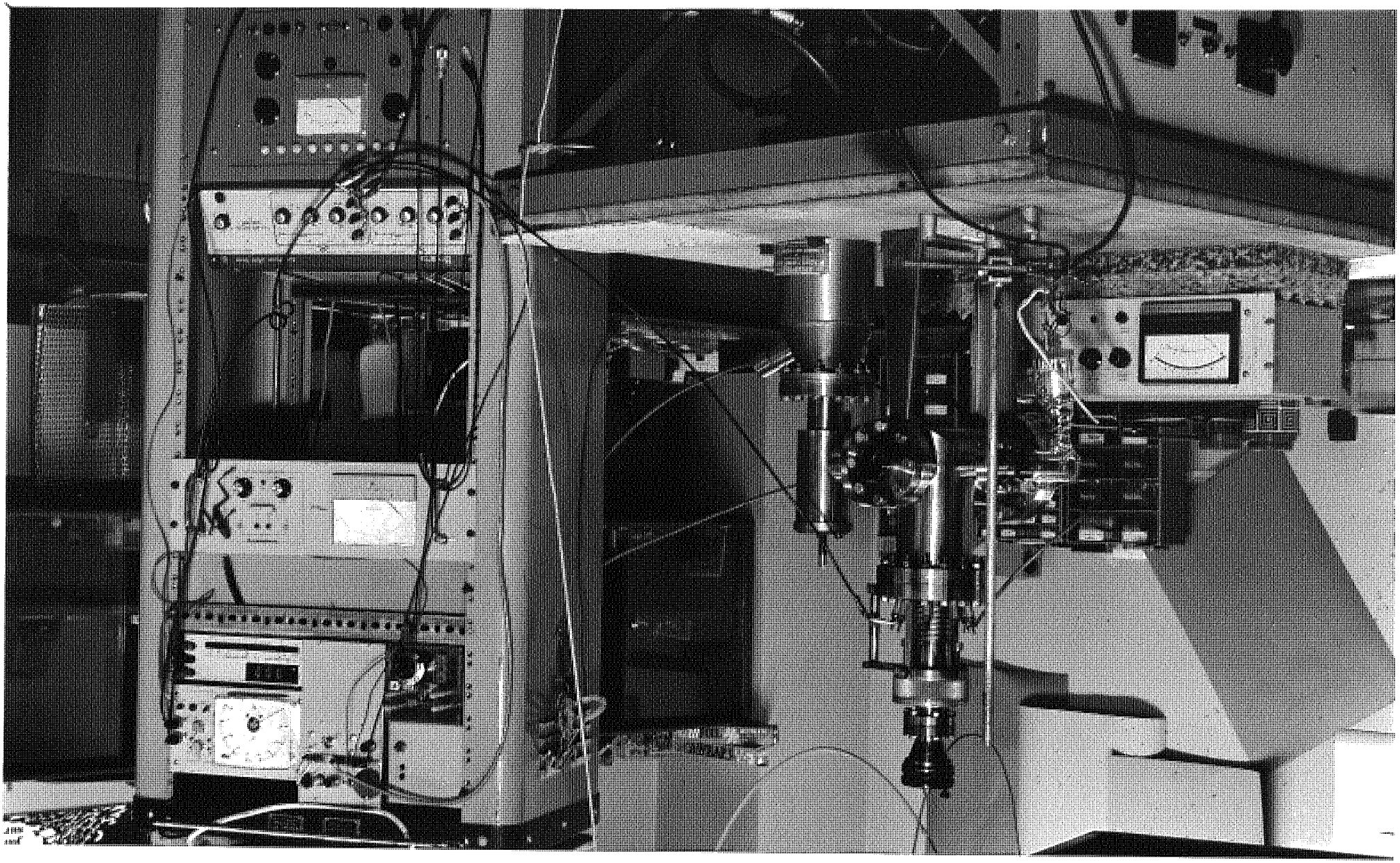

Fig. 4.9

The measuring circuit.

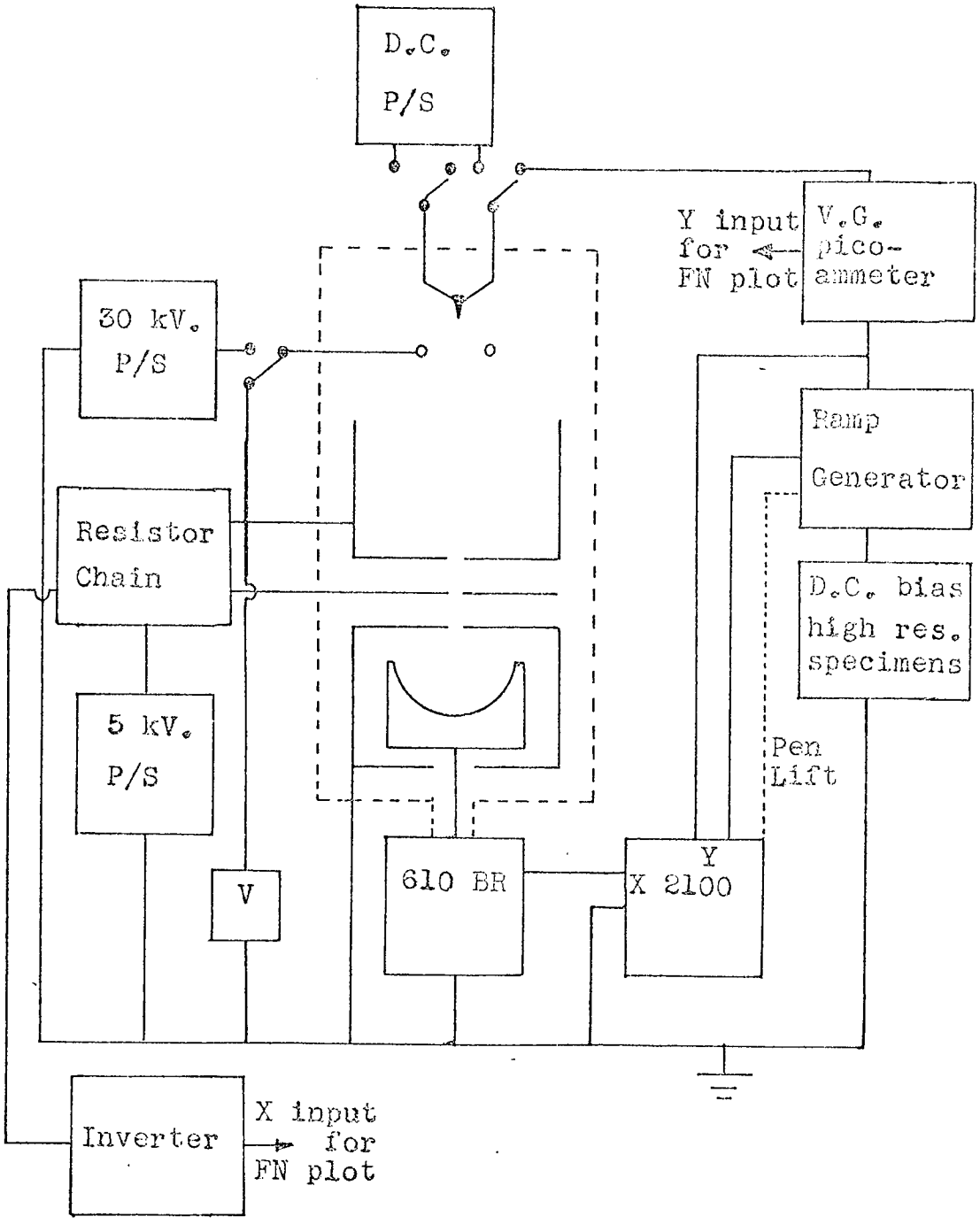

have supplied deflector plate voltages as well as the lens voltages. The resistor chain is shown in Fig. 4.10. Van Oostrum has shown (75) that for this type of analyser the resolution is at its highest when the ratio of the lens voltage to the anode voltage is 0.003 and that no reflection of electrons occurs for values below 0.01, consequently the resistorchain was designed to deliver a lens voltage of between 0.01 of the anode voltage and 0.0 volts. Another tapping was made to the low end of the resistor chain to supply a voltage to drive the inverter circuit which will be discussed later.

4.6 b The Ramp Generator

Two ramp generators were built, one a slow one-shot device and the other a fast repeating ramp, it was hoped to use the latter in conjunction with a differentiating circuit to provide an output on an oscilloscope. Unfortunately, the time constant of the electrometer was too great to be used with the fast ramp, also, as the response of the differentiating circuit was frequency dependent it worked much better at differentiating the noise than it did the relatively slowly varying collected current. The slow ramp generator shown in Fig. 4.11 was used for supplying the retarding potential and differentiation carried out manually.

The information contained in the retarding potential measurement occurs within a small voltage range of the collector work-function. If the retarding potential was applied to the pen recorder with respect to earth, most of the scan would be taken up overcoming the collector work-function, consequently the ramp generator was designed to run from one voltage V_1, below the onset, to another V_2 above saturation,

Fig. 4.10

The resistor chain.

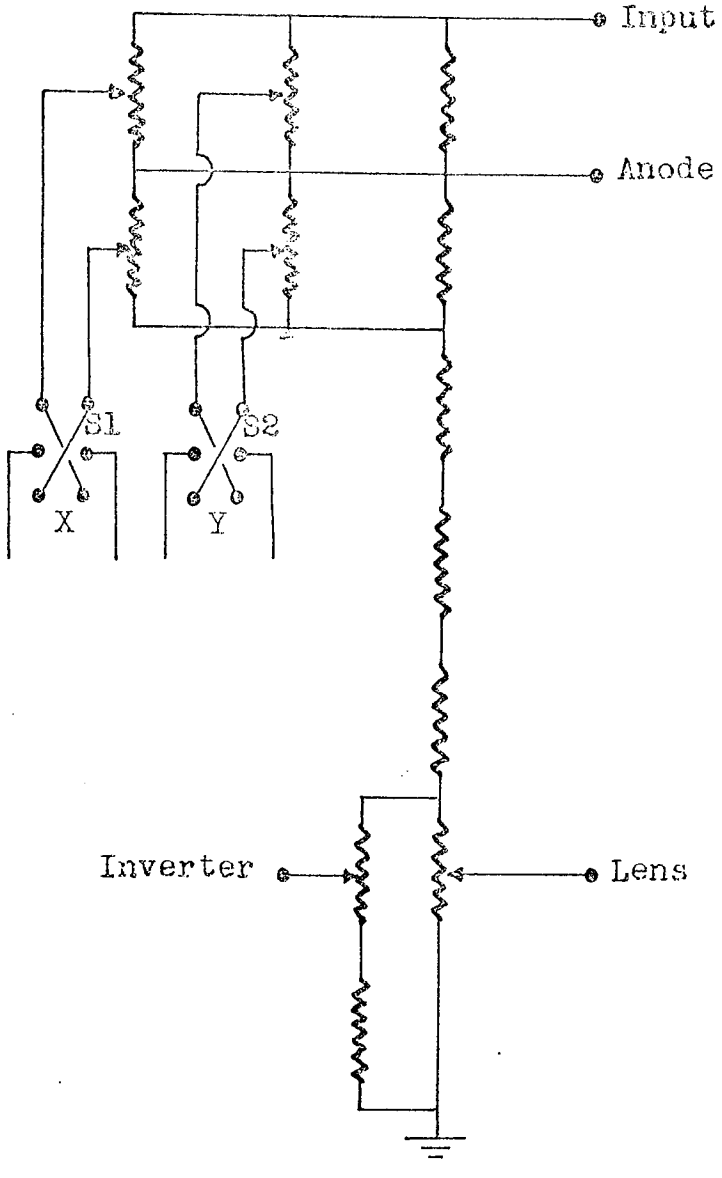

Fig. 4.11

The ramp generator.

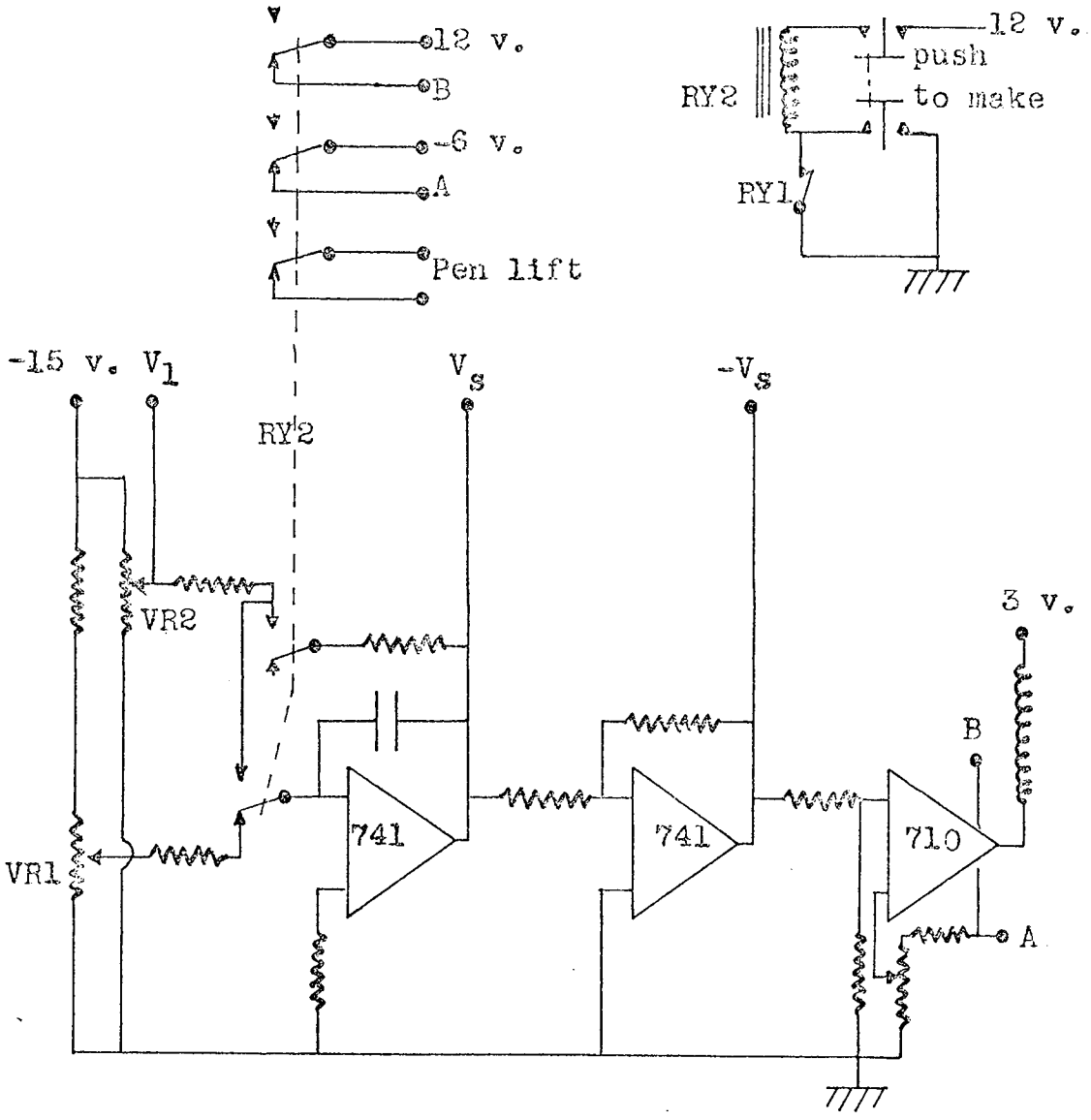

VR1 rate

VR2 set V_1

VR3 set V_2

the difference in the voltages used to drive the pen recorder. This allowed a typical sensitivity of 100 mV/cm for the pen recorder.

The ramp generator uses two operational amplifiers and a voltage comparator. When the ramp generator is switched on the first op.amp. operates as a unity gain inverting amplifier, this is fed with a voltage $-V_1$ set by the variable resistor VR2. This voltage is used as a reference for the pen recorder and is the initial value of the ramp. The output from the first op.amp. is $+V_1$ and this is inverted again by the second op.amp. to give an output of $-V_1$. The voltage comparator remains switched off. On pressing the ramp button S1 the first op.amp. is switched to integration mode and the voltage comparator is turned on. The integrator is fed with a constant voltage from VR1, which determines the rate of the ramp, as the output of the integrator is

$$V_o = -\frac{1}{RC}\int_0^T V\,dt$$

this produces a positive going ramp which is inverted by the second op.amp. to produce a negative ramp. The voltage comparator compares the ramp voltage with a reference, set by VR3, until it reaches a voltage $-V_2$ at which point its output switches to +5 volts turning off the reed relay and the circuit reverts to its initial state. The circuit could be run from batteries but was normally driven by a regulated d.c. power supply.

4.6 c The Inverter Circuit

In order to facilitate the recording of volt-ampere characteristics for the semiconductor specimens the inverting circuit shown in Fig. 4.12 was built which produces an output inversely proportional to the applied

Fig. 4.12

The inverter circuit.

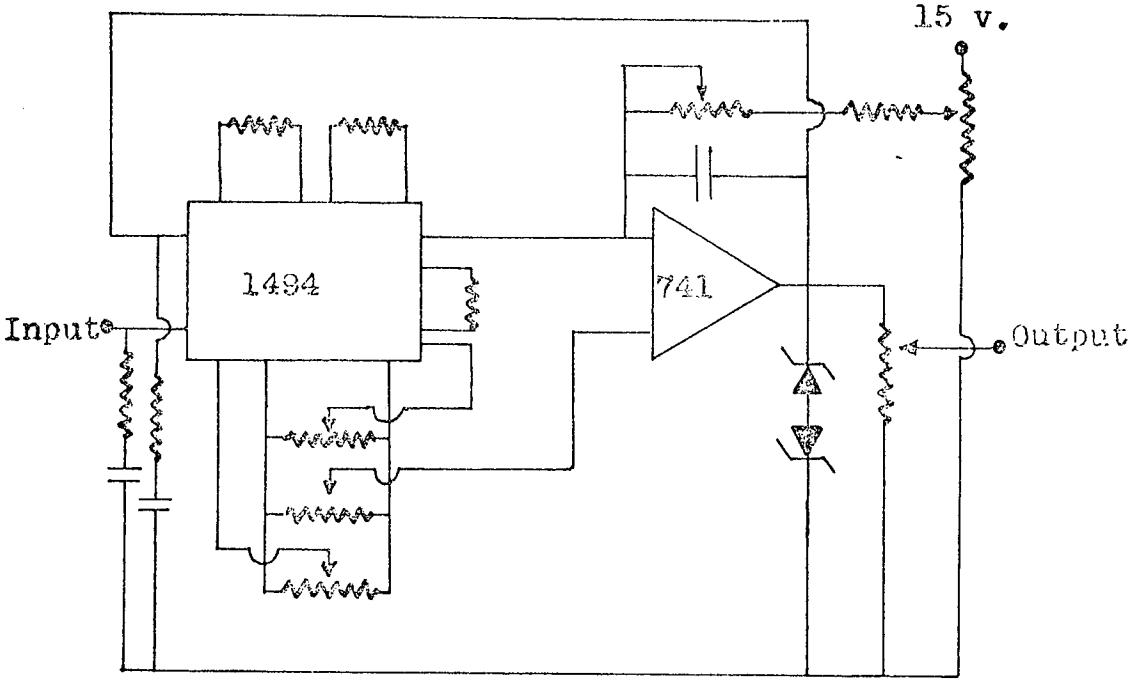

voltage. If this device is used to drive the X deflection of the pen recorder whilst the output from the log. picoameter is fed to the Y deflection total current Fowler-Nordheim plots can be recorded simply by turning up the applied voltage. The circuit consists of a four quadrant multiplier in the feedback loop of an operational amplifier, this type of circuit produces an output which is equal to one input voltage divided by another, thus by fixing the first input voltage and making the second proportional to the applied high voltage (from a tapping on the resistor chain) the output will be proportional to the inverse of the field emission voltage. The accuracy of the circuit is about 2% at high input voltages and decreases with reduction in input voltage, however this was not important as the method could not be used at low voltages because the induced current, caused by the increment in applied field was greater than the steady current. Consequently, the circuit was only used for total currents greater than 10^{-9} amps.

4.7 SAMPLE PREPARATION

Preparation of the tungsten emitters followed a procedure which was well established in this laboratory from commercially available wire which contains a (110) preferred orientation. The semiconductor specimens were supplied as cut from a single crystal boule . It was decided to use chemical methods to reduce the square section crystals to cylinders rather than mechanical methods, as it is well known that considerable damage can be produced in semiconductor crystals by grinding and that this damage can penetrate several microns.

4.7 a Tungsten Emitters

The tungsten specimens were electrolytically etched in a 1N

solution of sodium hydroxide using the sensing circuit described by Salmon (51) to switch off the current at the appropriate time. The 0.1 mm. wire used for the specimens was spot welded to a 0.2 mm. tungsten filament, which itself was spot welded across the tungsten rods of the specimen holder, prior to etching.

4.7 b Lead Telluride Emitters.

The lead telluride specimens were prepared from (111) oriented single crystals 1 mm. by 1 mm. by 15 mm. supplied by the Royal Radar Establishment. The emitters were made by electrolytic etching following the method due to Norr (76). An electrolyte of 20 gms. of potassium hydroxide dissolved in 45 ccs. of deionized water, 20 ccs. of glycerine and 20 cc. of methanol was used with a gold wire cathode at a current density of 0.2 Amp cm^{-2} at the crystal. The crystals were rotated in the electrolyte until a cylinder of about 0.5 mm. diameter was produced, the applied voltage being reduced as the diameter of the crystal reduced. The rotation was then stopped and the crystal diameter allowed to reduce to 0.1 mm. The crystals were then transferred to the specimen holder by attaching them to a loop in a 0.2 mm. tungsten filament with a drop of silver dag as this was known to produce an ohmic contact to lead telluride (77). Once the dag was set the final etch was performed in a drop of electrolyte suspended from a loop of gold wire. The etching process was observed through a travelling microscope. Initially, the crystal was allowed to pass through the drop of electrolyte until a neck was formed, the crystal was then raised until the neck was coincident with the upper meniscus. The etching was then monitored by observation of the etching current and when the current fell to zero the crystal was withdrawn and washed. It was found that a better tip was produced by

monitoring the cell current during the final etch rather than watching the end of the tip drop off. Tips produced in this way, although resolvable at 400 x magnification, produced emission at about 1 kV by use of the ring anode.

4.7 c Gallium Phosphide Emitters.

A (111) oriented gallium phosphide single crystal, supplied by the Royal Radar Establishment, was polished to a suitable emitter, unresolvable at 100 x magnification, in a mixture of 2 parts deionized water, 2 parts hydrochloric acid, 1 part nitric acid and 1 part sulphuric acid. The rate of removal of material in this mixture is extremely slow so the crystal, which was of similar dimensions to the lead telluride crystals, was left spinning in the etch for about twenty-four hours. When the diameter of the needle, thus produced, reached 250 microns the crystal was mounted on a tungsten filament in the same way as the lead telluride emitters. The crystal was then returned to the etch and allowed to etch through whilst observing the process with the aid of a travelling microscope. The crystal was then removed and washed in deionized water.

CHAPTER 5

PRESENTATION OF RESULTS

5.1 TUNGSTEN

Tungsten was chosen as a material with which to test the performance of the analyser as it is a simple task to produce reliable emitters and the emission characteristics are well known. From the tungsten results it should be possible to estimate the resolution of the analyser, if only by comparison with other work, and the work function of the collector, hence the position of the Fermi level in the emitter.

When the tip was mounted on the specimen holder it was set with its tip on the axis of rotation of the rotary motion drive and pointing along the axis of the analyser. After field evaporation a clean tungsten pattern was obtained almost in the centre of the screen with the emission from the (111) faces lying on the horizontal axis of the screen, consequently it was only necessary to rotate the emitter by a few degrees to get the emission over the probe hole. With the anode voltage fixed and the retarding potential set to its maximum value the collected current was measured as a function of the lens voltage. This function was only investigated over the range $V_L = 0.01\ V_A$ to $V_L = 0.00$ volts as it was expected that the highest resolution would occur within this range. As can be seen from Fig. 5.1 the change in collected current is not as great as that reported by Van Oostrum but it does go through a minimum value which should correspond to optimum resolution. The lens voltage, therefore, was set to the value corresponding to the minimum and left at that for the remainder of the experiment. This value was not regarded as critical, however, as Van Oostrum (75) only reports a 10% change of resolution over

the entire range of V_L allowed by the potential divider used.

The measured retarding potential vs collected current plots are shown in Fig. 5.2 together with the corresponding energy distributions. The energy distributions were obtained by finding the gradient of the experimental curves using the approximate relationship:

$$\left(\frac{dI_c}{dV_c}\right)_{V_c = V} = \frac{I_{c(V+h)} - I_{c(V-h)}}{2h}$$

The choice of the interval, h, is important as too large a value leads to a loss of resolution and too small a value leads to a large scatter in the values of dI_c/dV_c, in the limit producing results similar to those produced by the electronic differentiator mentioned in section 4.6 b. The total collected currents investigated were of the order of 10^{-12} amps. as the majority of the total emitted current came from the (100) faces and only a small fraction from the (111), and only a fraction of this could pass through the probe hole. Fig. 5.2a shows a comparison of the measured distribution with that of Young and Muller (6). From the measured distributions shown the width at half height of the energy distribution is 0.220 ± 0.010 eV. In addition, as the Fermi level should be 0.050 eV above the peak of the distribution (38), the work-function of the collector is 3.98 ± 0.05 eV.

The excellent agreement between the measured distribution and that of Young and Muller (6) shows that the resolution of the analyser is as good as theirs if not better. Van Oostram (75) has estimated, from measurements at cryogenic temperatures, the resolution of his analyser to be of the order of 0.010 eV, thus the resolution of the present analyser is probably not much worse than 0.01 eV.

Fig. 5.1

Plot of I_c against V_L/V_A to determine the optimum value of V_L.

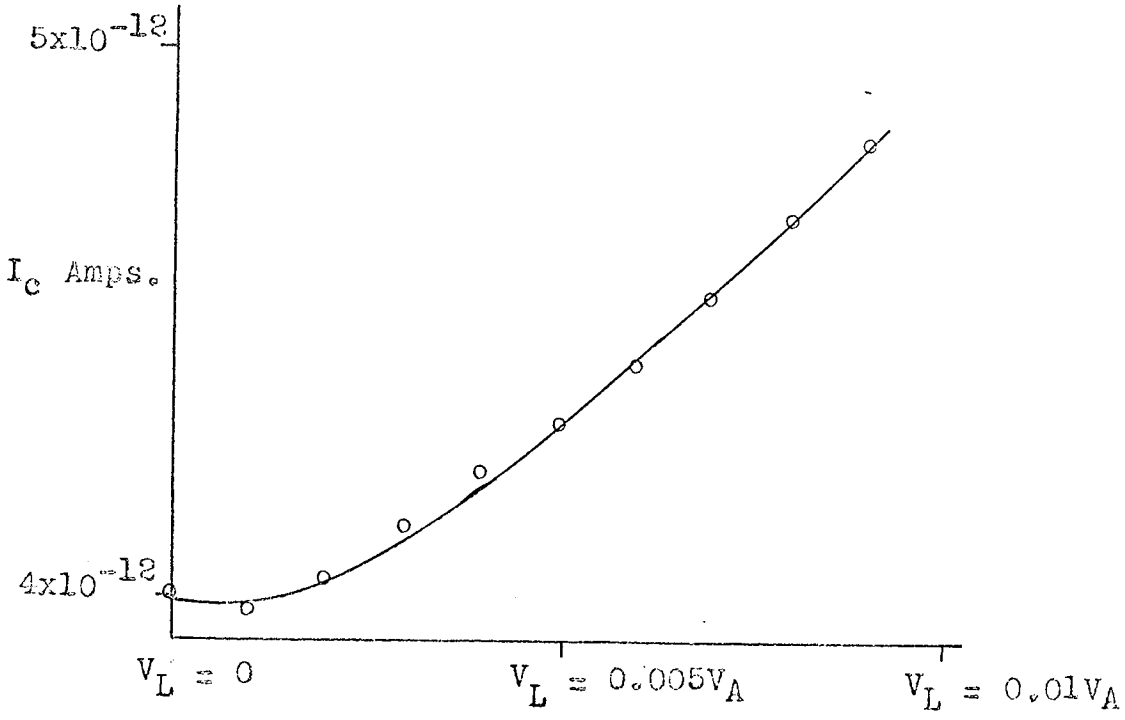

Fig. 5.2(a)

Tungsten

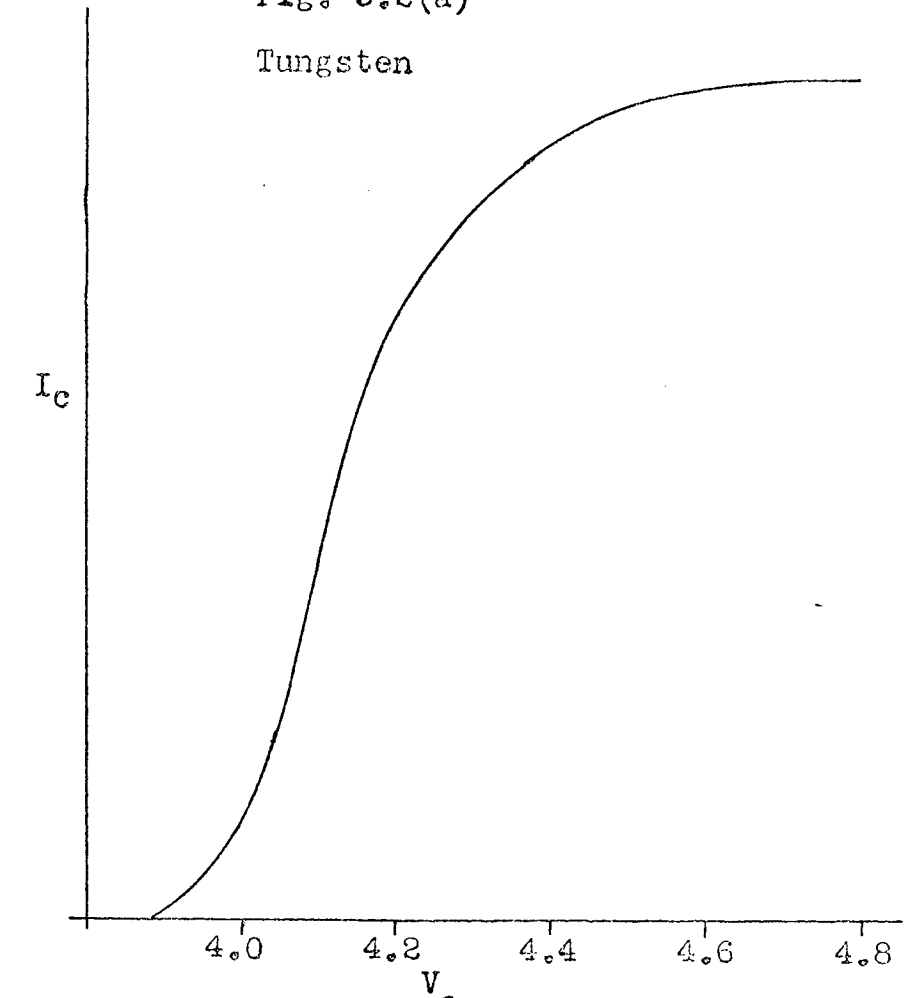

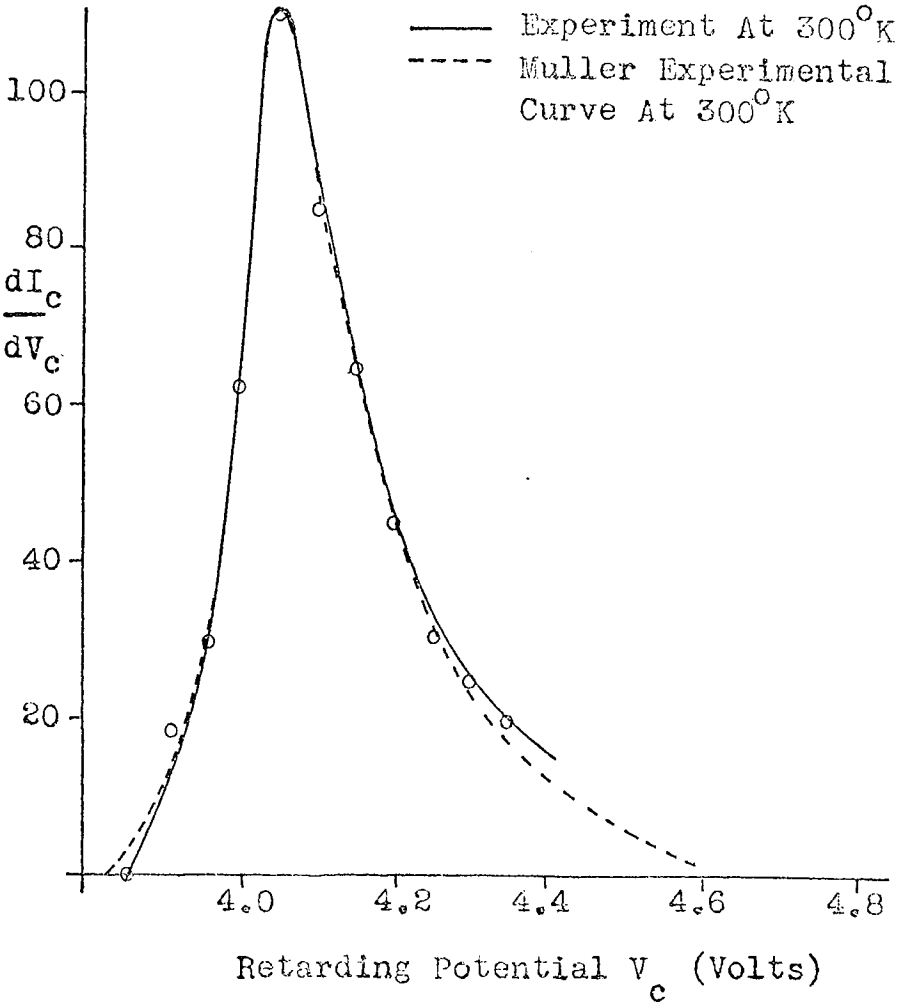

Fig. 5.2(b)

Tungsten

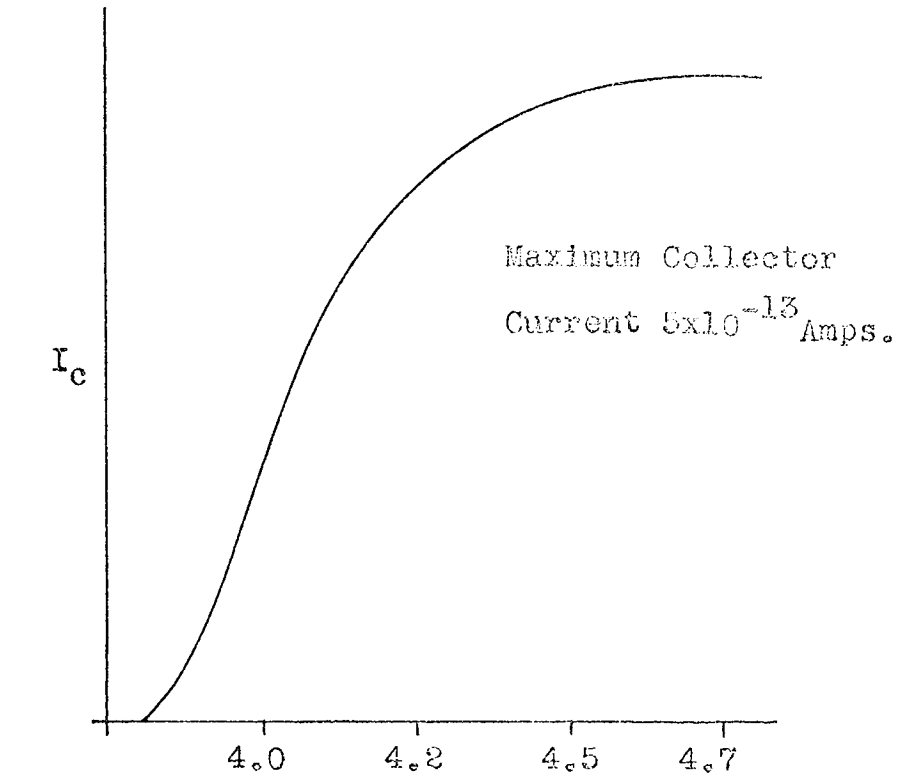

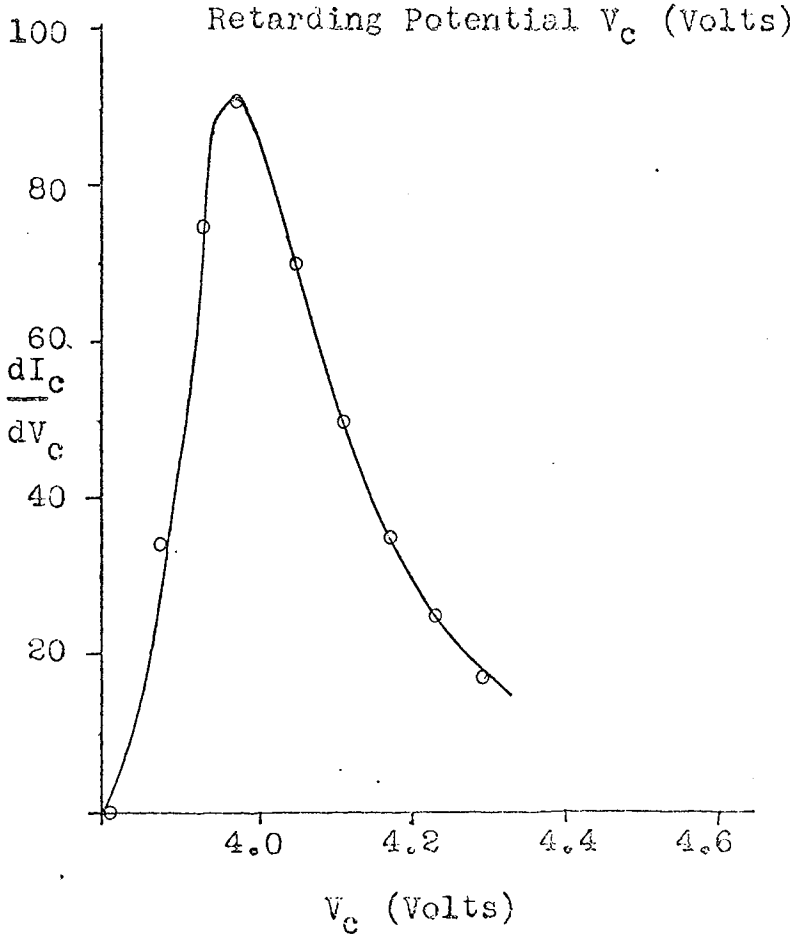

Fig. 5.2(c)

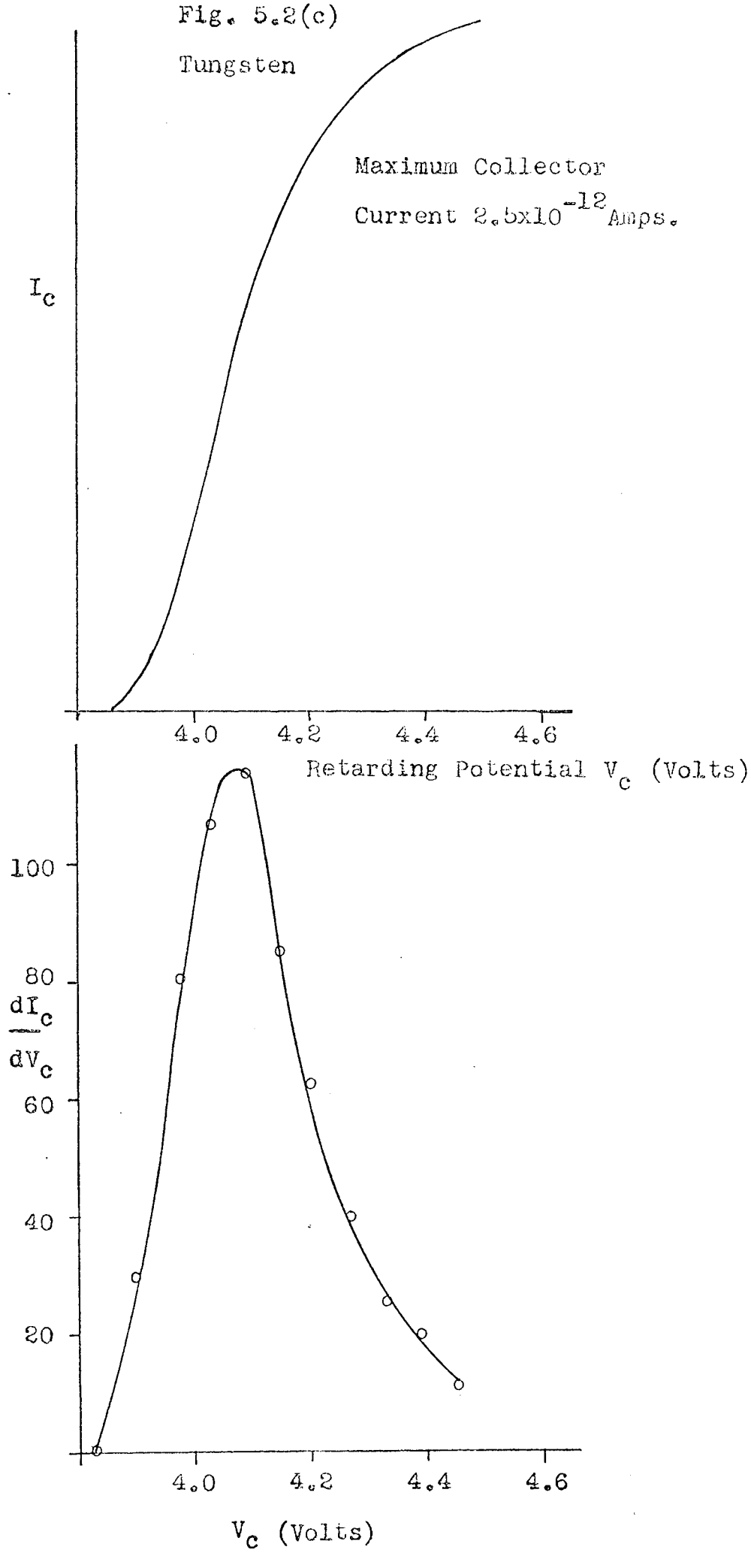
Tungsten
Maximum Collector
Current 2.5x10^{-12} Amps.
I_c
4.0
4.2
4.4
4.6
Retarding Potential V_c (Volts)
100
80
$\frac{dI_c}{dV_c}$
60
40
20
4.0
4.2
4.4
4.6
V_c (Volts)

No attempt was made to screen the analyser from magnetic fields, other than avoiding magnetic materials in constructing the system. The reason for this was two-fold : a) Van Oostram (75) used magnetic deflection to scan the emission pattern across the probe hole, with no detrimental effect to the resolution and b) the magnetic effects discussed by Salmon (51) would be reduced by a factor of ten simply by geometric considerations. The decision to ignore magnetic screening is justified by the good agreement between the measured distributions and those of other workers.

5.2 LEAD TELLURIDE

5.2 a THE MAIN RESULTS

The energy distributions shown in Fig. 5.3 were obtained from emitter 7 after thorough field evaporation at 10 k.v., the corresponding emission pattern was composed of three stable spots positioned at the points of an equilateral triangle which is of the correct symmetry for a (111) orientation. The most convenient spot was chosen for analysis as each spot should possess identical characteristics. Initially, with this emitter, application of the high voltage produced a flash at 1 kV followed by an emission pattern, at 4 kV, which consisted of a stable large triangular spot from which the distributions shown in Fig. 5.4 were recorded. The emission pattern must be associated with a clean surface as heating or field evaporation (up to 10 kV) produced no change. The distributions shown in Fig. 5.4 b and Fig. 5.4 c were taken consecutively with only a few minutes elapsing between the two with no change in the applied conditions, the change in the number of low energy electrons illustrated in this case was often observed after a change in applied voltage. Similar results were obtained with emitter

6, Fig. 5.5; initial application of the high voltage produced a flash at 2 kV followed by a stable pattern of three spots at the points of an equilateral triangle at 4 kV. Field evaporation or heating of the specimen produced no change in the pattern indicating the presence of a clean surface.

Emitter 5 behaved somewhat differently as no initial flash was observed and the pattern, at first turbulent, became stable and symmetrical after a few minutes of emission. The energy distributions, however, were found to lie up to several volts below the Fermi level and were considerably wider than the distributions from other emitters Fig. 5.6. Investigation showed that no charge in the distributions could be produced by shifting the tip by large amounts and so it was concluded that the odd behaviour of this emitter was not due to poor resolution arising from tip misalignment. The variation of the position and width of the distribution with total current is shown in Table 5.1. An attempt to clean the emitter was made by passing a current through the support filament whilst observing the emission pattern. Heating gently produced turbulence in the emission pattern and then a change. Energy distributions recorded at this stage, Fig. 5.7, resemble those in Fig. 5.6 in that the onset changes with total current. Further heating produced a very turbulent pattern which became suddenly bright and flashed leaving a single spot visible only when the applied voltage was increased to its maximum, energy distributions recorded from this spot are shown in Fig. 5.8. The behaviour of this emitter must be attributed to a poor contact or a grossly contaminated surface as the same crystal was used later, with a new endform etched on it and with more silver dag applied to the contact, as emitter 7.

Table 5.1

Fig. No.	$I_{c\ Max}$ (Amps.)	I_t (Amps.)	Onset (eV.)	Half-Width (eV.)
-	2×10^{-13}	8×10^{-11}	4.7	.400
5.6a	8×10^{-13}	5×10^{-10}	4.6	.400
-	3×10^{-12}	7×10^{-9}	5.1	.450
5.6b	6×10^{-12}	1×10^{-8}	5.4	.480
5.6c	3×10^{-11}	5×10^{-8}	6.1	.500
5.6d	5×10^{-11}	1×10^{-7}	6.4	.860

Fig. 5.9 shows a series of scans from emitter 4 at different applied voltages before any attempt had been made to clean the emitter. The emission pattern resembled that for emitter 5 before cleaning in that there was no initial flash and the turbulent pattern soon stabilized to a non-triangular form. The energy distributions show a slight shift with applied voltage but not as great as that found for emitter 5. Field evaporation, however, produced a distribution near the Fermi level at a current level which had previously shifted the distribution well below it Fig. 5.10.

The first lead telluride emitters mounted in the analyser failed to produce emission at voltages up to 5 kV and it was not until the ring anode was included that significant currents could be drawn. The first tip used with the ring anode, emitter 3, only gave maximum collected currents of less than 1×10^{-11} amps. as the anode was too far from the tip. Distributions recorded from this tip will not be presented except to note that a peak of about 0.4 eV. total width was observed after field evaporation.

Fig. 5.3(a)

PbTe Emitter 7

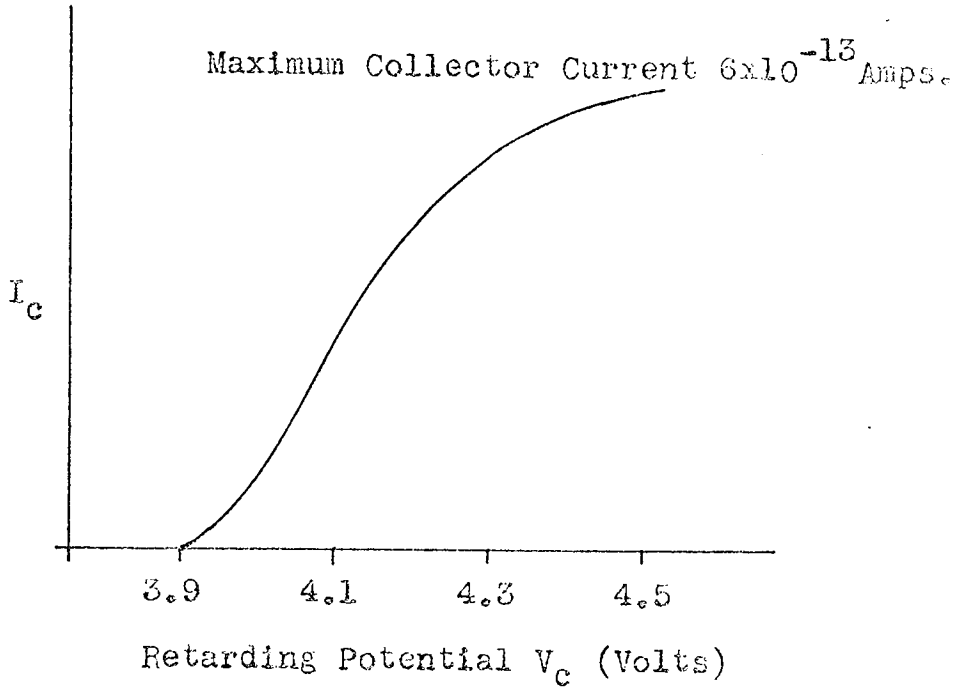

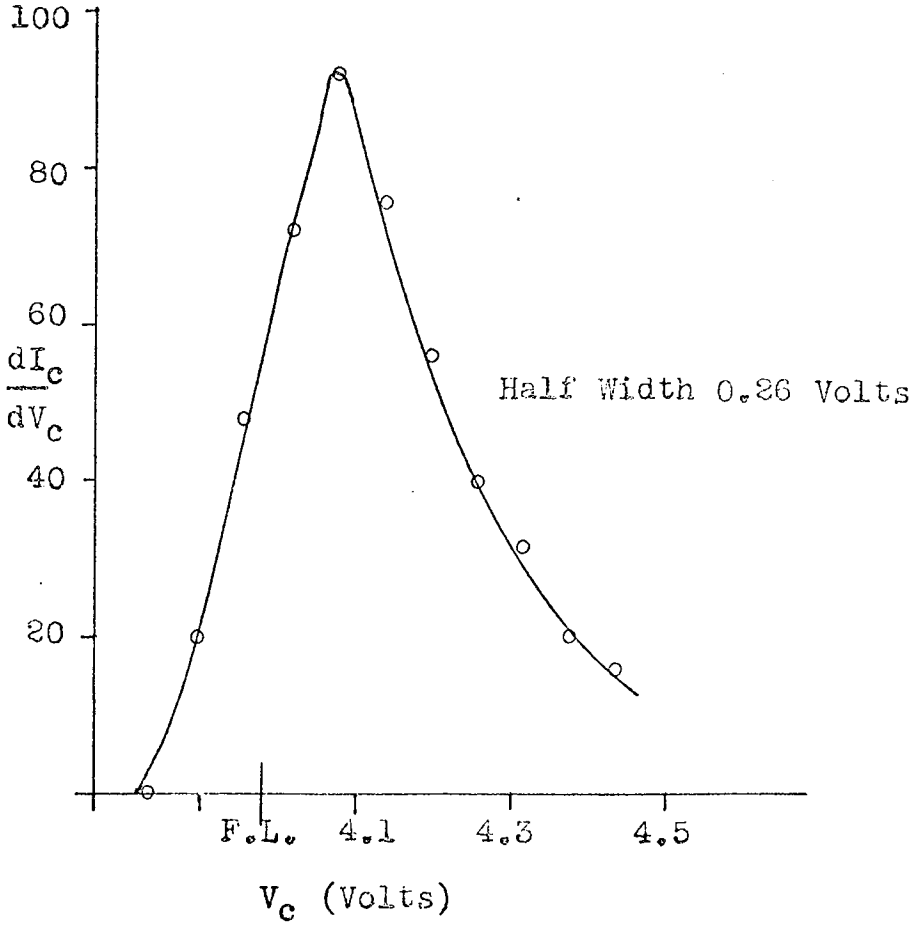

Fig. 5.3(b)

PbTe Emitter 7

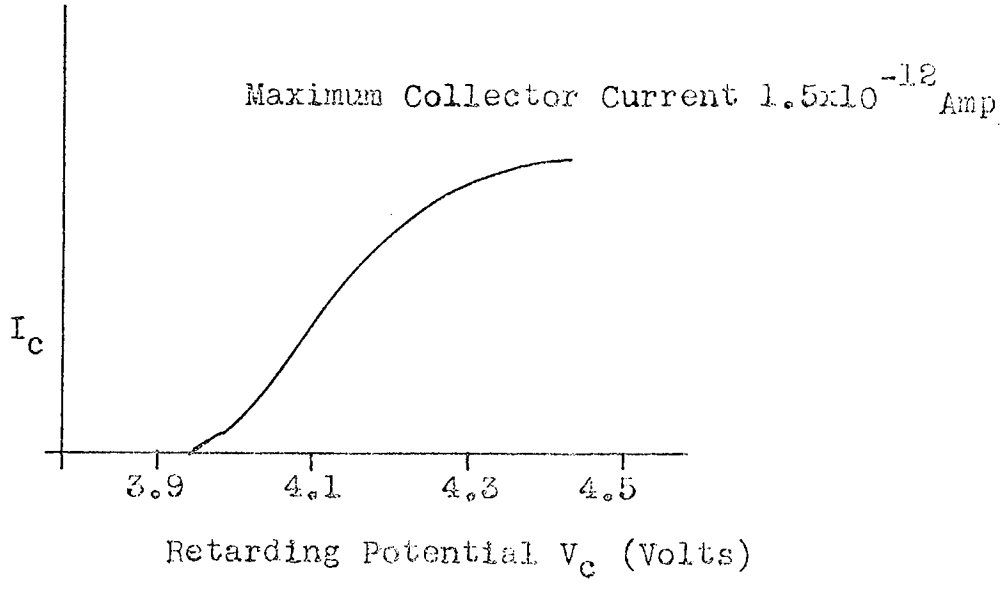

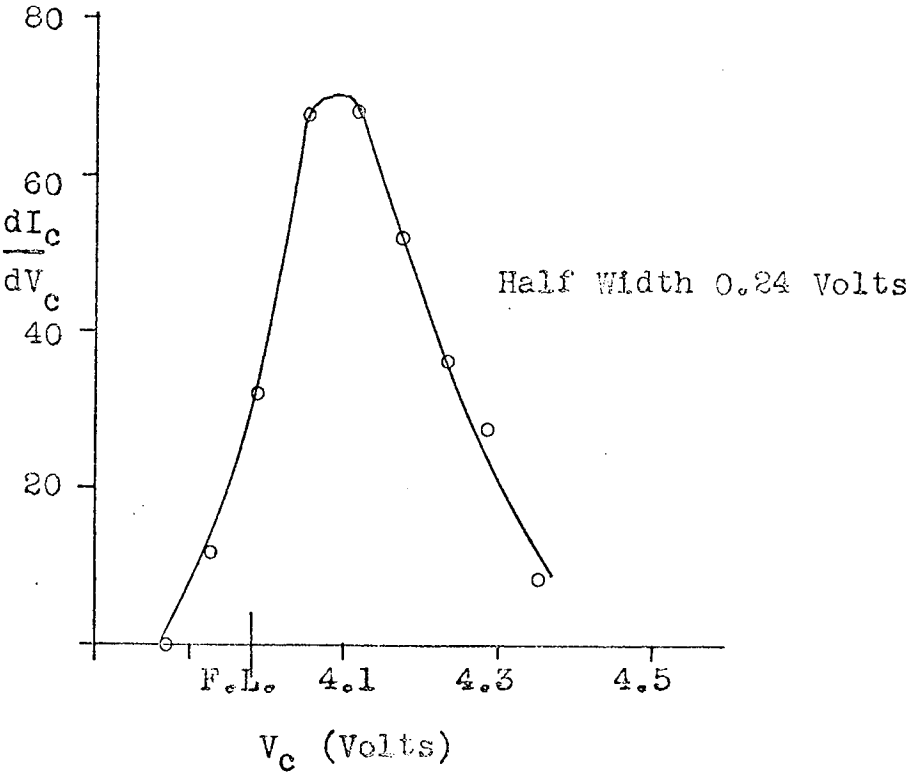

Fig. 5.4(a)

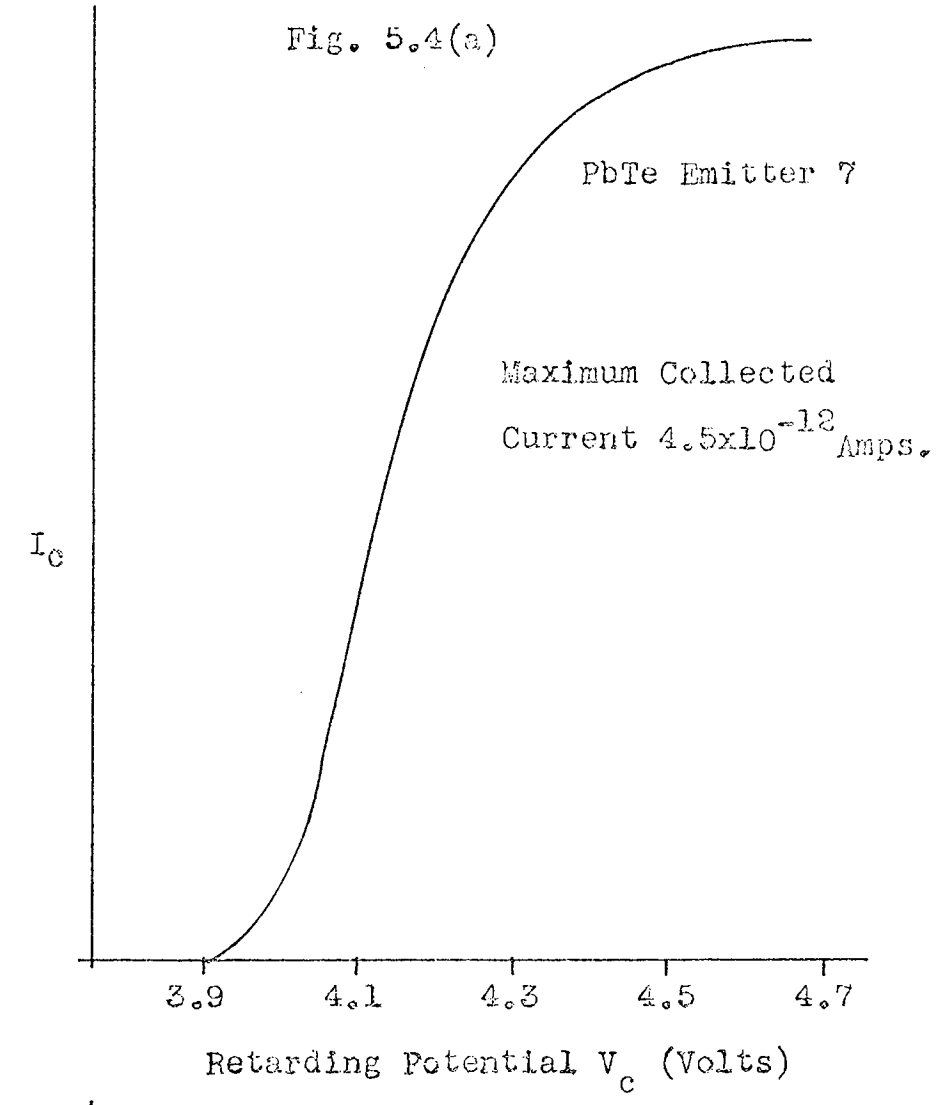
PbTe Emitter 7
Maximum Collected
Current 4.5x10^{-12} Amps.
I_c
3.9
4.1
4.3
4.5
4.7
Retarding Potential V_c (Volts)

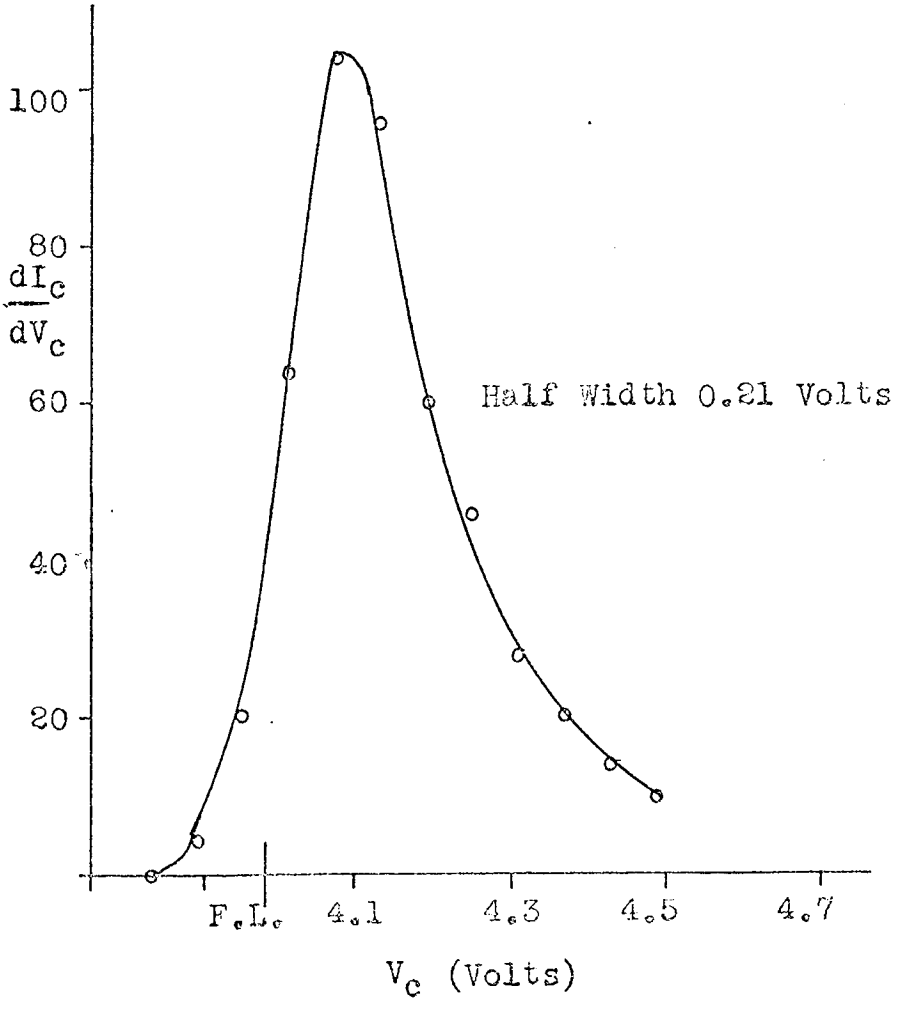
100
80
$\frac{dI_c}{dV_c}$
60
40
20
Half Width 0.21 Volts
F.L.
4.1
4.3
4.5
4.7
V_c (Volts)

Fig. 5.4(b)

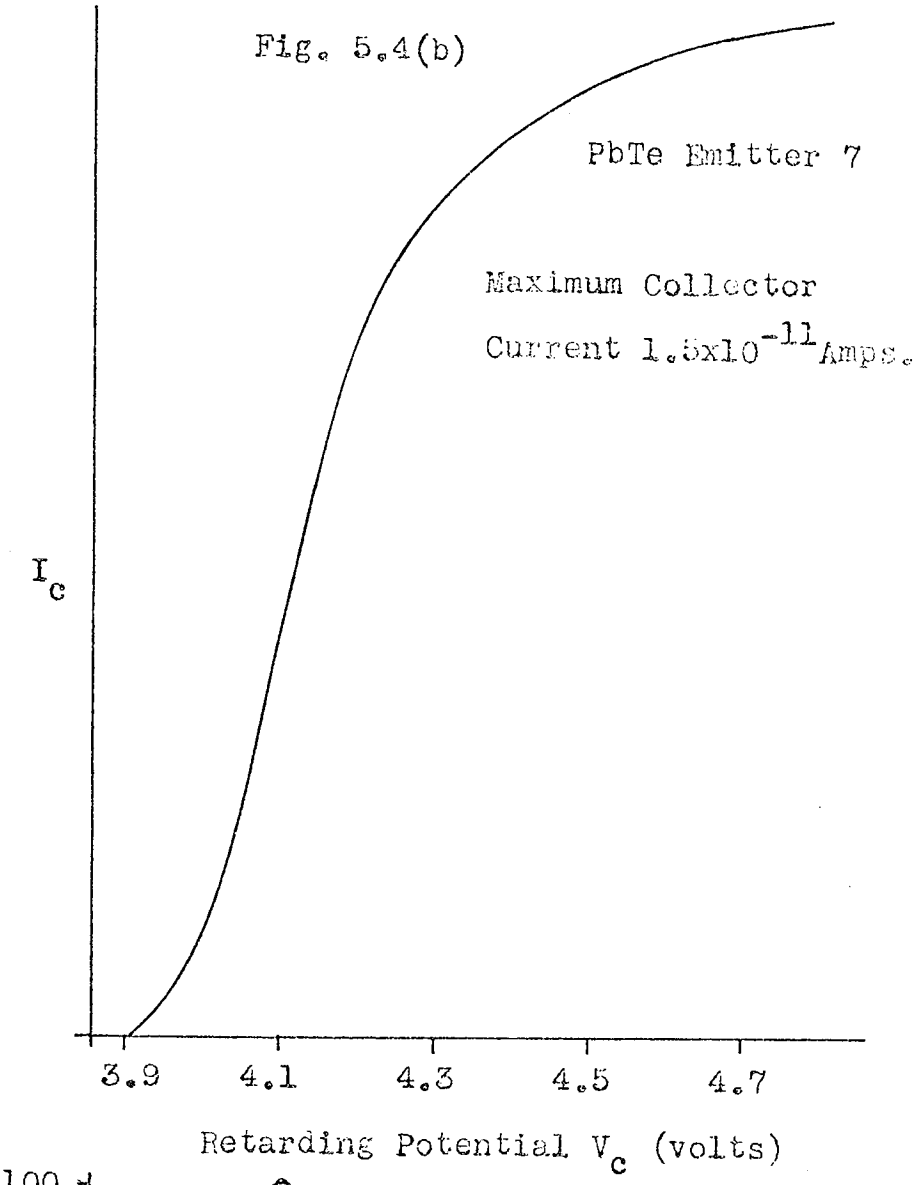
PbTe Emitter 7
Maximum Collector
Current 1.5×10^{-11} Amps.
I_c
3.9
4.1
4.3
4.5
4.7
Retarding Potential V_c (volts)

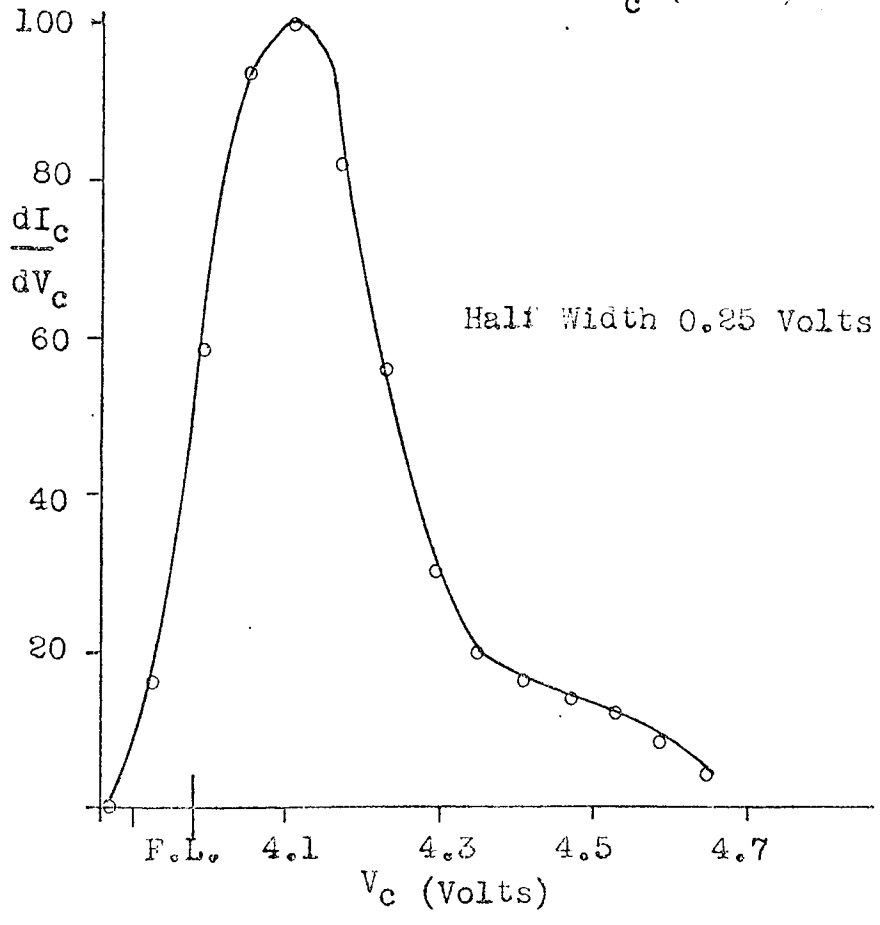
100
80
$\frac{dI_c}{dV_c}$
60
40
20
Half Width 0.25 Volts
F.L.
4.1
4.3
4.5
4.7
V_c (Volts)

Fig. 5.4(c)

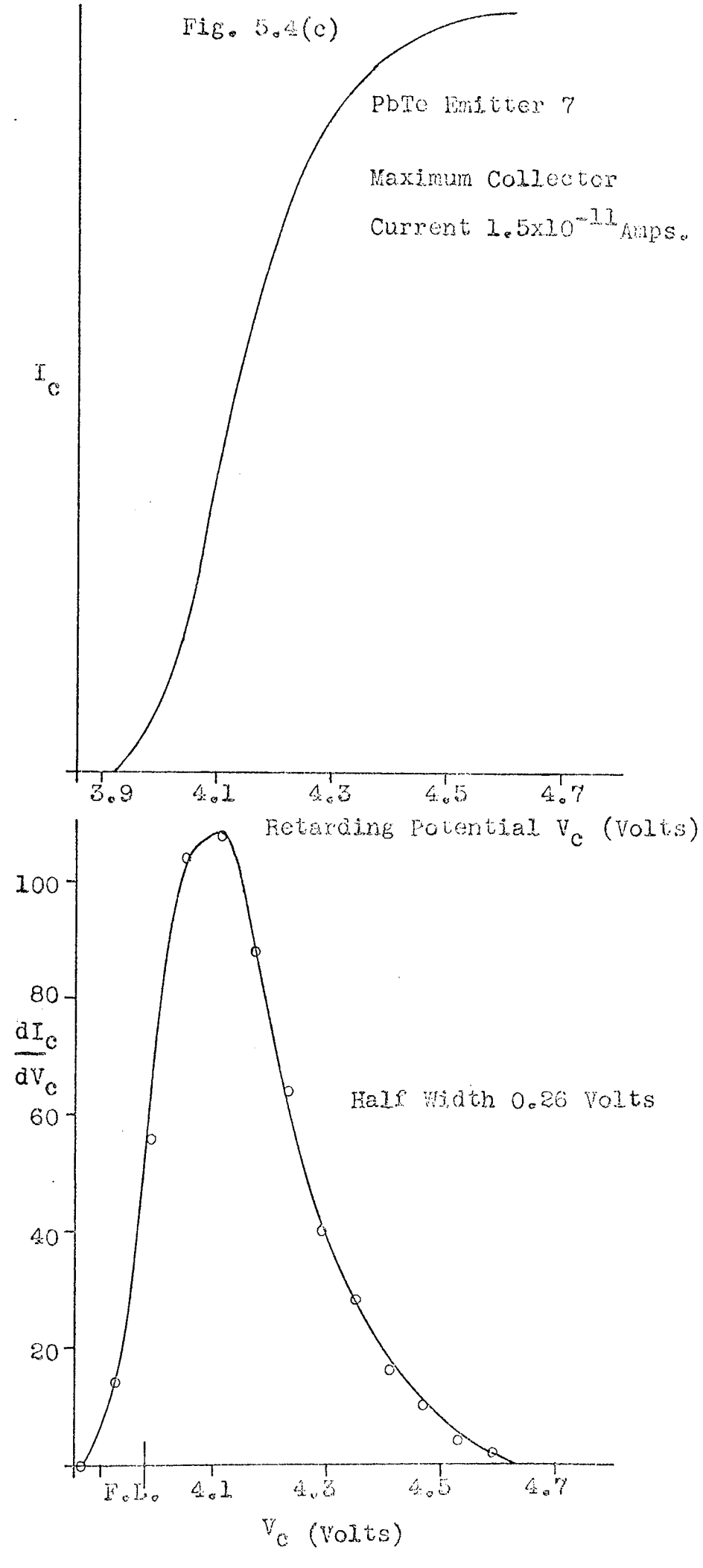
PbTe Emitter 7
Maximum Collector
Current 1.5x10^{-11} Amps.
I_c
3.9
4.1
4.3
4.5
4.7
Retarding Potential V_c (Volts)
100
80
$\frac{dI_c}{dV_c}$
60
40
20
Half Width 0.26 Volts
F.L.
4.1
4.3
4.5
4.7
V_c (Volts)

Fig. 5.4(d)

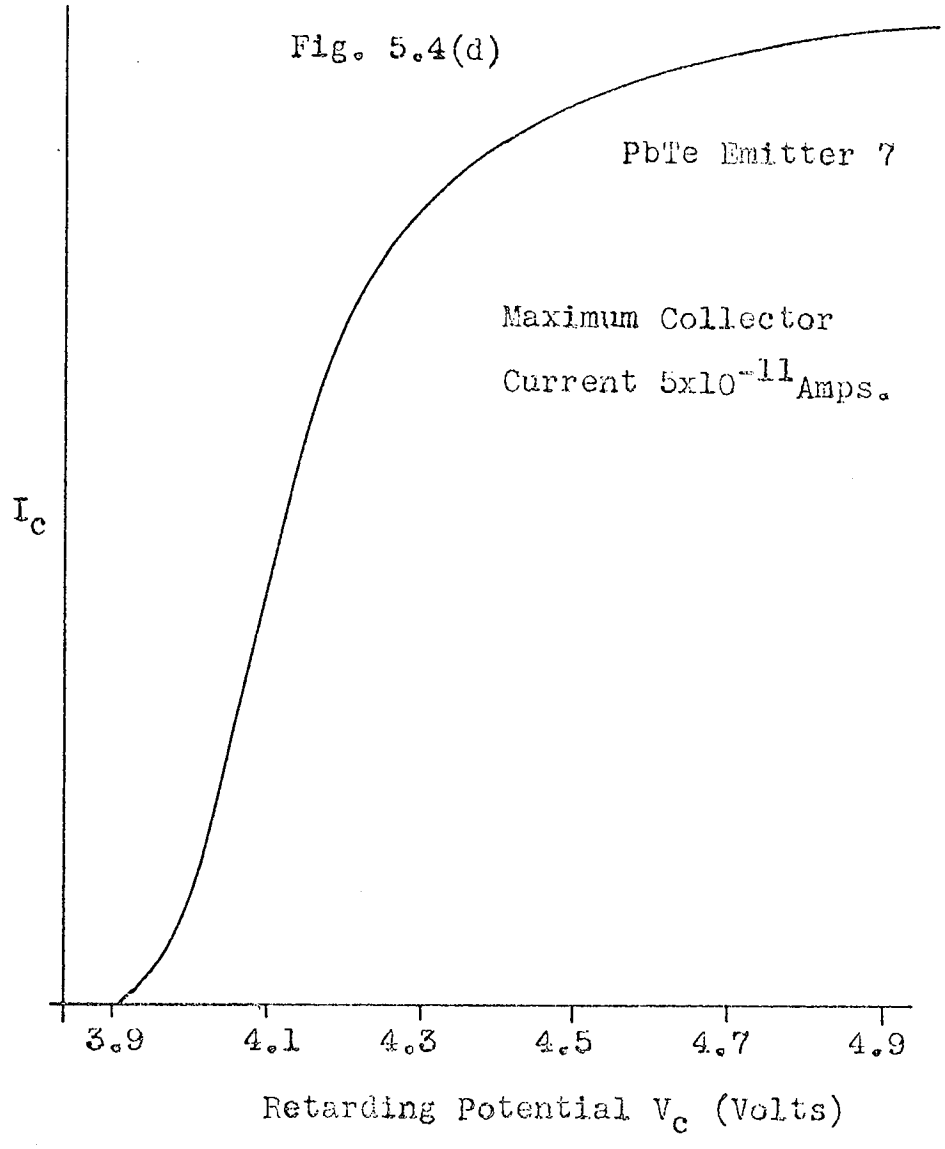
PbTe Emitter 7
Maximum Collector
Current 5x10⁻¹¹ Amps.
I_c
3.9
4.1
4.3
4.5
4.7
4.9
Retarding Potential V_c (Volts)

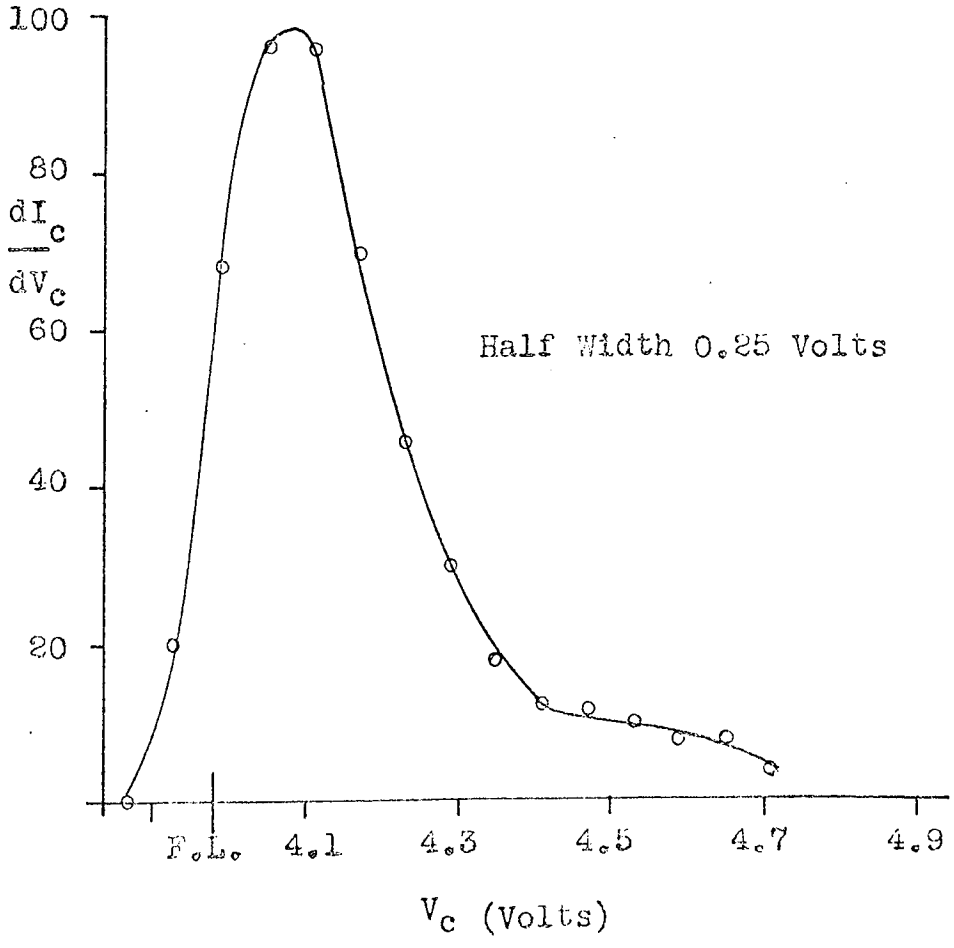
100
80
$\frac{dI_c}{dV_c}$
60
40
20
Half Width 0.25 Volts
F.L.
4.1
4.3
4.5
4.7
4.9
V_c (Volts)

Fig. 5.5(a)

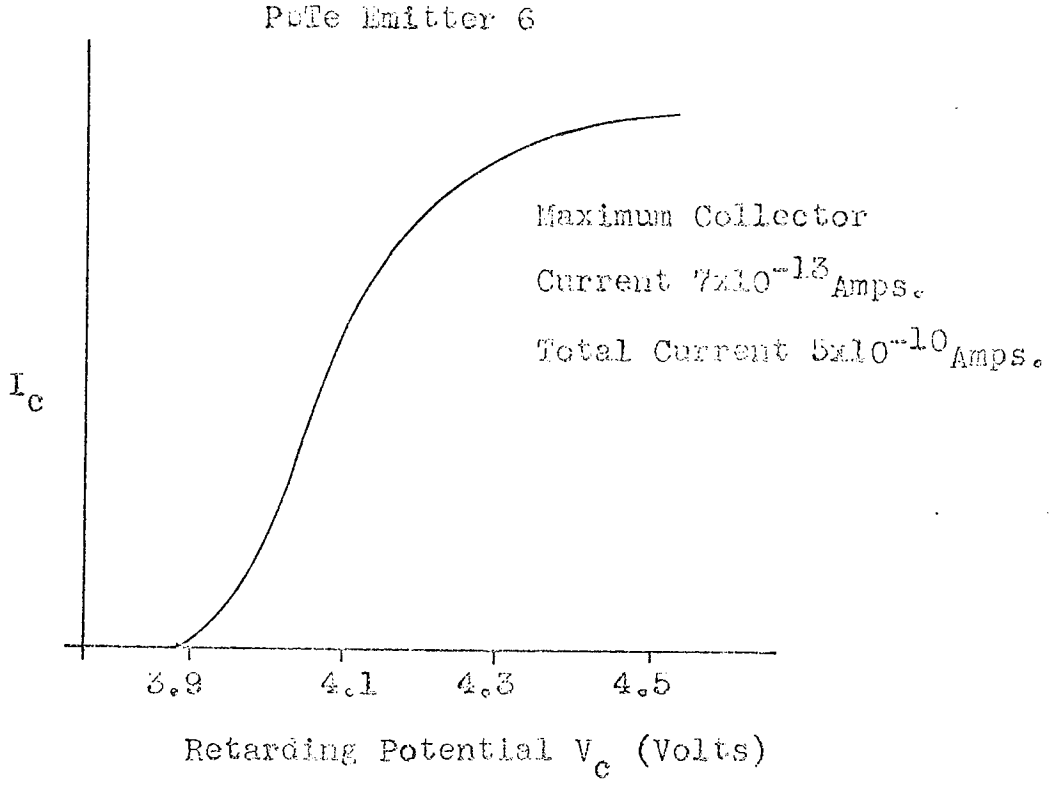
PuFe Emitter 6
Maximum Collector
Current 7×10^{-13} Amps.
Total Current 5×10^{-10} Amps.
I_c
3.9
4.1
4.3
4.5
Retarding Potential V_c (Volts)

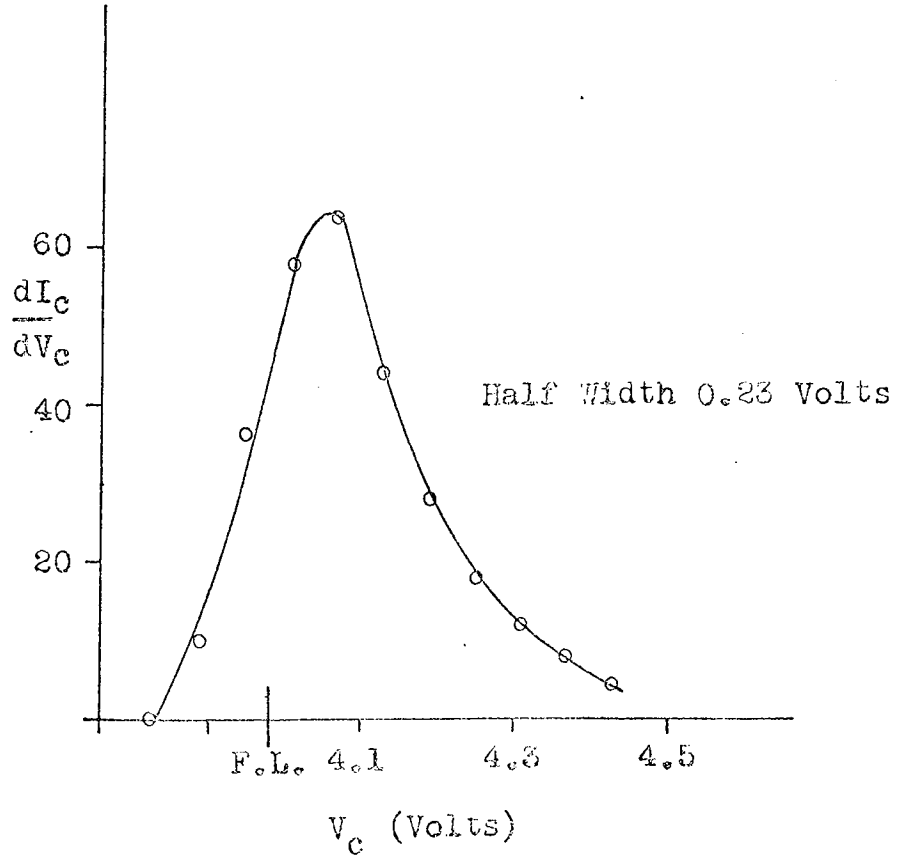
60
$\frac{dI_c}{dV_c}$
40
20
Half Width 0.23 Volts
F.L. 4.1
4.3
4.5
V_c (Volts)

Fig. 5.5(b)

PbTe 6

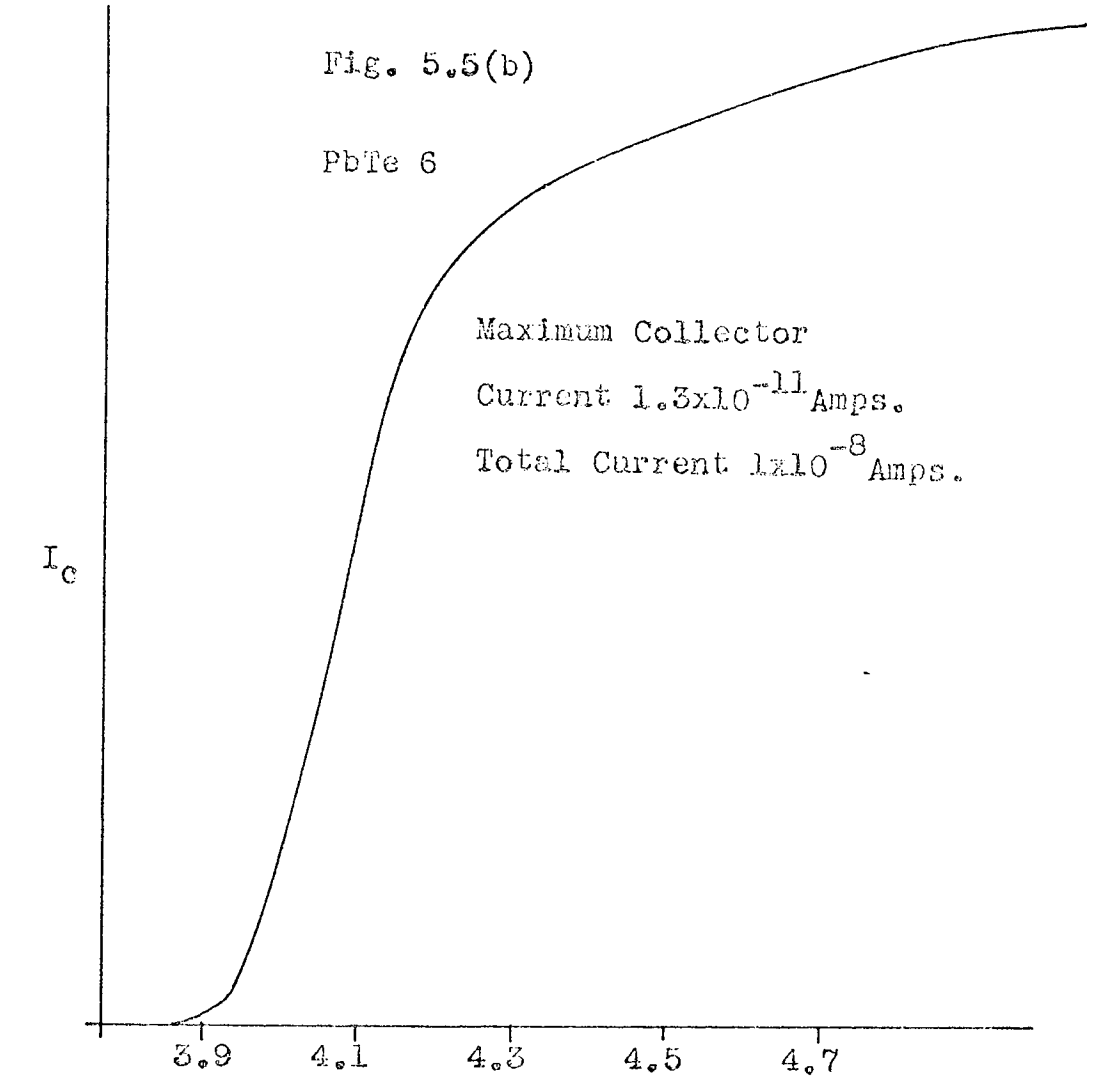

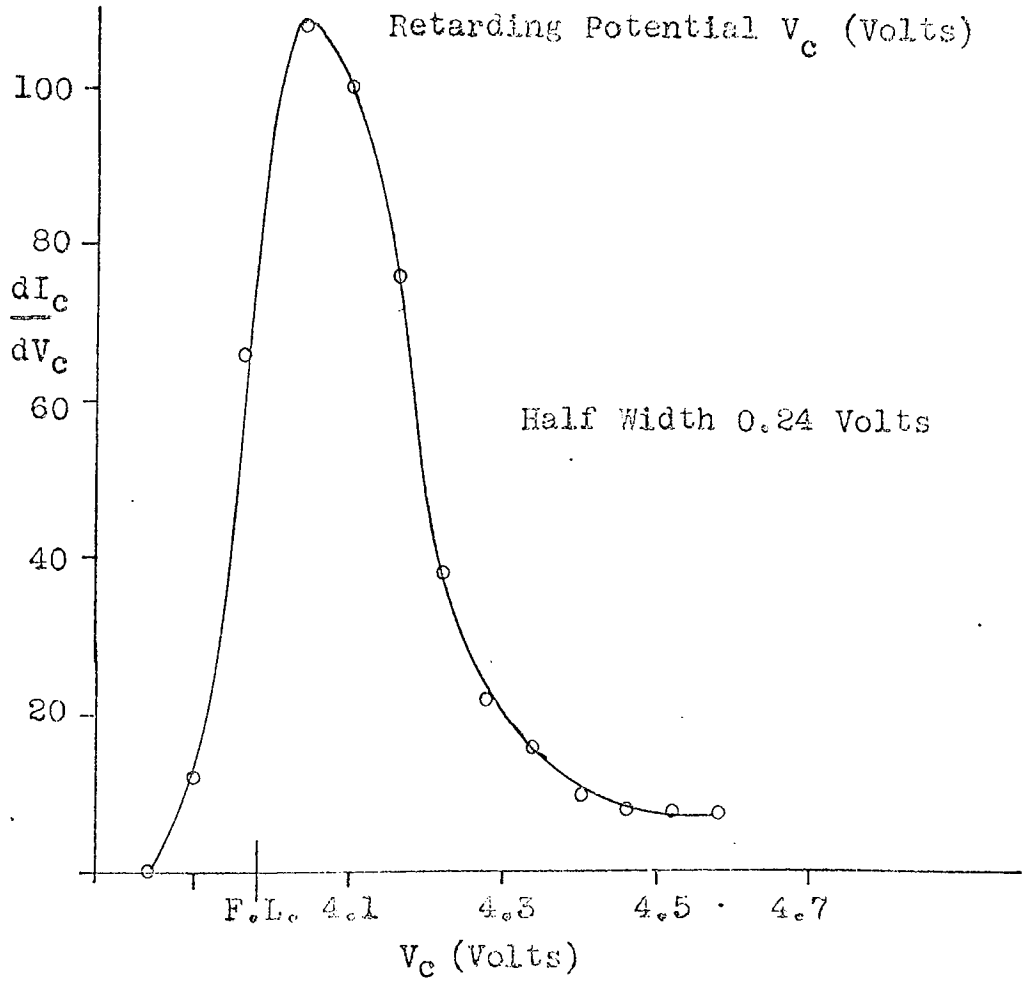

Fig. 5.5(c)

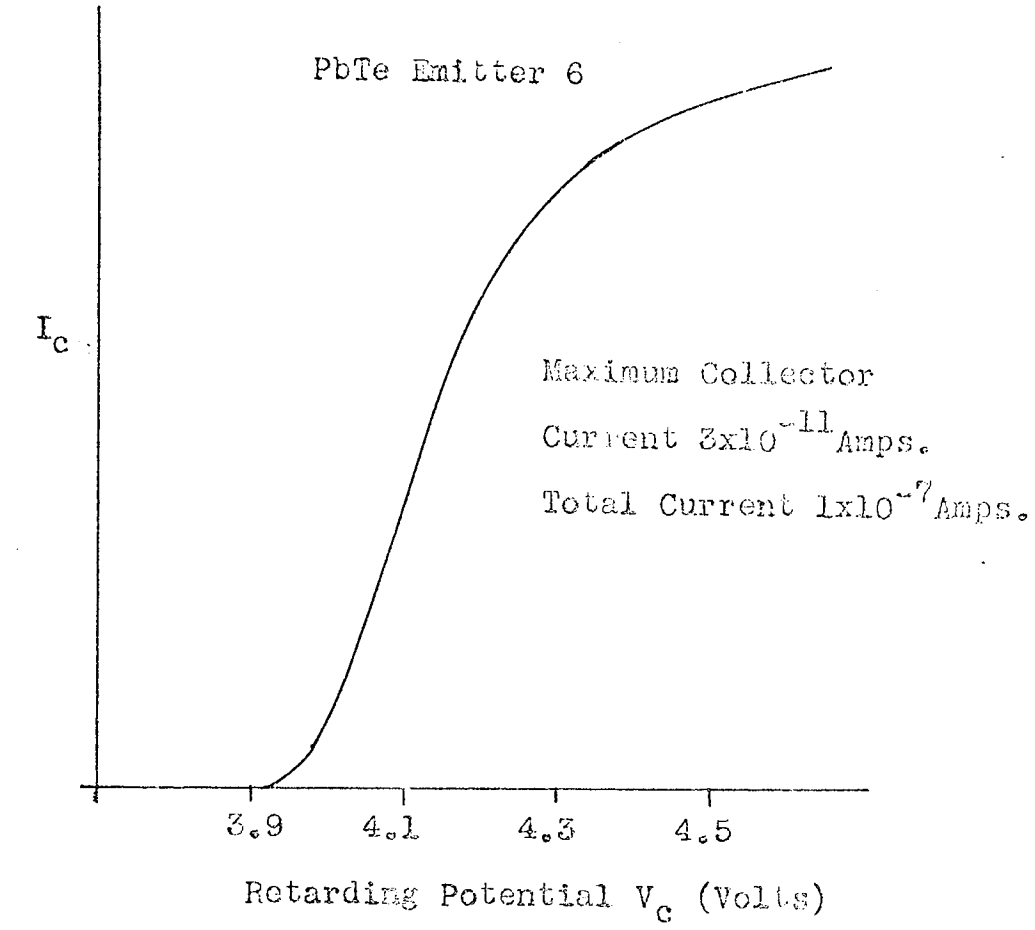
PbTe Emitter 6
I_c
Maximum Collector
Current 3×10^{-11} Amps.
Total Current 1×10^{-7} Amps.
3.9
4.1
4.3
4.5
Retarding Potential V_c (Volts)

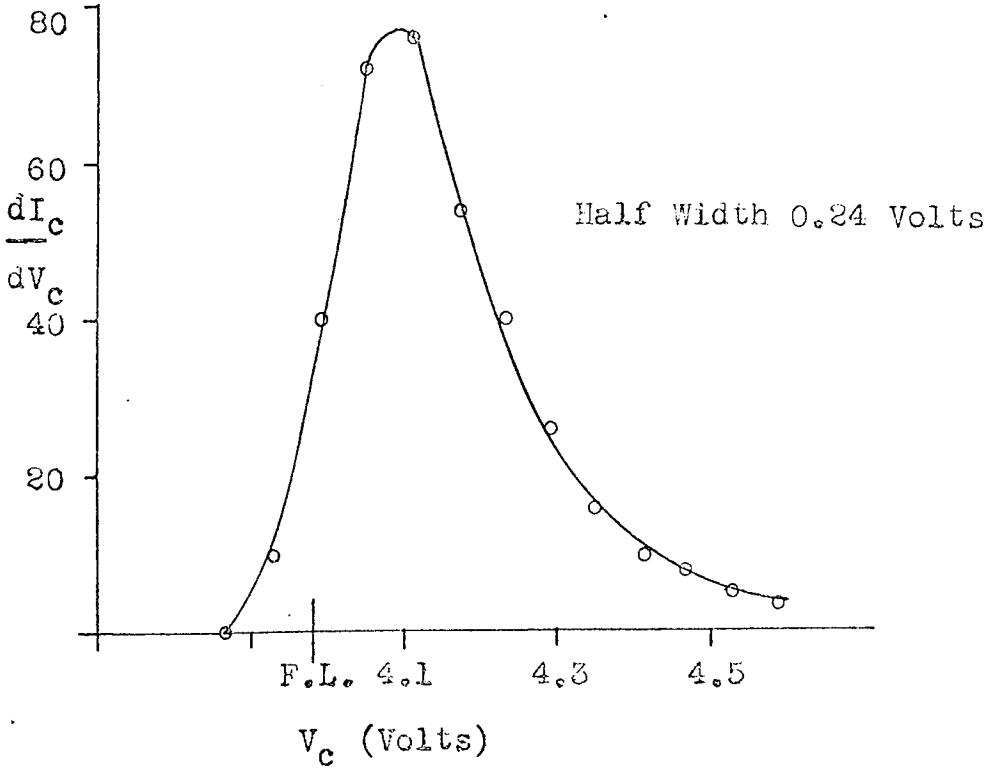
80
60
$\frac{dI_c}{dV_c}$
40
20
Half Width 0.24 Volts
F.L. 4.1
4.3
4.5
V_c (Volts)

Fig. 5.6(a)

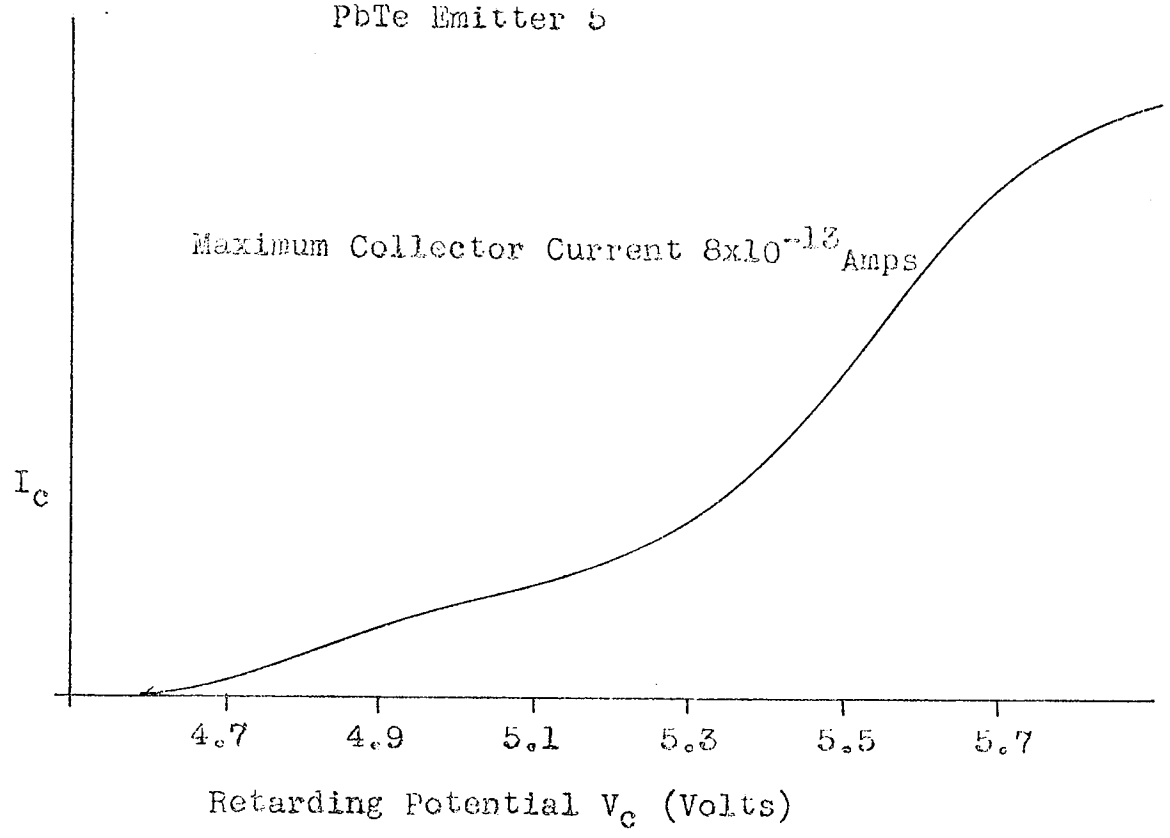
PbTe Emitter 5
Maximum Collector Current 8x10^-13 Amps
I_c
4.7
4.9
5.1
5.3
5.5
5.7
Retarding Potential V_c (Volts)

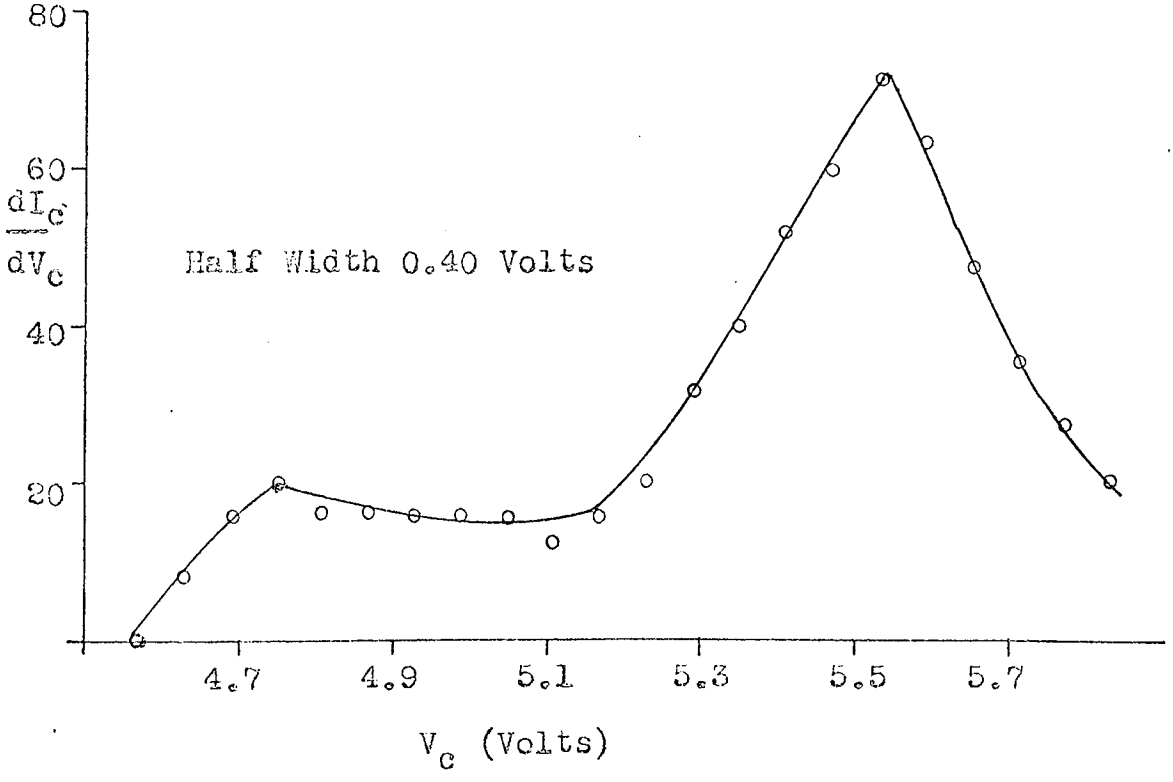
80
60
40
20
$\frac{dI_c}{dV_c}$
Half Width 0.40 Volts
4.7
4.9
5.1
5.3
5.5
5.7
V_c (Volts)

Fig. 5.6(b)

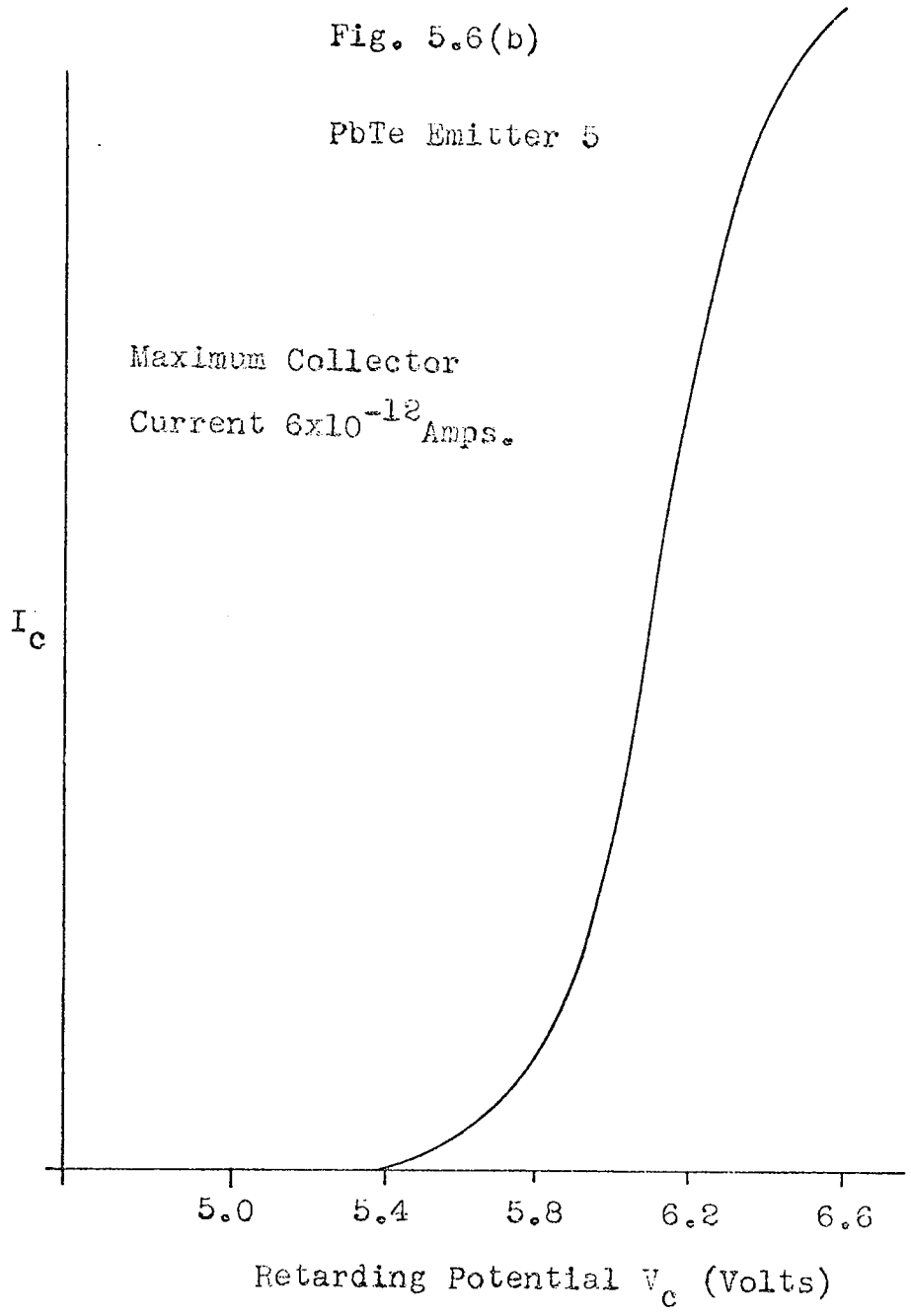
PbTe Emitter 5
Maximum Collector
Current 6x10^{-12} Amps.
I_c
5.0
5.4
5.8
6.2
6.6
Retarding Potential V_c (Volts)

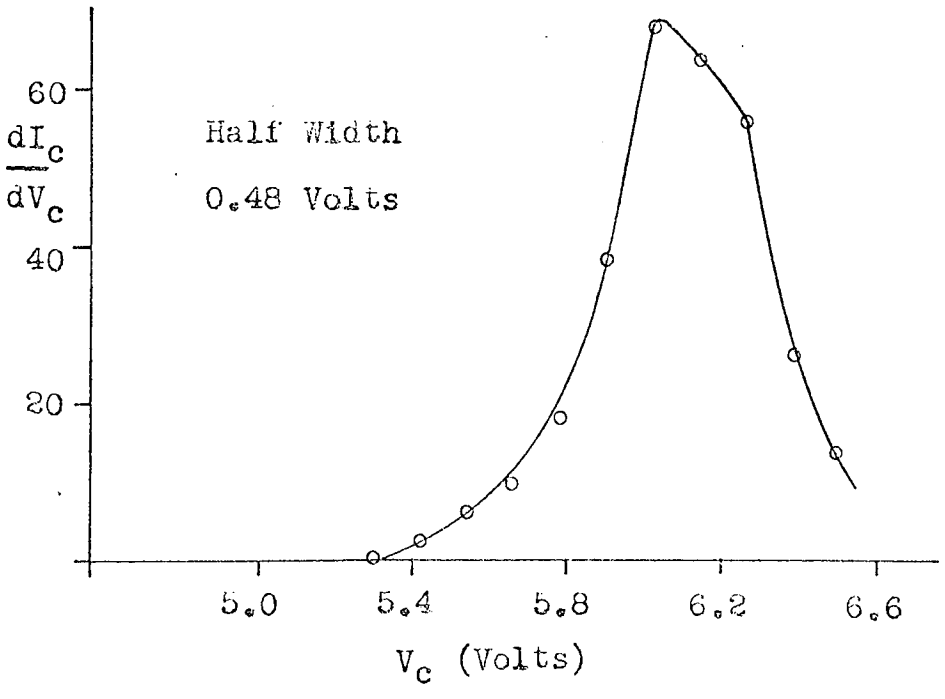
60
$\frac{dI_c}{dV_c}$
40
20
Half Width
0.48 Volts
5.0
5.4
5.8
6.2
6.6
V_c (Volts)

Fig. 5.6(c)

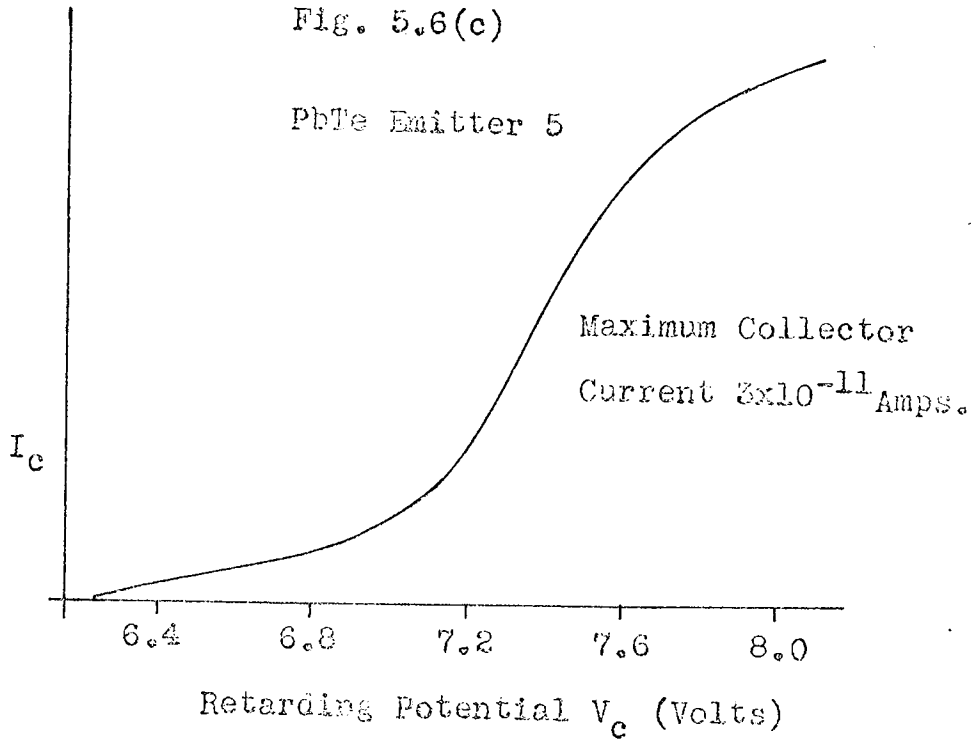
PbTe Emitter 5
Maximum Collector
Current 3x10⁻¹¹ Amps.
I_c
6.4
6.8
7.2
7.6
8.0
Retarding Potential V_c (Volts)

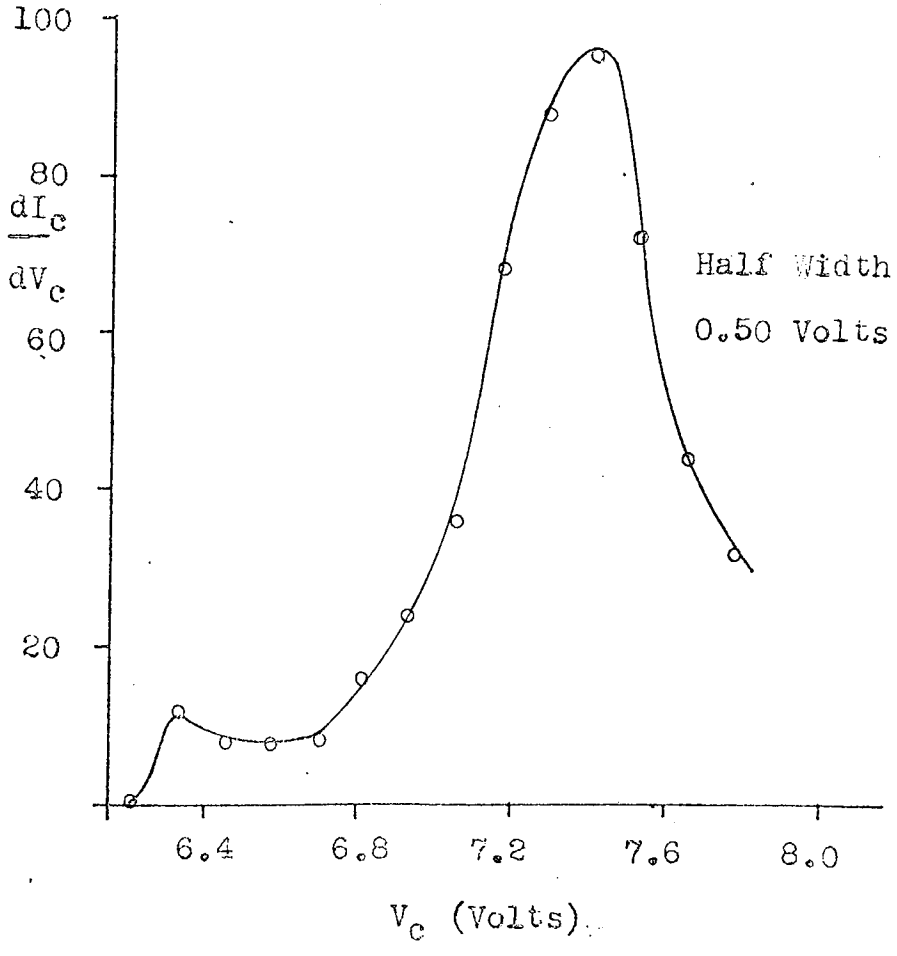
100
80
$\frac{dI_c}{dV_c}$
60
40
20
Half Width
0.50 Volts
6.4
6.8
7.2
7.6
8.0
V_c (Volts)

Fig. 5.6(d)

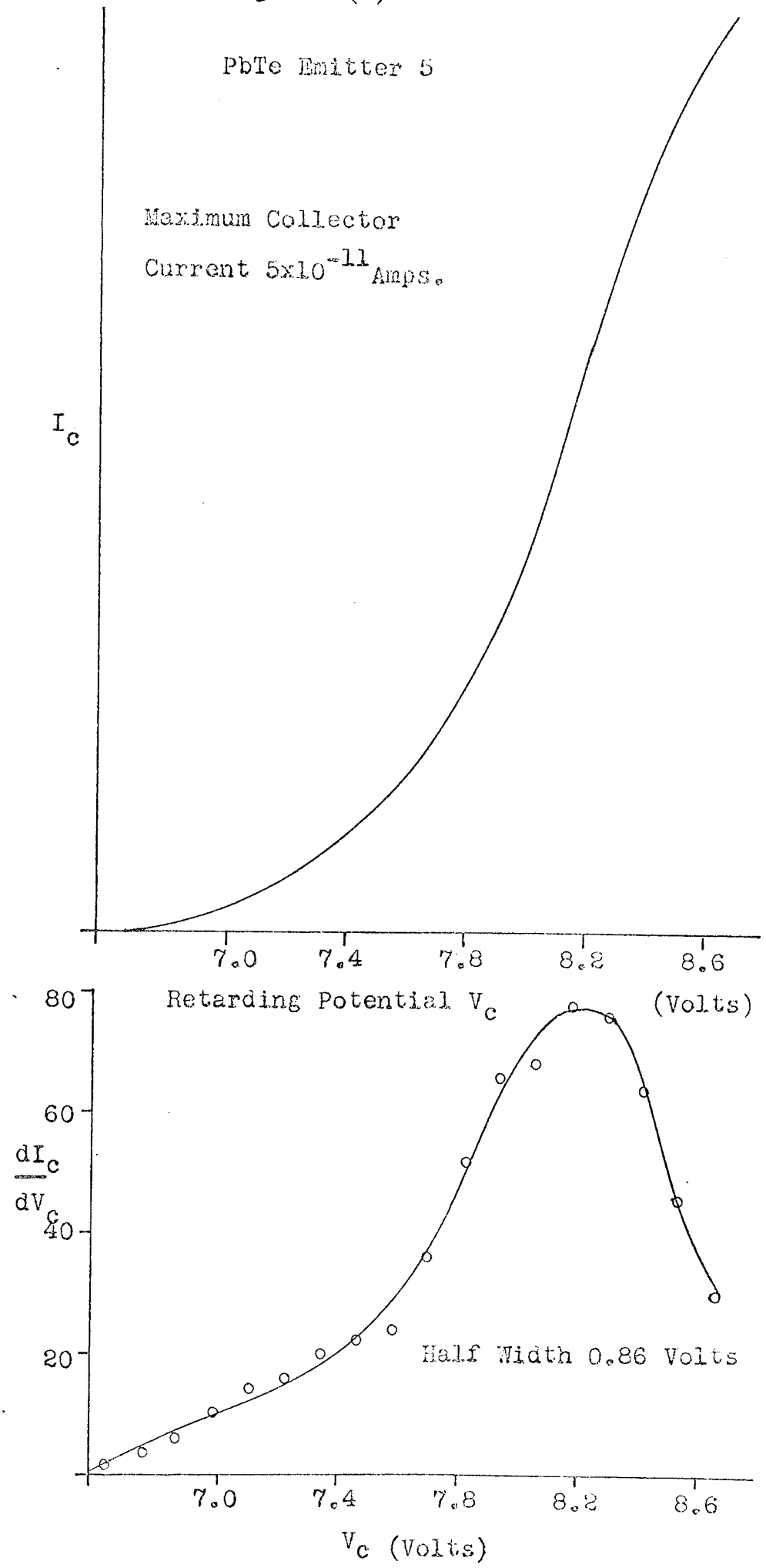
PbTe Emitter 5
Maximum Collector
Current 5×10^{-11} Amps.
I_c
7.0
7.4
7.8
8.2
8.6
Retarding Potential V_c (Volts)
80
60
40
20
$\frac{dI_c}{dV_c}$
Half Width 0.86 Volts
7.0
7.4
7.8
8.2
8.6
V_c (Volts)

Fig. 5.7(a)

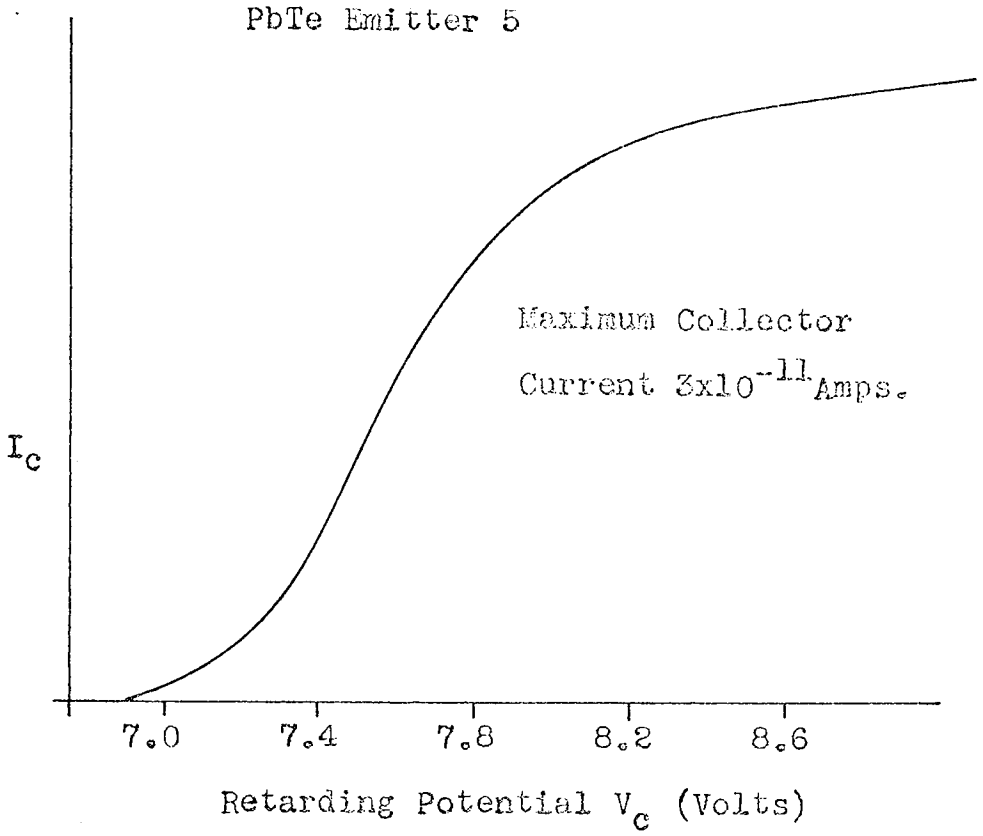
PbTe Emitter 5
Maximum Collector
Current 3×10^{-11} Amps.
I_c
7.0
7.4
7.8
8.2
8.6
Retarding Potential V_c (Volts)

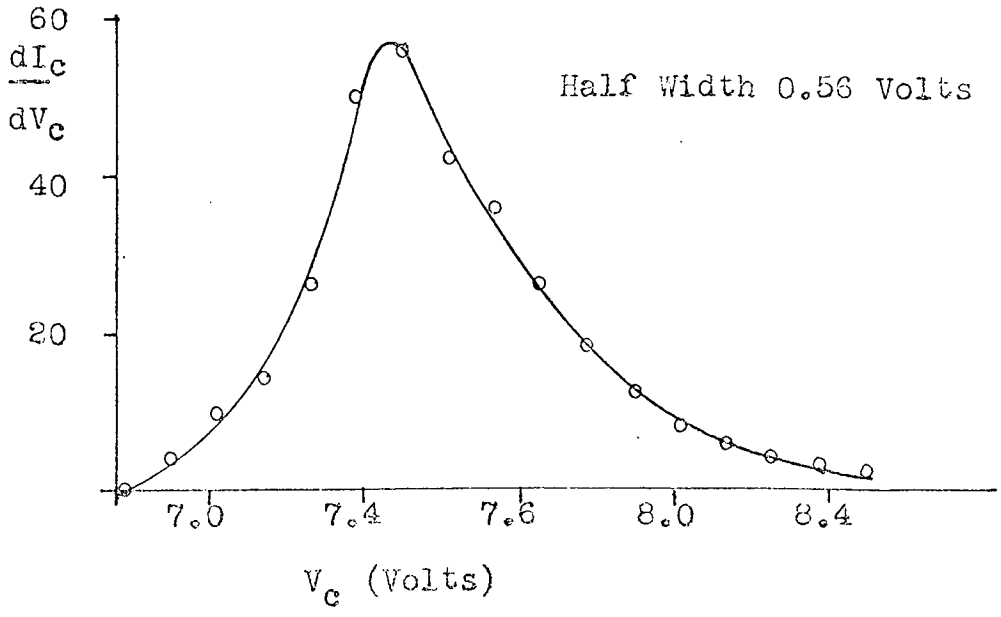
60
$\frac{dI_c}{dV_c}$
40
20
Half Width 0.56 Volts
7.0
7.4
7.6
8.0
8.4
V_c (Volts)

Fig. 5.7(b)

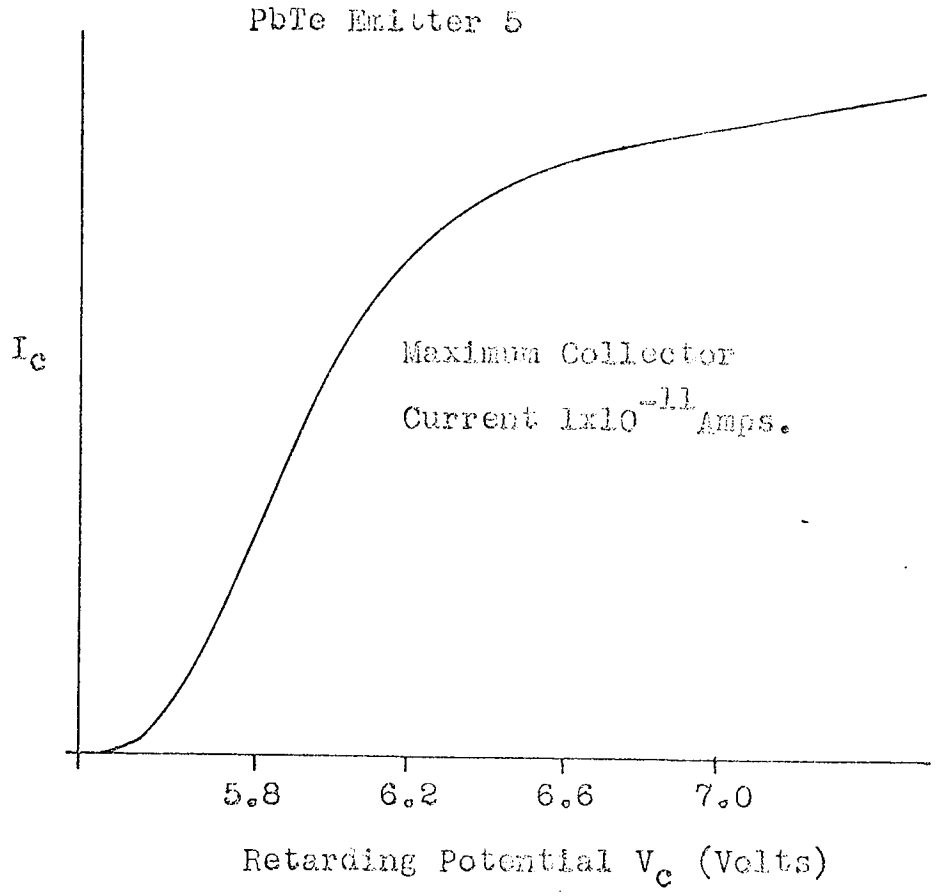
PbTe Emitter 5
I_c
Maximum Collector
Current $1x10^{-11}$ Amps.
5.8
6.2
6.6
7.0
Retarding Potential V_c (Volts)

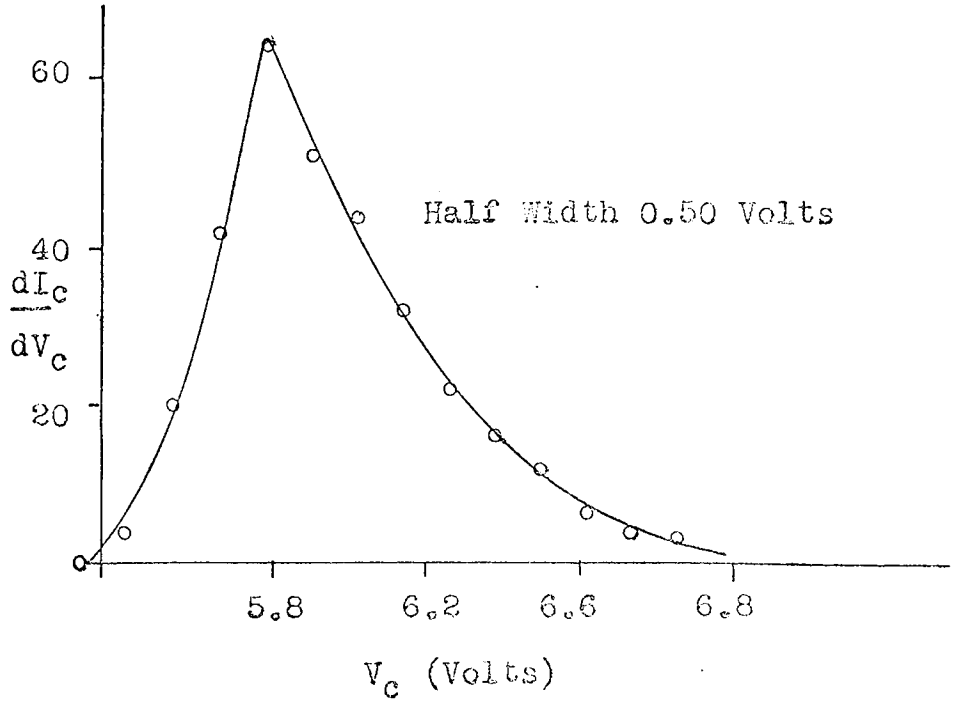
60
40
20
$\frac{dI_c}{dV_c}$
Half Width 0.50 Volts
5.8
6.2
6.6
6.8
V_c (Volts)

Fig. 5.8(a)

PbTe Emitter 5

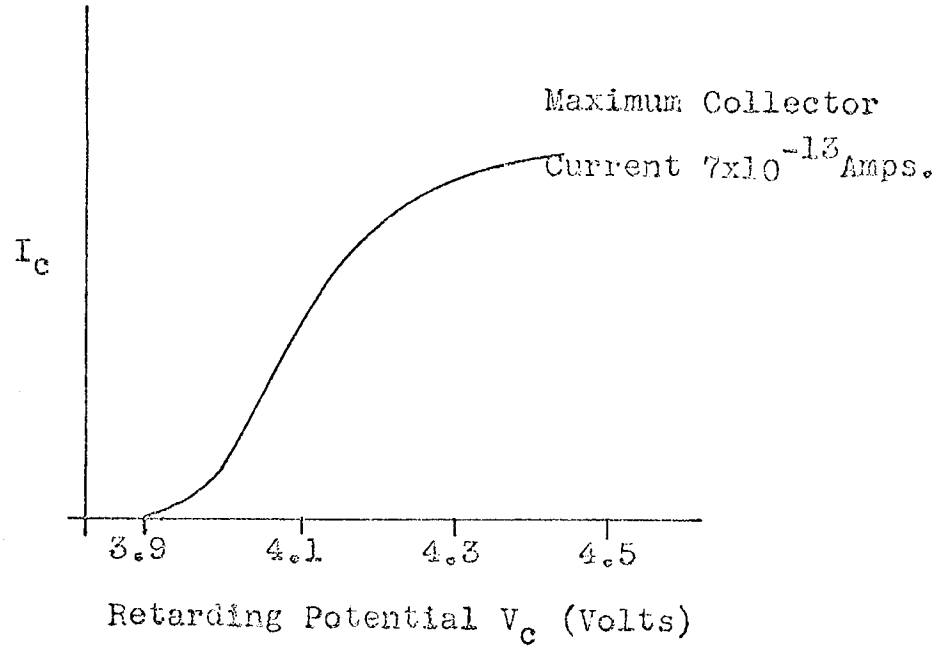

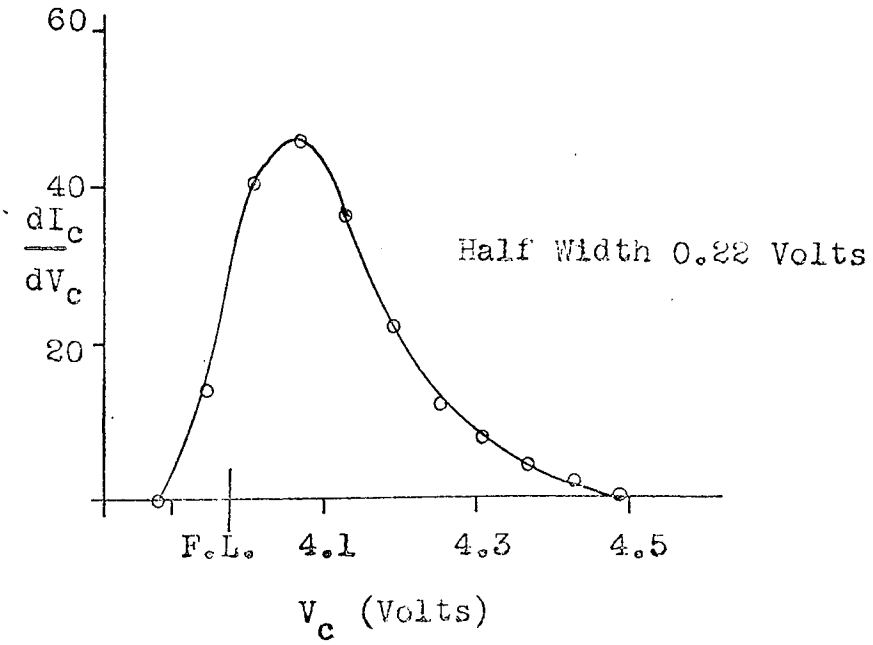

Fig. 5.8(b)

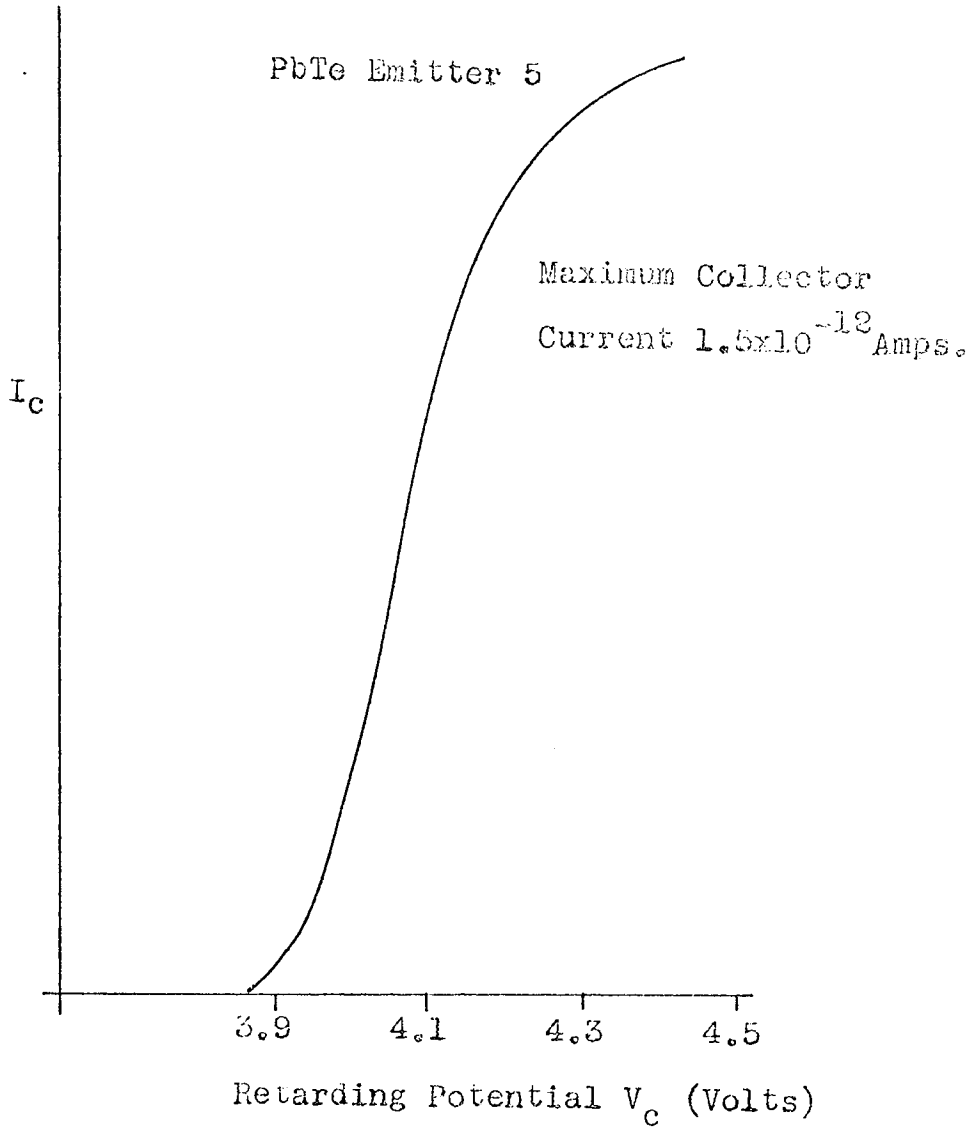
PbTe Emitter 5
Maximum Collector
Current 1.5x10^{-12} Amps.
I_c
3.9
4.1
4.3
4.5
Retarding Potential V_c (Volts)

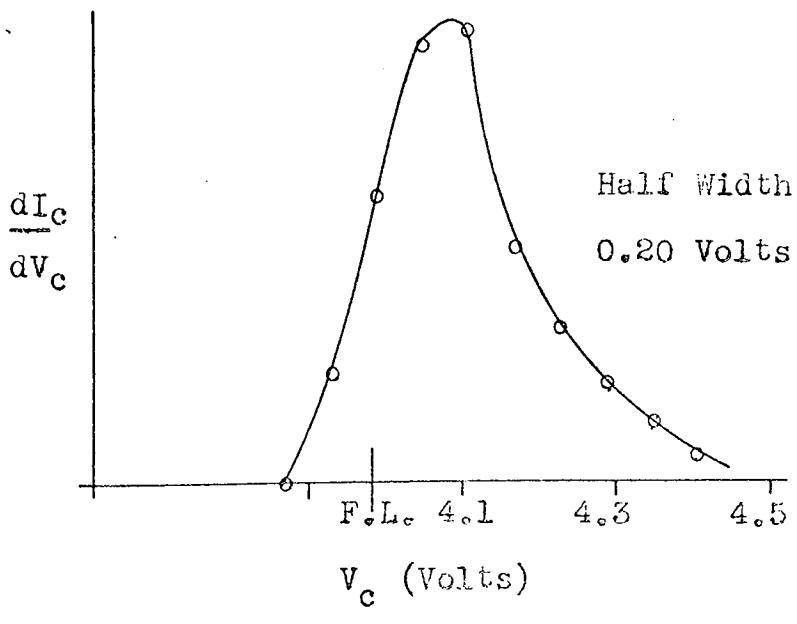
$\frac{dI_c}{dV_c}$
Half Width
0.20 Volts
F.L.
4.1
4.3
4.5
V_c (Volts)

Fig. 5.9(a)

PbTe Emitter 4

Maximum Collector Current 1.5×10^{-11} Amps.

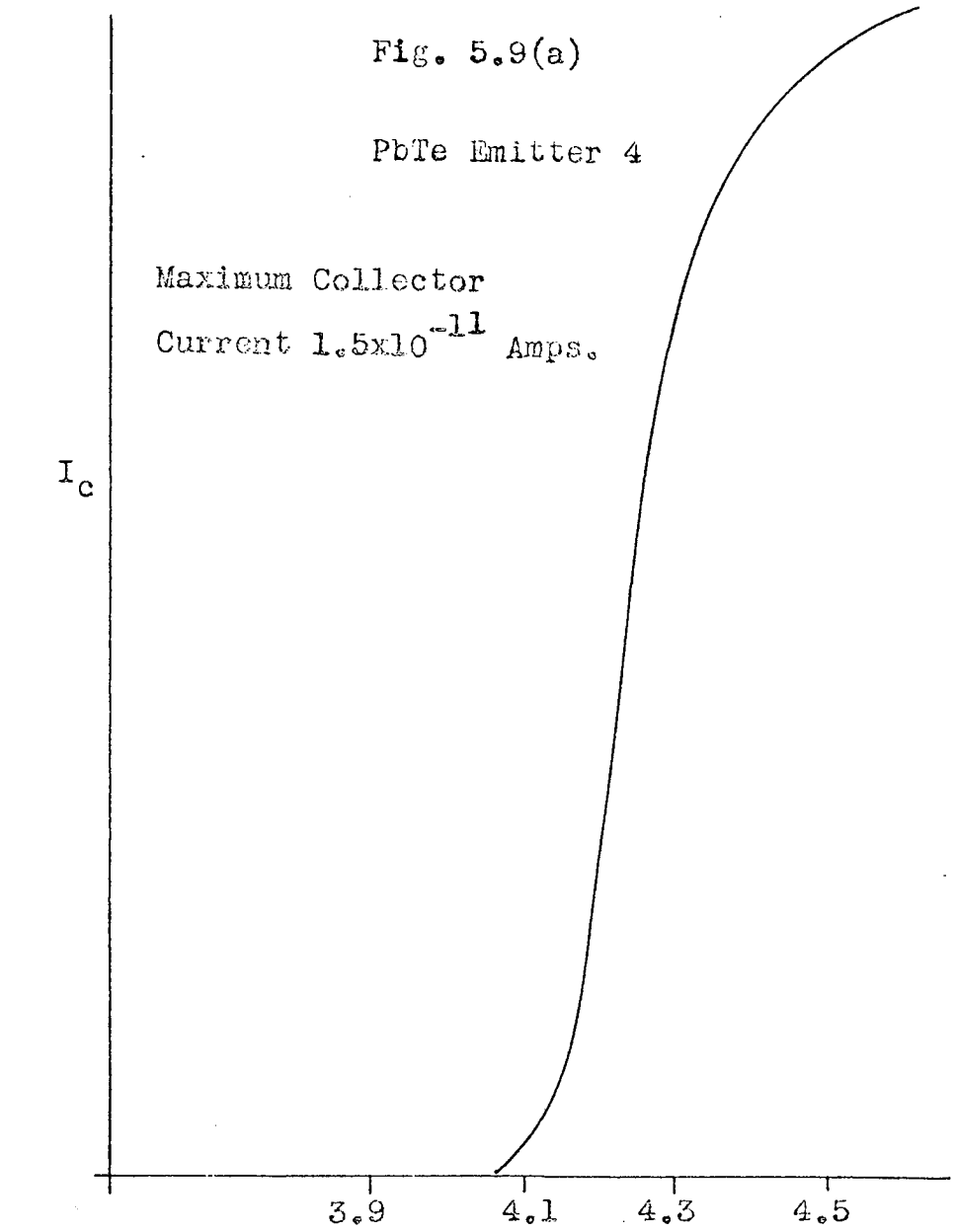

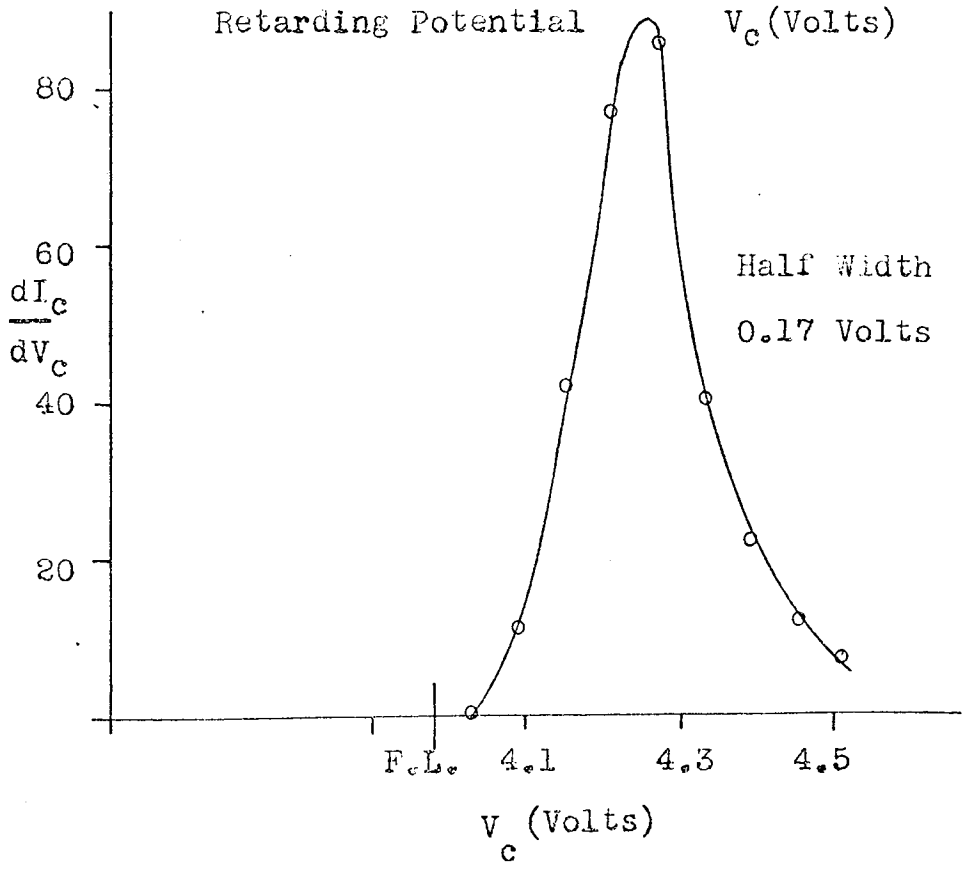

Fig. 5.9(b)

PbTe Emitter 4

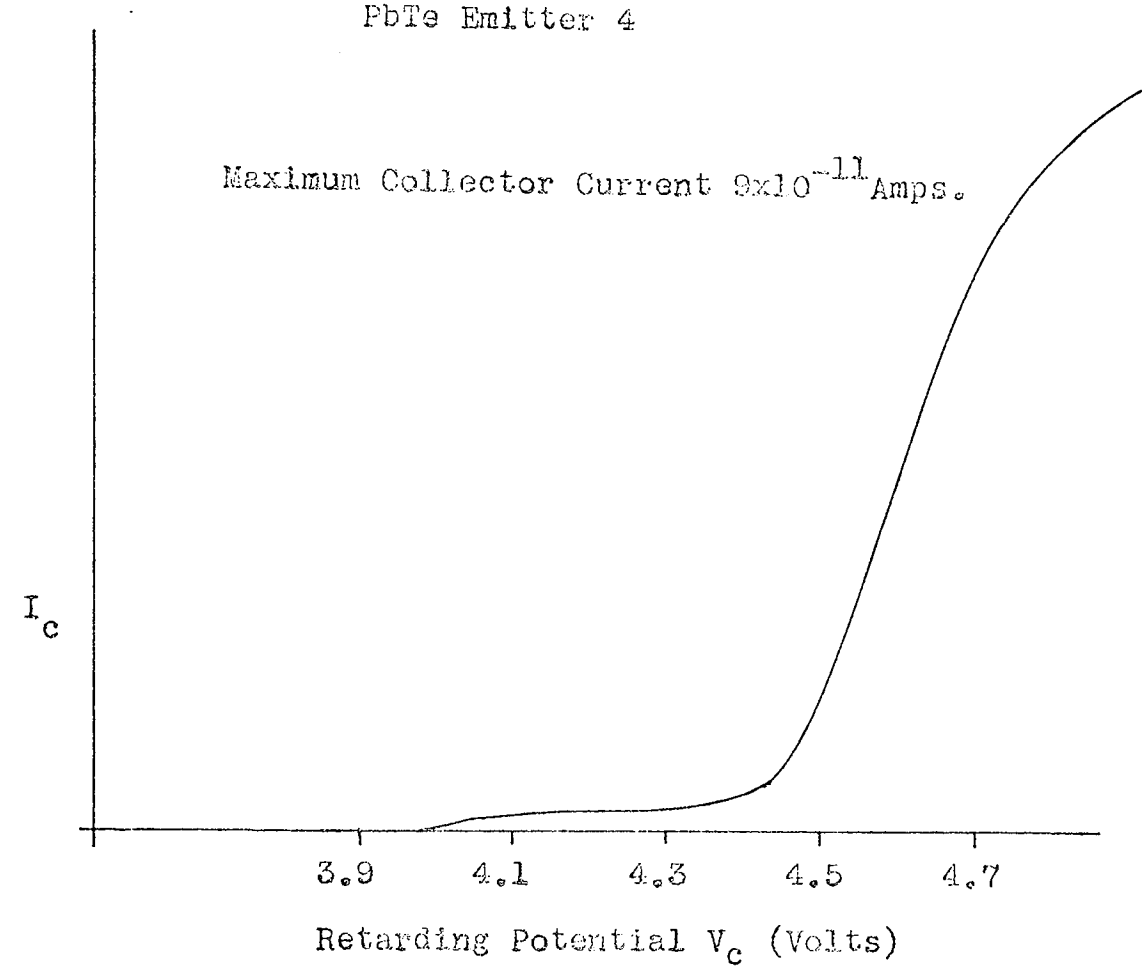

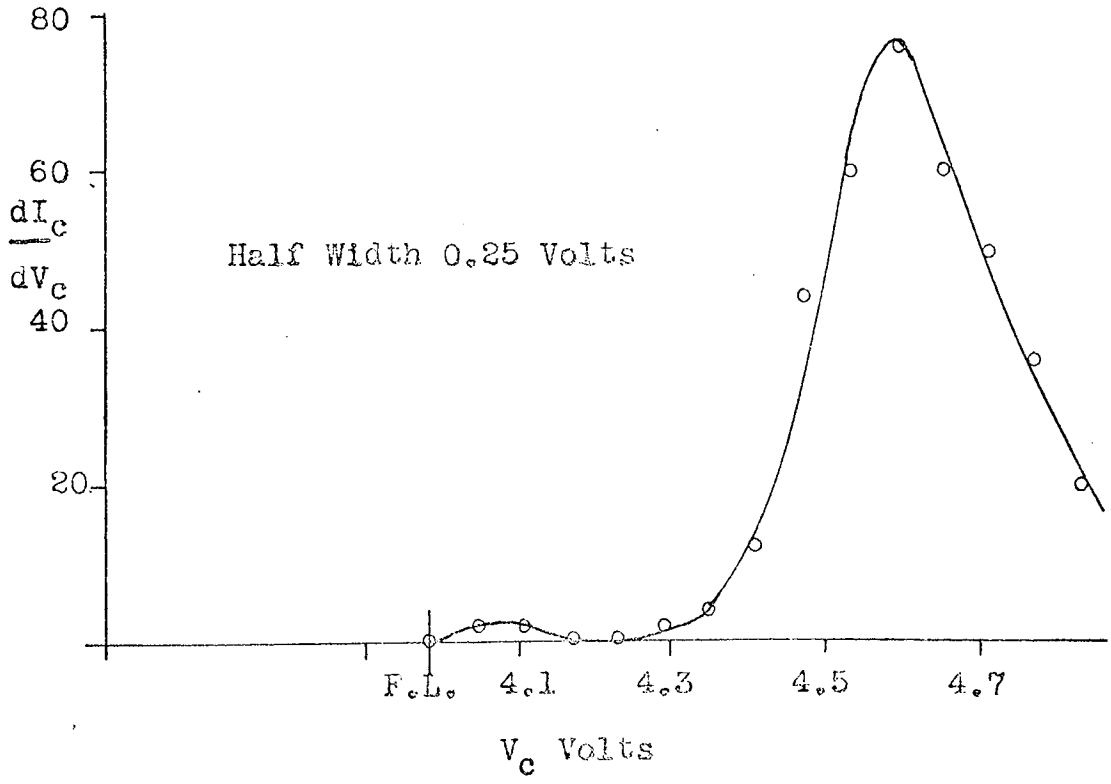

Fig. 5.9(c)

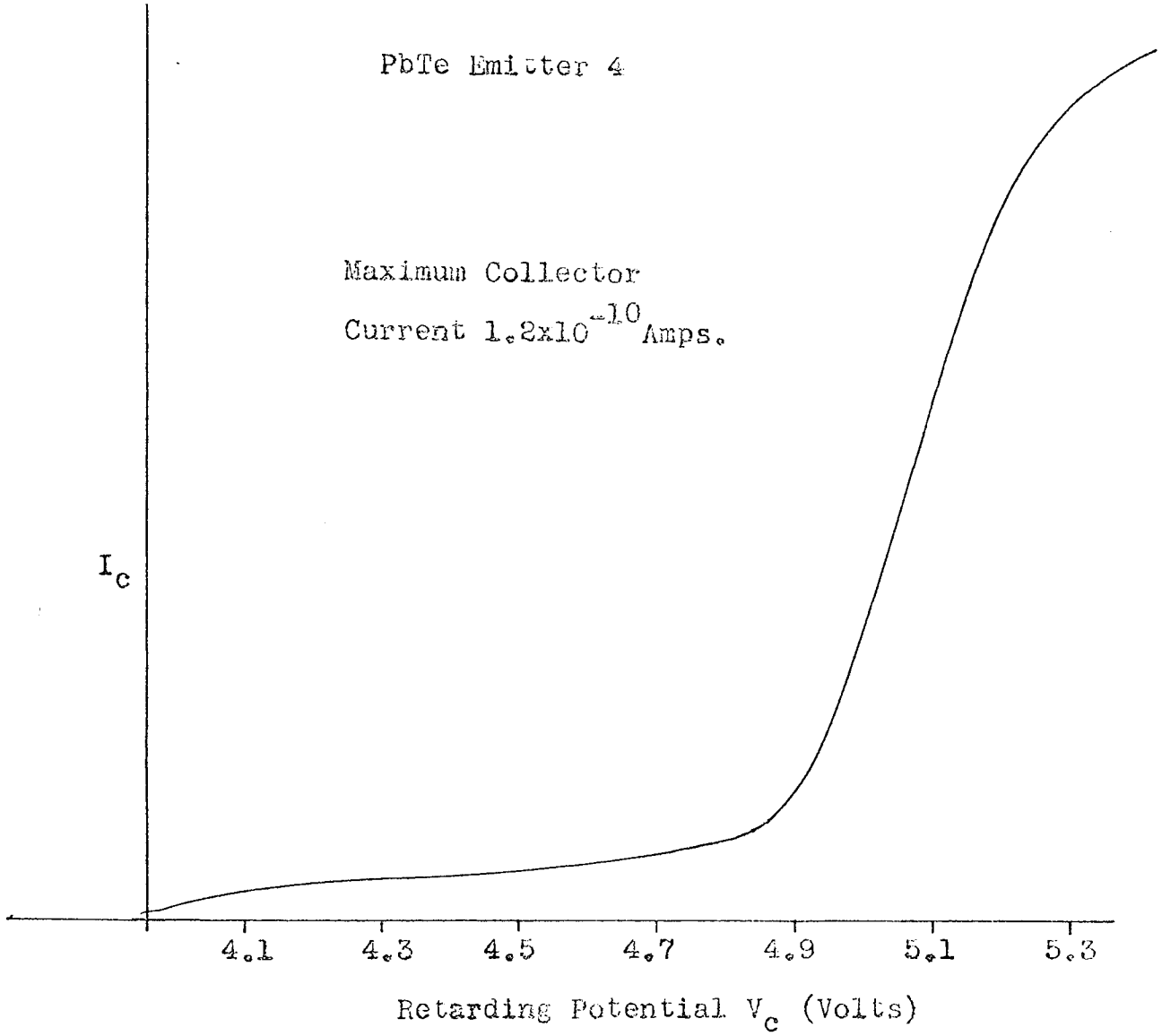
PbTe Emitter 4
Maximum Collector
Current 1.2x10^-10 Amps.
I_c
4.1
4.3
4.5
4.7
4.9
5.1
5.3
Retarding Potential V_c (Volts)

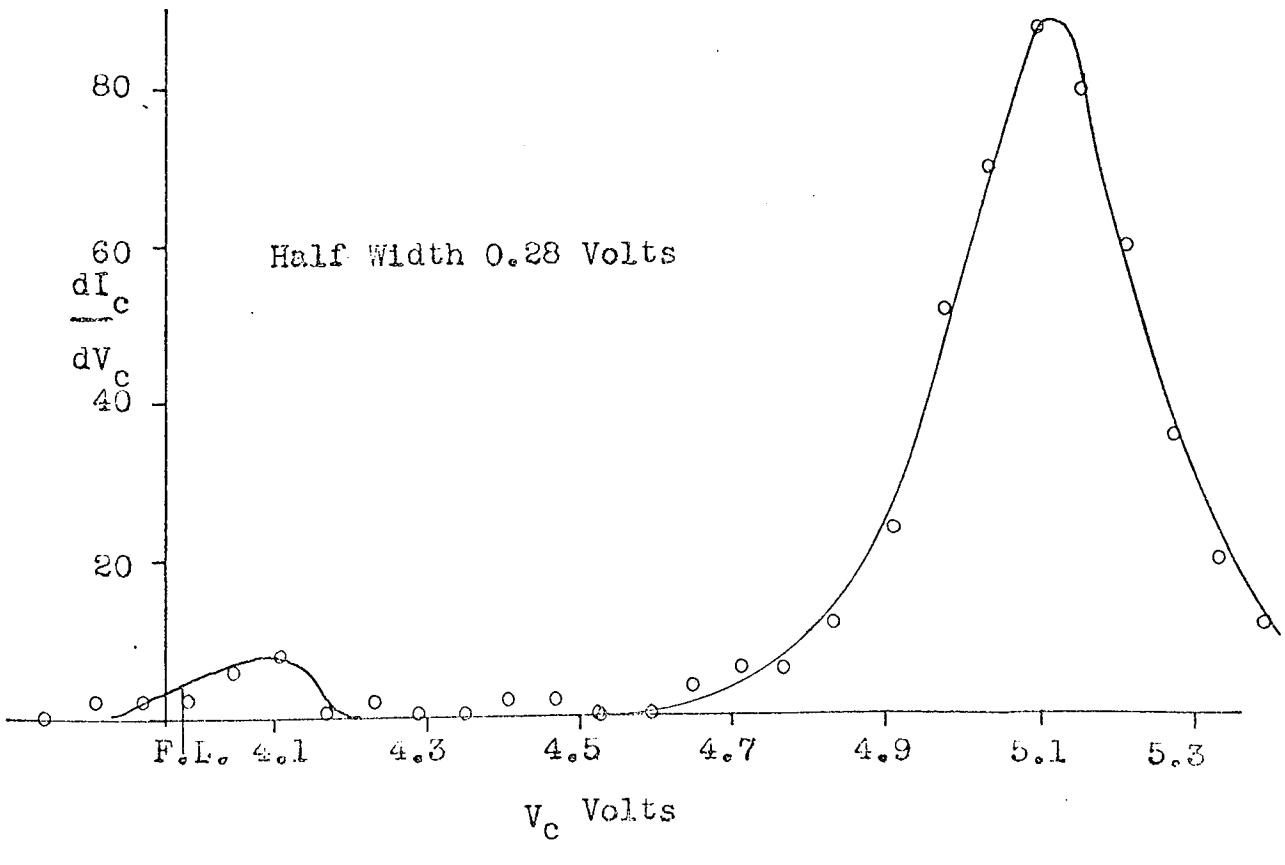
80
60
40
20
dI_c / dV_c
Half Width 0.28 Volts
F.L. 4.1
4.3
4.5
4.7
4.9
5.1
5.3
V_c Volts

Fig. 5.10

PbTe Emitter 4

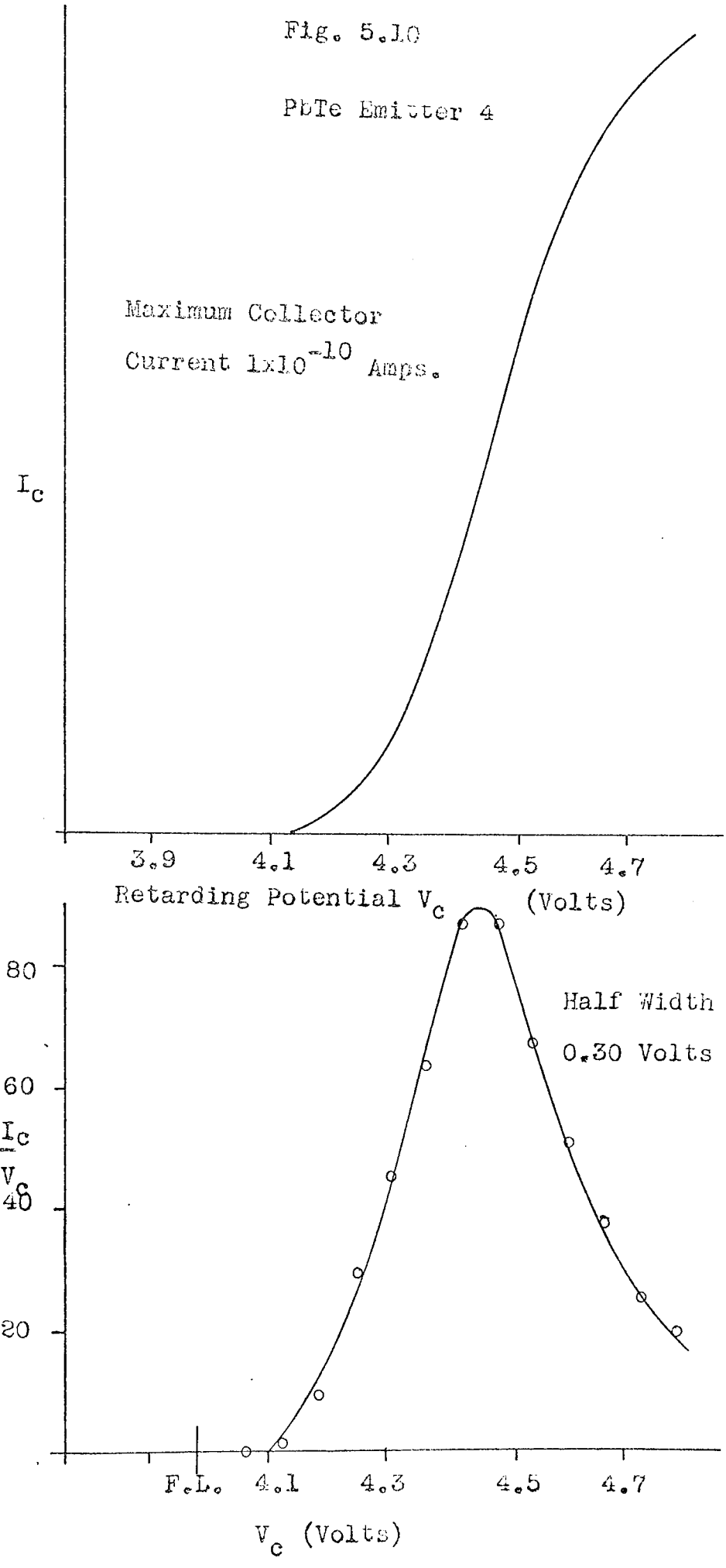

Many more scans were taken than those presented above, generally with several scans taken at any one set of conditions. The distributions presented are representative of the salient features of the distributions observed for each of the specimens.

5.2 b SOME PRELIMINARY RESULTS

Before the main work on lead telluride was undertaken it had been necessary to show that suitable tips could be made from the material and that it was a viable field emitter. The majority of this preliminary work was carried out in the analyser built by Salmon (51) but during the course of the work the electrical properties of the instrument, particularly the insulation of the glassware between the collector and anode leadthrough, deteriorated preventing further investigation without recourse to another instrument. It was for this reason that an analyser, after the design of Van Oostrom (75), was built with which most of the measurements were made. The results from the preliminary work will be presented briefly. The energy distributions shown in this section are not corrected for secondary electron effects (6) but this does not affect the halfwidth of the distributions in this particular instrument (51), these secondary effects do not occur with the Van Oostrom (75) design.

A lead telluride emitter prepared by the method described in section 4.7 b was placed in the simple field emission microscope used for the carbon fibre work and currents up to 1×10^{-5} amps. drawn from it, thus demonstrating that lead telluride was a suitable material for field emission studies. The current voltage characteristics measured at this stage will not be presented. Having established that lead telluride could be used as a successful field emitter two tips were mounted in Salmon's (51) analyser together with two tungsten tips. The results from the tungsten

tips will not be presented as a reliable energy distribution could not be obtained. This was attributed to the fact that the tips were not on the axis of the analyser when the emission pattern was over the probe hole. It was noticed, however, that not only did the halfwidth of the distribution change with tip position but the onset voltage also changed. This should be borne in mind when interpreting the lead telluride distributions measured with this instrument.

The lead telluride emitters were set as closely as possible to the optimum resolution position by use of a cathetometer. Initial application of the high voltage to the emitters produced a turbulent pattern which soon stabilized. The tip was then field evaporated at steadily increasing voltages until a change was produced in the pattern, at about twice the voltage necessary to see a field emission image, revealing a stable central spot. Fig. 5.11 shows some energy distributions taken at this stage at different values of emission current. These results were taken with the room lights on but a scan taken in total darkness Fig. 5.11.c shows no differences. Further field evaporation at successively higher voltages, following shifts in the tip position to keep the pattern over the probe hole, produced a pattern of three spots at the points of an equilateral triangle which developed into an equilateral triangle with a central dark "Y" shaped zone. During the field evaporation electrical breakdown, from the anode lead to the specimen stage, resulted in a temporary incapacity of the ramp generator, consequently the distributions had to be taken manually using the method of Salmon (51). These distributions are shown in Fig. 5.12. By this stage the collected current had become very noisy, due in part to the deterioration of the electrical properties of the glassware in the analyser. The distributions shown in Fig. 5.12 only

Fig. 5.11(a)

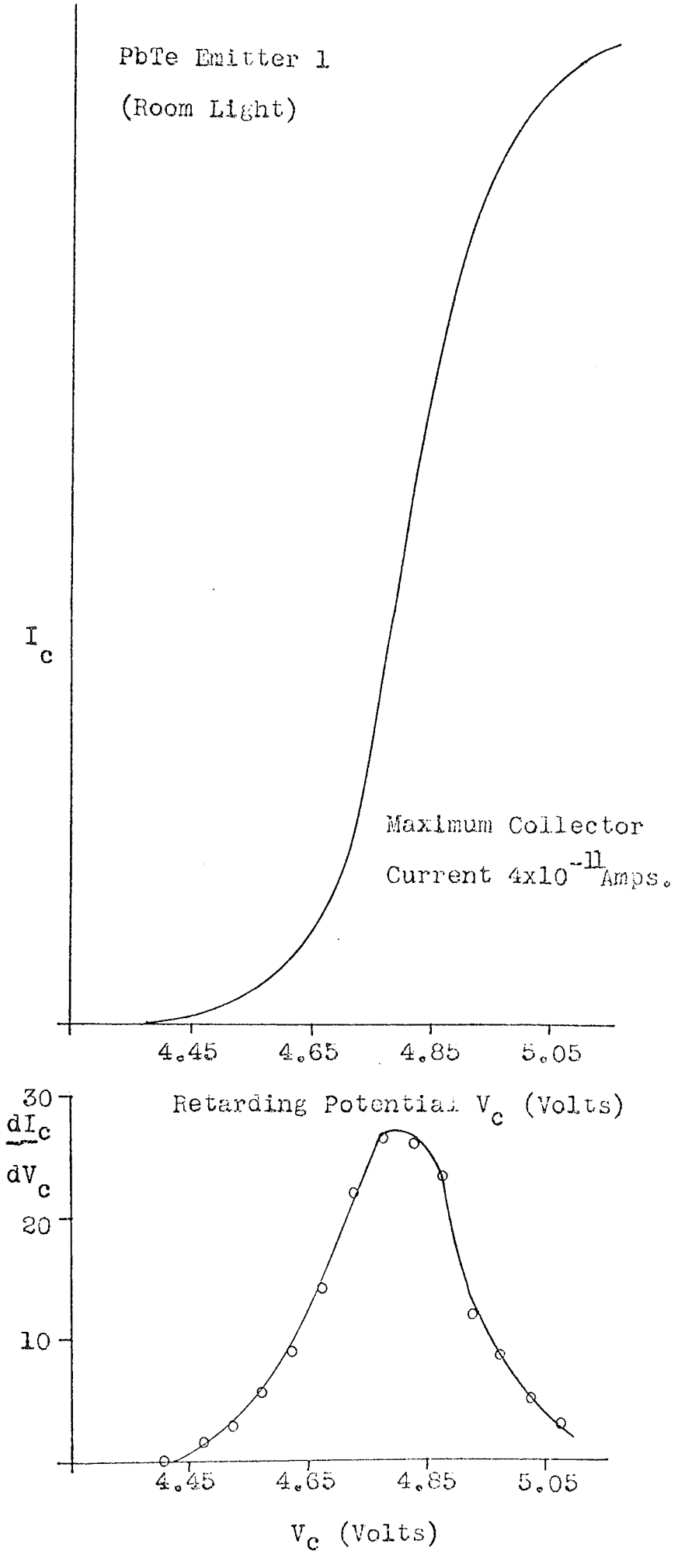
PbTe Emitter 1
(Room Light)
I_c
Maximum Collector
Current 4×10^{-11} Amps.
4.45
4.65
4.85
5.05
Retarding Potential V_c (Volts)
30
$\frac{dI_c}{dV_c}$
20
10
4.45
4.65
4.85
5.05
V_c (Volts)

Fig. 5.11(b)

PbTe Emitter 1

(Room Light)

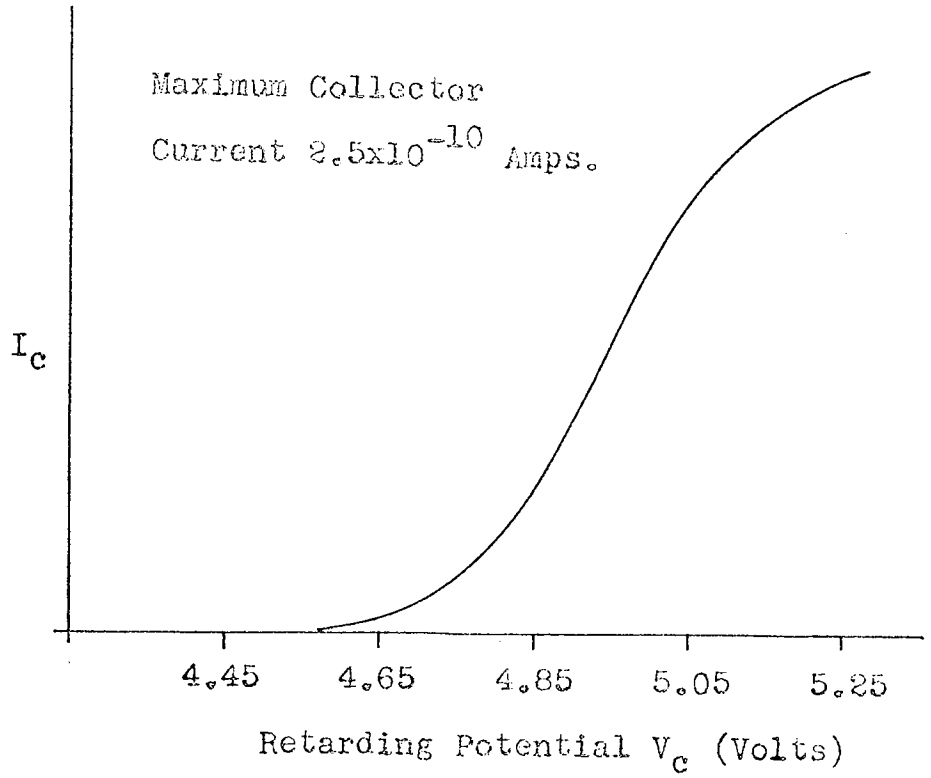

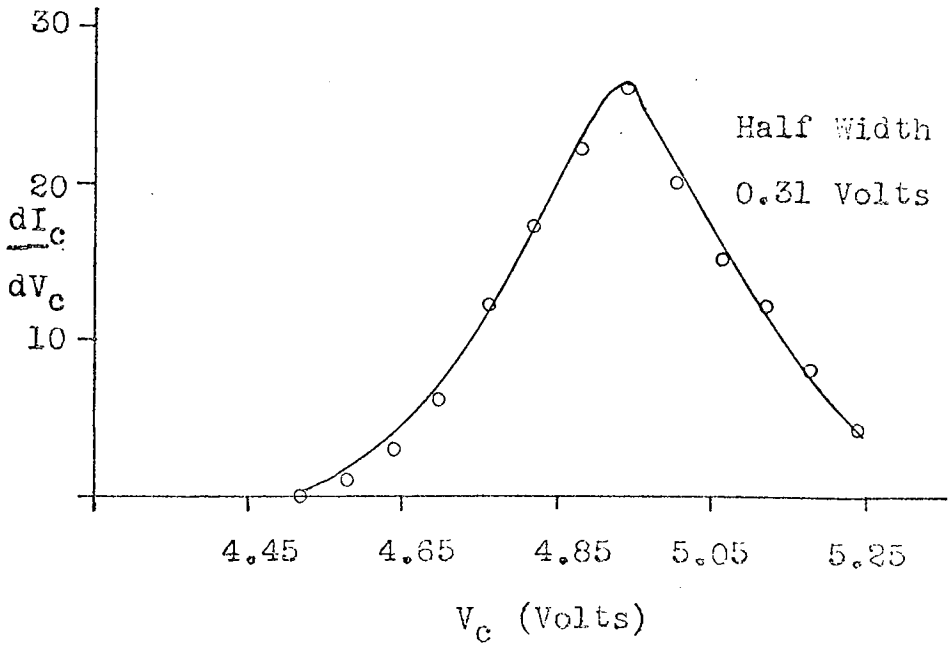

Fig. 11(c)

PbTe Emitter 1

(Total Darkness)

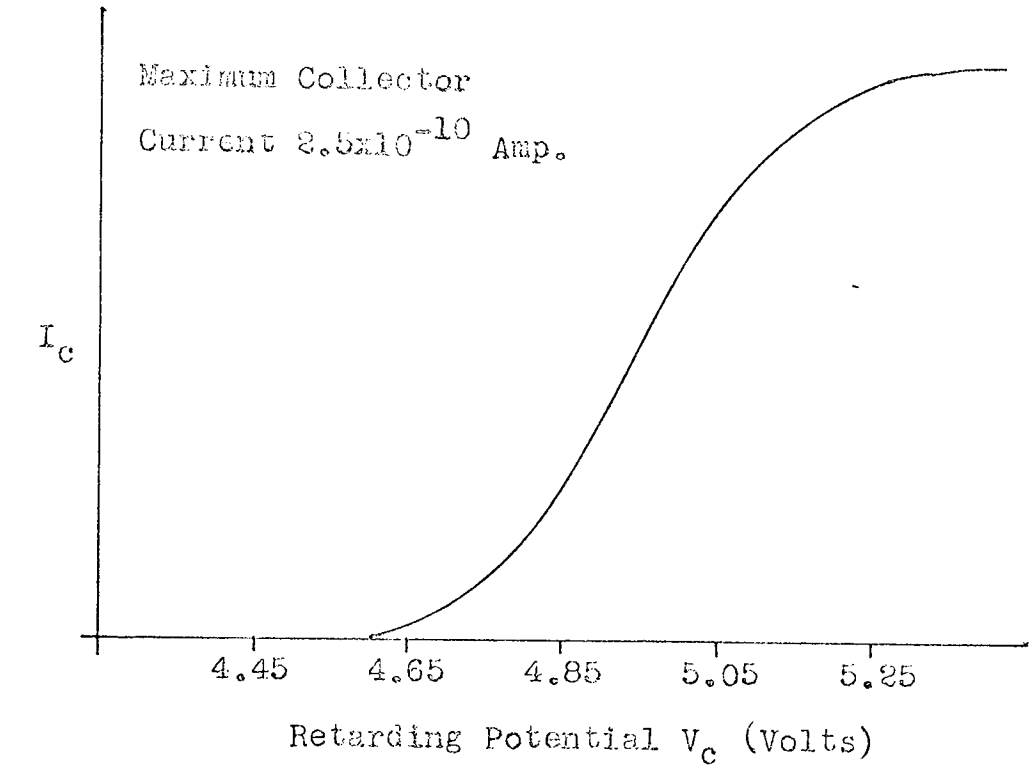

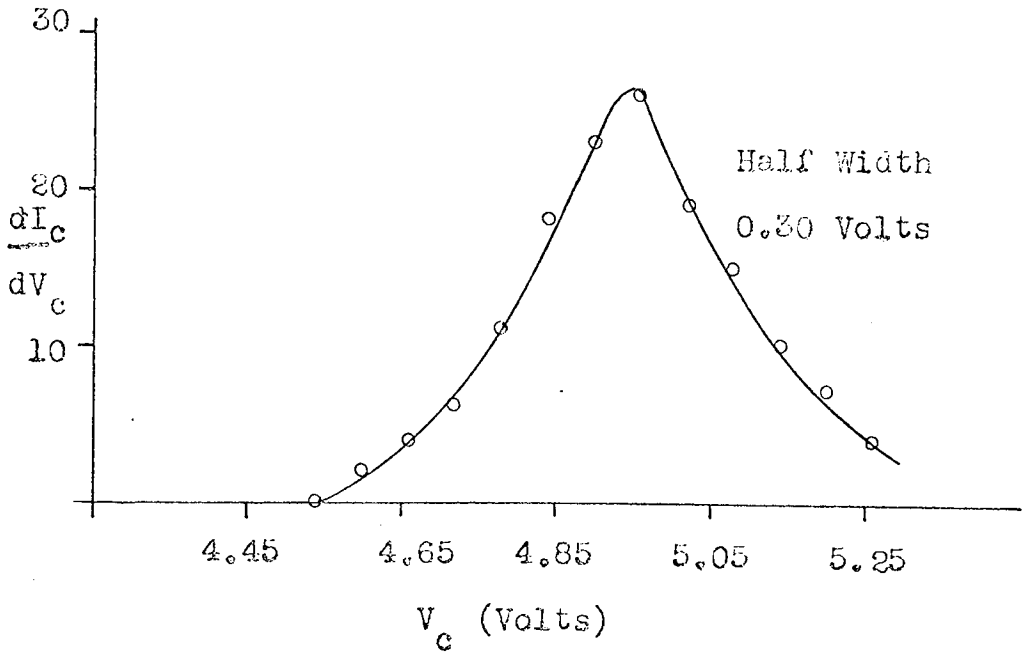

Fig 5.12(a)

PbTe Emitter 1

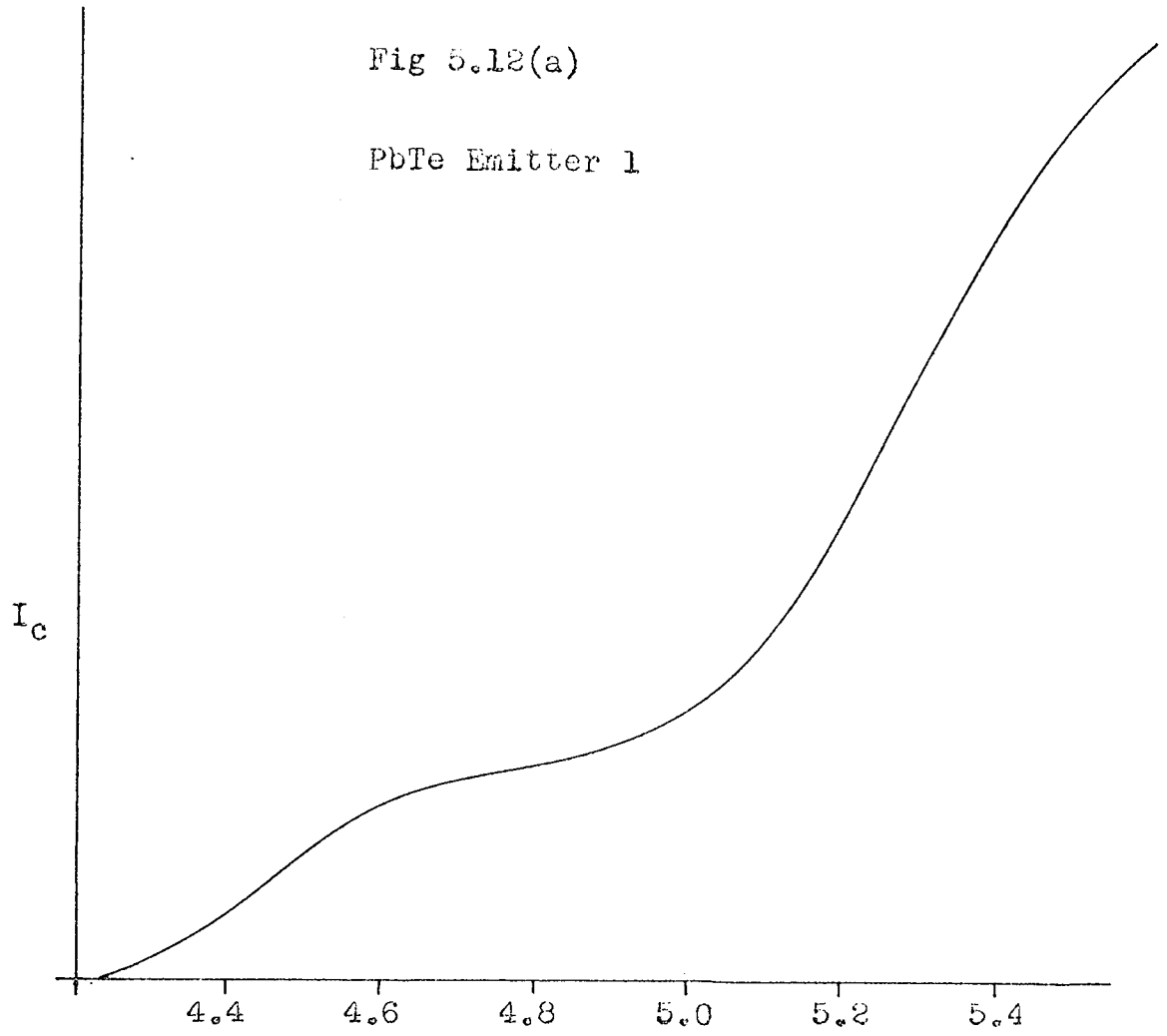

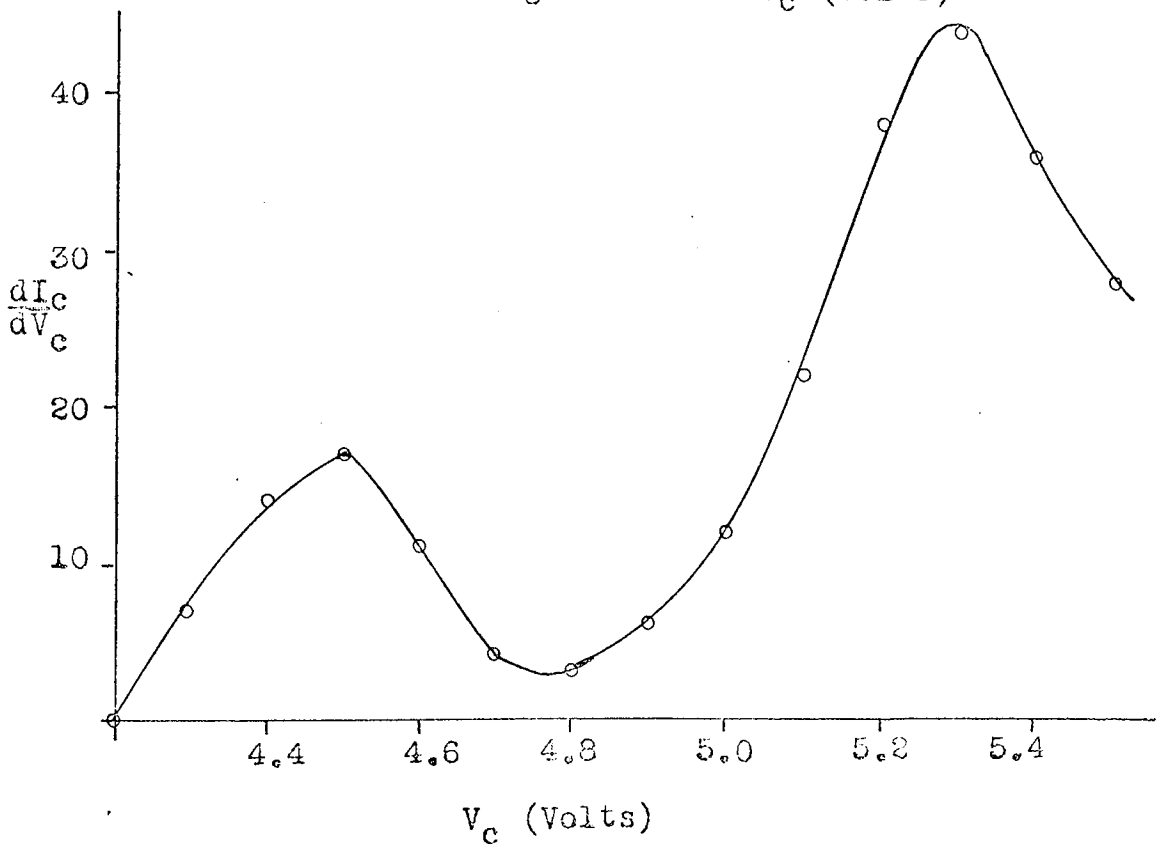

Fig. 5.12(b)

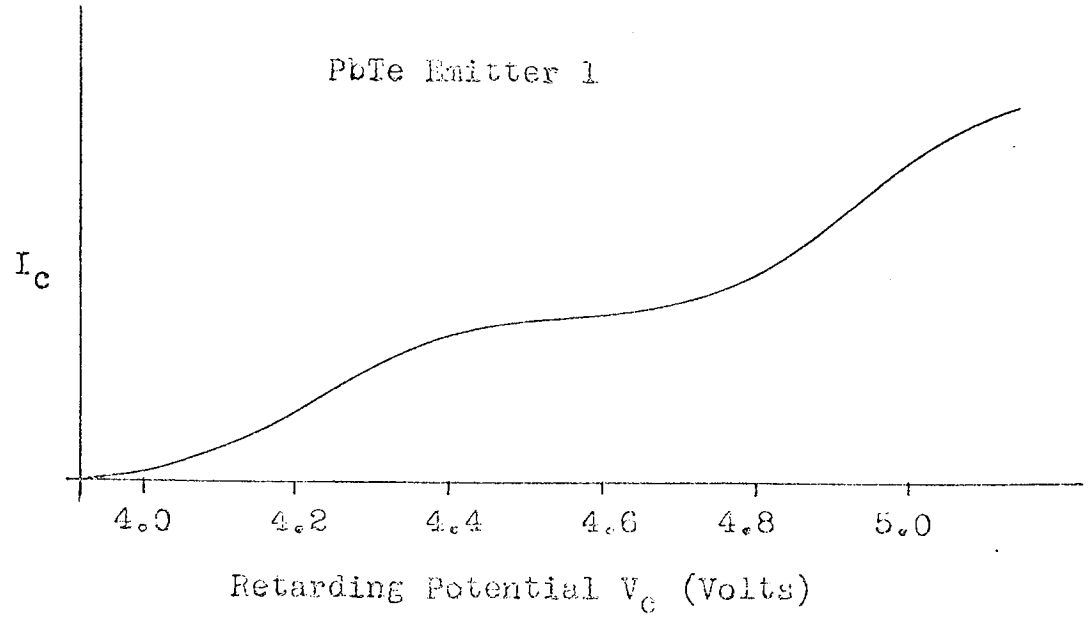
PbTe Emitter 1
I_c
4.0
4.2
4.4
4.6
4.8
5.0
Retarding Potential V_c (Volts)

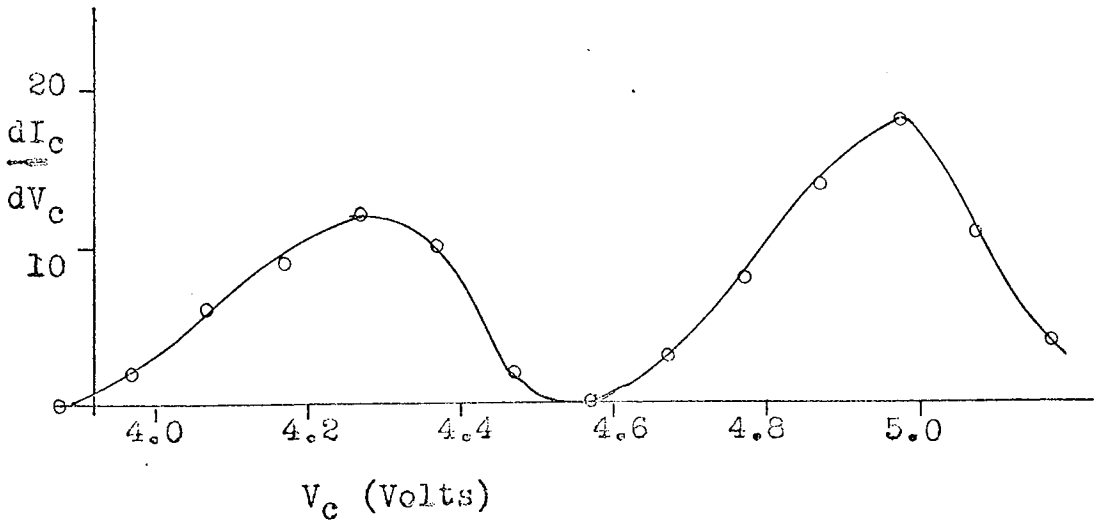
20
$\frac{dI_c}{dV_c}$
10
4.0
4.2
4.4
4.6
4.8
5.0
V_c (Volts)

Fig. 5.12(c)

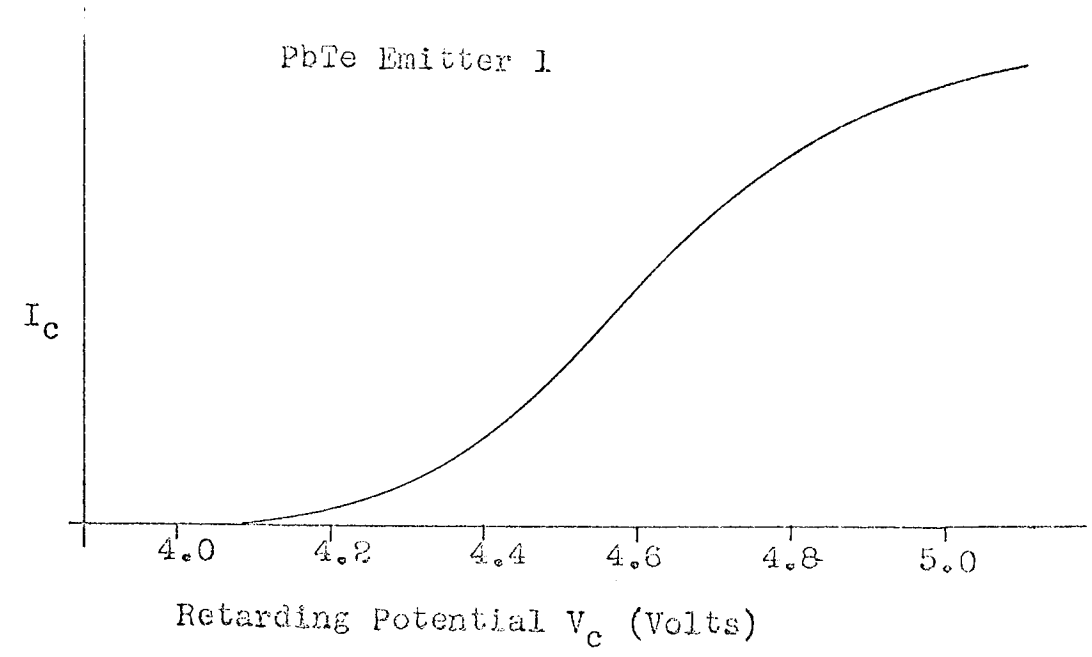
PbTe Emitter 1
I_c
4.0
4.2
4.4
4.6
4.8
5.0
Retarding Potential V_c (Volts)

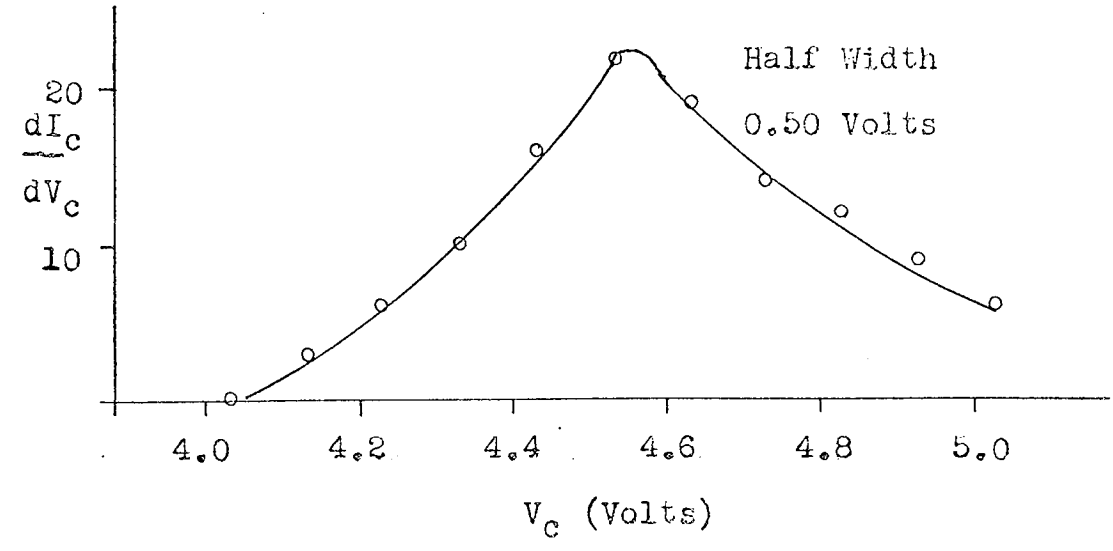
20
$\frac{dI_c}{dV_c}$
10
Half Width
0.50 Volts
4.0
4.2
4.4
4.6
4.8
5.0
V_c (Volts)

represent the general trend of the I_c/V_c curves as the excessive noise makes interpretation difficult.

Field evaporation of the second emitter produced a triangular emission pattern similar to that seen with the first tip. The curves produced, however, were so noisy they could be interpreted as giving energy distributions with halfwidths varying from 0.270 eV to 0.450 eV with no change of conditions. These results, therefore, will not be presented.

5.3 GALLIUM PHOSPHIDE

A preliminary investigation of gallium phosphide was undertaken using the Van Oostrom type analyser following the work on lead telluride. As gallium phosphide is a high resistance material considerable difficulty was experienced in obtaining sensible scans from the specimen. After field evaporation of a specimen a peripheral region between the clean emitting tip and the grossly contaminated shank is formed from which emission can occur, the emission from this region fluctuates, thus the voltage drop along the shank of a high resistance specimen fluctuates whilst the emission from the clean tip remains stable. This mechanism tends to shift the energy distribution along the retarding potential axis as the resistive drop changes. With the gallium phosphide specimen this difficulty was complicated by the fact that the pressure in the system was not much better than 1×10^{-9} torr causing contamination to occur more rapidly than with the lead telluride specimens. The distribution shown in Fig. 5.13 was taken immediately after field desorption whilst the emission current remained sufficiently stable to give a reasonable scan.

5.4 FOWLER-NORDHEIM PLOTS

Fowler-Nordheim plots were not taken as often as would have been desired as the V.G. picoameter used for measurement of the total current was not always in working order. Fig. 5.14 shows a plot taken for tip 5 and Fig. 5.15 a plot using the analogue device, discussed in Chapter 4, over the same range. It was not possible to measure Fowler-Nordheim characteristics for the gallium phosphide emitter due to the extremely unstable nature of the emission current.

Fig. 5.13

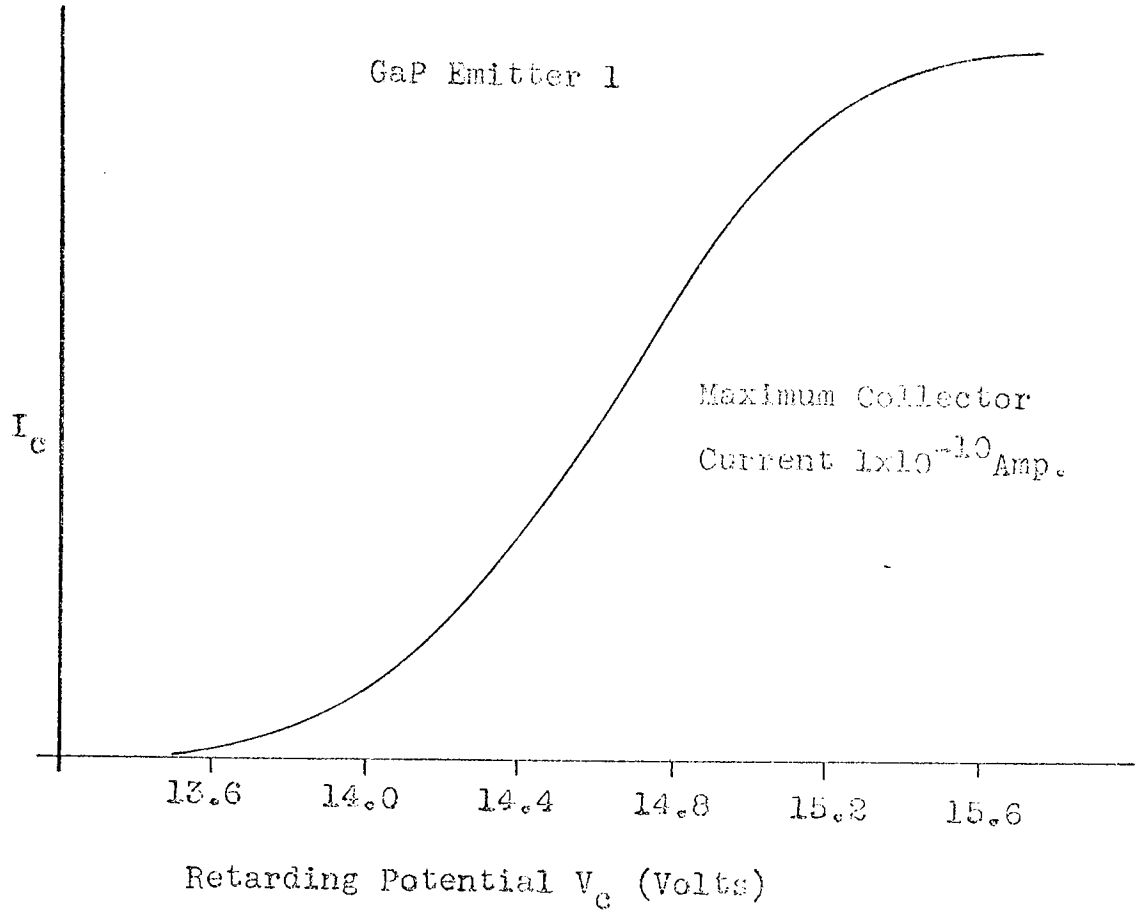
GaP Emitter 1
Maximum Collector
Current 1×10^{-10} Amp.
I_c
13.6
14.0
14.4
14.8
15.2
15.6
Retarding Potential V_c (Volts)

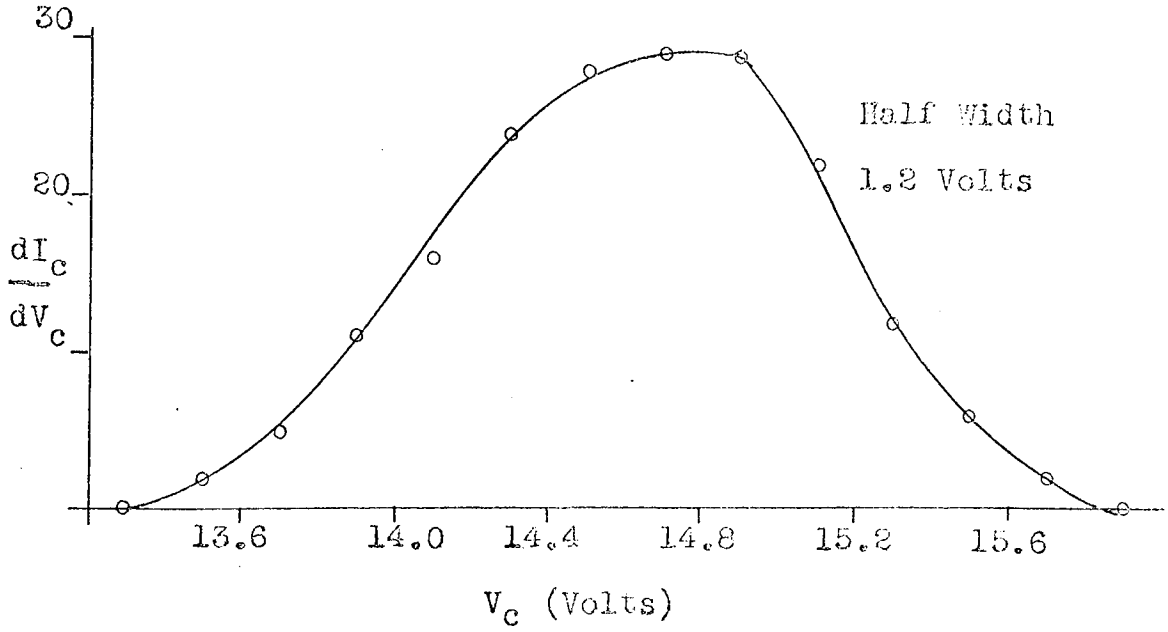
30
20
$\frac{dI_c}{dV_c}$
Half Width
1.2 Volts
13.6
14.0
14.4
14.8
15.2
15.6
V_c (Volts)

Fig. 5.14

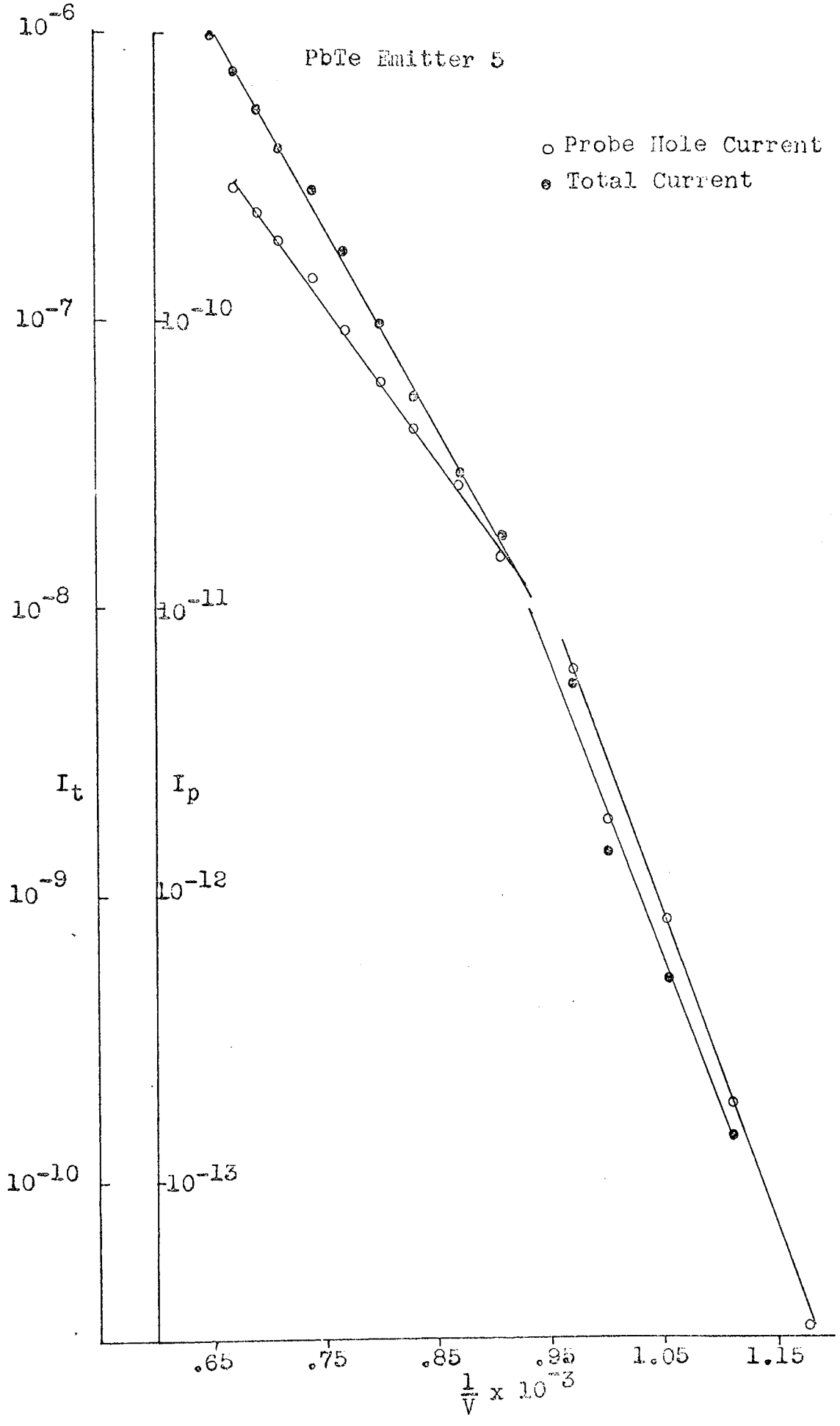
PbTe Emitter 5
o Probe Hole Current
• Total Current
10^{-6}
10^{-7}
10^{-8}
10^{-9}
10^{-10}
I_t
10^{-10}
10^{-11}
10^{-12}
10^{-13}
I_p
.65
.75
.85
.95
1.05
1.15
$\frac{1}{V} \times 10^{-3}$

Fig. 5.15

PbTe Emitter 5

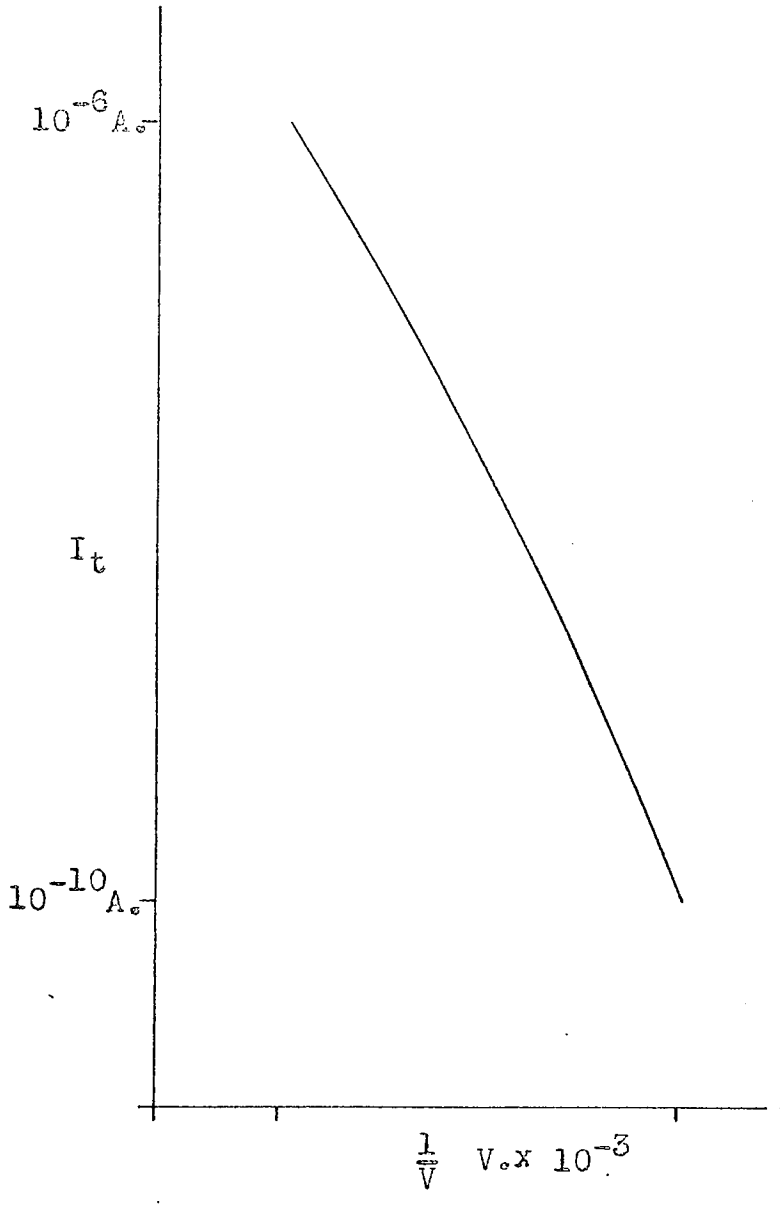

CHAPTER 6

DISCUSSION OF RESULTS

6.1 THE RESULTS FROM SALMON'S ANALYSER

The preliminary results from Salmon's analyser showed initially that emission from a field evaporated surface of lead telluride could give reasonably narrow energy distributions. The double humped distributions, however, must be artefacts of the analyser, as they bear no apparent resemblance to the electronic structure of the emitter either in the width or separation of the peaks. They were obtained from a clean surface, as indicated by the presence of a stable symmetrical emission pattern, but the emitter had been shifted from the position in which narrow distributions were obtained. The double humped structure is possibly due to inhomogeneity in the collector. In fabricating the collector the tin oxide coating did not completely cover the glass sphere and so a layer of aquadag had been applied to the non-conducting area. This would result in the collector having two regions of different workfunction and consequently electrons of equal energy falling across the boundary would be collected at different values of retarding potential producing a double humped distribution. The patch of aquadag was located 20° to 30° away from the axis of the system (within the limit of angular confinement of the electrons imposed by the collimating tube and apertures used in the anode) so, although paraxial electrons, originating from a tip at the position of optimum resolution, could not fall upon it, electrons from a tip off the axis could. This is consistent with the fact that double humped distributions were only found with wide peaks and Salmon's observation that double humps were associated with emission from the edge of the pattern, leading him to conclude that he was seeing emission from

from contamination states. Salmon's interpretation should not be dismissed, however, as the double humped distributions observed in the present work were narrower than those observed by Salmon and were never observed with the tungsten emitters.

The nature of the collector could also account for the observed broadening of the energy distributions with collected current, observed for tungsten as well as the other materials. The thin film of tin oxide forming the collector has a finite resistance and this could introduce a voltage drop between the point at which the electrons were collected and the collector leadthrough thus apparently broadening the energy distribution with increasing currents. This hypothesis is consistent with the observation from the present work that the onset voltage (from the tungsten results) shifted with the tip position; as the tip was manipulated the collected electrons would reach different parts of the collector and so experience a different voltage drop depending on the resistance of the collector between the point of collection and the feedthrough.

The broadening with current density could equally well be attributed to the interactions discussed by Salmon (51) as this design of instrument seems particularly sensitive to such anomolous effects. No such effects, however, were observed with the Van Oostrom analyser over the range of emitted currents investigated.

Despite the inability, in the present work, to produce sensible results from tungsten specimens and the subsequent deterioration of the analyser it had been capable of giving reasonable measurements when correctly used. This is illustrated by the work on carbon fibres presented in Chapter 3 and the work of Salmon (51) is in no way disputed.

6.2 THE MAIN RESULTS FROM LEAD TELLURIDE

The emission pattern of three spots at the points of an equilateral triangle was taken to be indicative of a clean surface as it was of the correct symmetry and usually found after field desorption. In some cases, however, such a pattern was found simply by increasing the applied voltage, but in such instances the pattern was always preceded by a flash at a lower voltage. This sequence is similar to effects observed as the field is increased in a field-ion microscope, before any pattern is visible a flash is seen as the surface contamination desorbs followed by a clean pattern at higher fields. Lead telluride is a highly ionic material so, although the polarity of the voltage is reversed with respect to the field-ion situation, the negative ions in the structure will experience a force similar to that experienced by the ions in the field-ion specimen and could be stripped off by the field. This mechanism would create a clean surface simply by turning up the emission voltage and would explain why patterns produced after a flash were insensitive to heating and field desorption.

Fig. 6.1 shows a typical experimental distribution from a clean lead telluride emitter compared with the theoretical prediction of Modinos (39) for a germanium emitter (with the parameter taken to be five times larger than that for the distributions which resemble the experimental work of Shepherd and Peria (38)). In this case the emission from the surface states is much greater than the valence band emission. The similarity between the experimental results of the present work and the theory is striking. Table 6.1 shows the parameters for germanium, used by Modinos to analyse his results, with the corresponding parameters for lead telluride as far as they are known.

Fig. 6.1

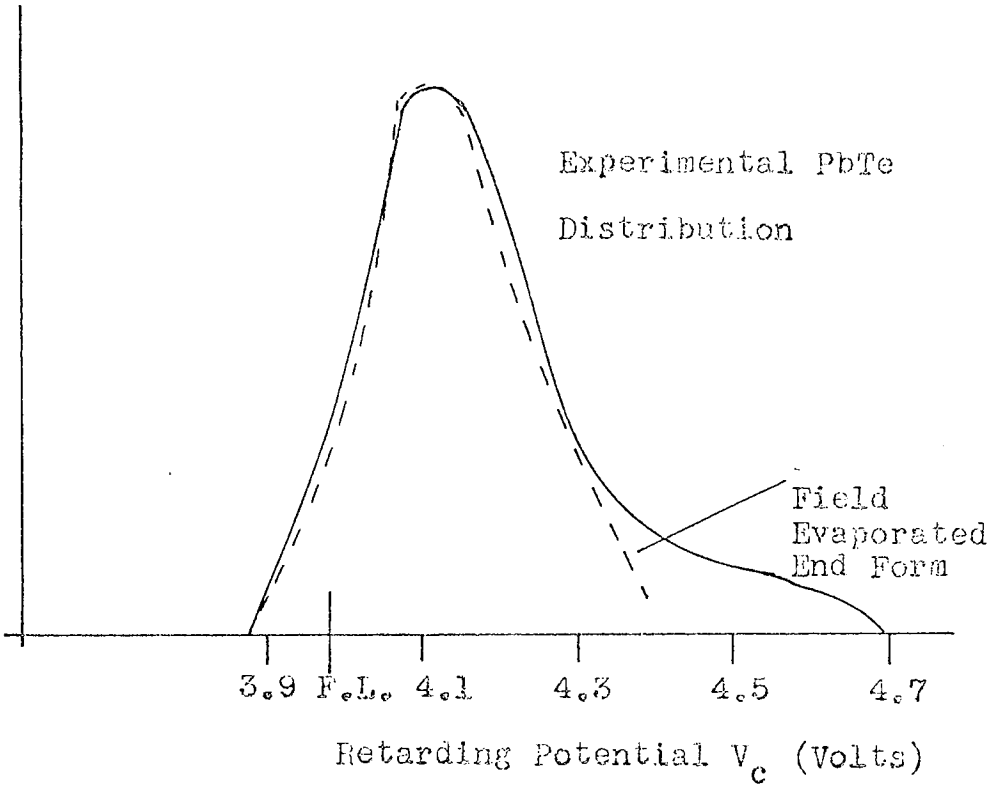
Experimental PbTe
Distribution
Field
Evaporated
End Form
3.9 F.L. 4.1 4.3 4.5 4.7
Retarding Potential V_c (Volts)

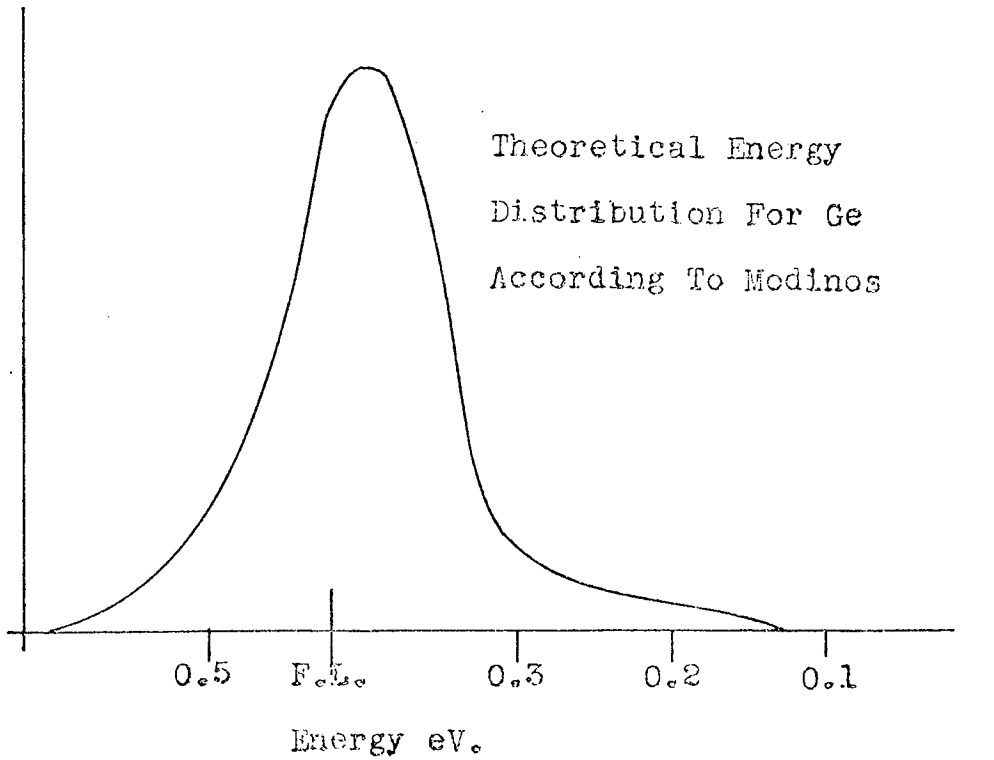
Theoretical Energy
Distribution For Ge
According To Modinos
0.5 F.L. 0.3 0.2 0.1
Energy eV.

TABLE 6.1

PARAMETER	GERMANIUM	LEAD TELLURIDE	
M_c	0.55 m	0.034 m	(78)
M_v	0.3 m	0.032 m	(78)
N_i	$1.5 \times 10^{13} cm^{-3}$	$1.5 \times 10^{16} cm^{-3}$	(78)
ε	16	380	(78)
Eg	0.67 eV	0.31 eV	(78)
ψ	4 eV	$4.6 \pm .3$ eV	(79)
No	10^{14} $eV^{-1} cm^{-2}$	2×10^{13} $eV^{-1} cm^{-2}$	(80)
Eo	-0.05 eV	+ 0.05 eV	(80)
S	10^{-17} cm^2	-	
θ	0.01 $\AA^{-1}$	-	

As can be seen the greatest differences are the effective masses, dielectric constant and intrinsic concentration of carriers. If the parameters for the surface states are of roughly the same order as those for germanium the surface state emission from lead telluride will be of similar magnitude to that from germanium but will dominate the energy distribution as the valence and conduction band emission will be relatively suppressed by virtue of the very small effective masses. In the expression for the total energy distribution emitted from the valence band :

$$P(E_v) = \frac{4\pi M_v e}{h^3 c_{v0}} f_v(E_v) \exp(-b_{v0} - c_{v0} E_v)(1 - \exp(-c_{v0} r_v E_v))$$

where M_v is the effective mass of the valence band hole and $r_v \equiv \frac{M_v}{M}$ M is the free electron mass, the majority of the terms will differ only slightly between lead telluride and germanium. The pre-exponential will, however, be reduced by a factor of about ten by the lower effective mass, which is about a factor of ten less than that for germanium, and the last term in the expression :

$$1 - \exp(-c_{v0}\,\Gamma_v\,E_v)$$

will be reduced also as it too contains the effective mass, thus attenuating the valence band emission from lead telluride relative to valence band emission from germanium. By a similar argument conduction band emission from lead telluride is suppressed whilst the surface state emission remains of similar magnitude.

The greater intrinsic concentration in lead telluride means that, despite the greater dielectric constant, the space charge region will not penetrate as deeply into the bulk as in germanium, the energy bands, if bent, will be bent more sharply. The existence of such a high intrinsic concentration of carriers, however, implies that, as the field lines must terminate on charges (and assuming a similar density of surface charge) band bending will be considerably less than in germanium under similar conditions.

The energy distributions obtained, narrow metalike distributions with a maximum just below the Fermi level, occasionally with a low energy shoulder, could be interpreted as emission from a degenerate conduction band with intermittent surface state emission due to some contamination. This interpretation would be consistent with the observation that the distribution does not widen or shift with increasing field, as would be expected if the conduction band was always degenerate. It is more likely, however, that most of the emission comes from the surface states due to the reasons outlined above and that the low energy shoulder is valence band emission. The band gap of lead telluride is so small that conduction band emission as well as valence band and surface state emission must be present but the

resolution and sensitivity of the analyser are not sufficient to adequately isolate the separate components of the distribution.

The time dependence of some of the results indicates that after a slight change of field the surface state and valence band emission can be resolved but after a few minutes at constant field the surface state band has broadened slightly and completely obscured the valence band emission. This slow relaxation must be associated with the surface states coming to equilibrium after a change of field but is not thought to be related to the more common slow surface states often observed on contaminated semiconductor surfaces. The slow states are formed by exposing a specimen to a humid atmosphere, at air pressure, for several days; time dependent effects lasting up to several hours can then be observed. The states, once formed, are known to remain in moderate vacuua but can be lost by heating to 200°C in a vacuum of about 10^{-9} torr (81). It seems unlikely, therefore, that the time dependent effects observed are due to conventional slow states as these would have been destroyed by the bakeout cycle and the subsequent attainment of ultra-high vacuum conditions, moreover, the presence of a stable symmetrical field emission pattern indicates that the surface is clean.

Time dependent effects have been observed by Fursei et. al. (82) in pulsed field emission currents drawn from p-type silicon. These effects occur within a fraction of a second and are attributed to the rate of carrier generation in the bulk; similar effects were not observed with n-type material. The time dependant effects observed in the present work justify further investigation as their time scale falls midway between that for slow states and that for the fast effects reported by Fursei.

The lack of movement of the peak with changing field whilst not confirming the argument in favour of surface state emission does not destroy it. As explained above, band bending in lead telluride is not as great as in germanium, consequently, for the limited range of fields used in the present work, significant band bending would probably not occur and so no shift in the position of the peak would be expected. The large shift and broadening observed with one specimen must be interpreted as a non-ohmic contact or emission from a grossly contaminated surface in poor electrical contact with the bulk as harsh field evaporation produced a narrow distribution, moreover the same specimen, with a new endform etched on the crystal and more silver dag applied to the contact between the crystal and the support filament, produced consistent narrow distributions. A non-ohmic contact between the emitting surface and the support structure could account for the large shift in onset, a plot of total current against onset voltage was more logarithmic than linear, and could explain the broadening as the effective retarding potential would be less than that applied. The broadening of the distribution could be due, in part, to the "hot electron" effect. Electrons could be injected into the specimen at a point in the energy bands well above that at which they would reside were they in thermal equilibrium or had they come through an ohmic contact. If the lifetime of the electrons in these states is longer than the time taken for the electrons to reach the surface they would be emitted with energies well above those normally observed. Although the number of such electrons is probably small they could constitute a significant emission current as their tunnelling probability would be larger than for electrons near the Fermi level at the surface. This explanation would account for the high energy tail observed with this specimen.

6.3 GALLIUM PHOSPHIDE

The energy distribution obtained from the one specimen used is only a preliminary result and so will not be considered in great detail. Gallium phosphide is a large band gap material and consequently has a high resistance, this makes positioning of the distribution with respect to the Fermi level impossible. The voltage drop along the specimen was of approximately the same order as that found by Salmon (51) for cadmium sulphide; the band gaps of gallium phosphide and cadmium sulphide are of similar proportion. The energy distributions for high resistance materials are difficult to measure as small fluctuations in total current can shift the distribution up or down the retarding potential axis as described by Salmon (51) and previously in the present work. The energy distribution shown, however, is thought to be representative of the distribution for gallium phosphide despite the danger in making judgements from one specimen. The large halfwidth of the distribution could possibly be explained in terms of a poor contact to the crystal but, even so, it is difficult to see the halfwidth reducing to a value comparable to that obtained for lead telluride. The result closely resembles the single peaked distributions of Salmon for cadmium sulphide.

6.4 THE ROLE OF SURFACE STATES IN THE EMISSION PROCESS

The experimental results of the present work, outlined above, together with those of Salmon for cadmium sulphide (51), Hughes and White (36) for gallium arsenide, Arthur (35) for germanium, and Shepherd and Peria (38) again for germanium, show a slight correlation between the energy gap of the material used and the halfwidth of the experimental distribution, Table 6.2.

TABLE 6.2

MATERIAL	ENERGY GAP (eV)	DISTRIBUTION HALFWIDTH (eV)	
Pb Te	0.30	0.24	Present Work
Ge	0.67	0.4	(35)
"	"	0.2 + valence band shoulder	(38)
GaAs	1.37	0.6	(36)
GaP	2.26	1.2	Present Work
CdS	2.40	0.6 to 0.7	(51)

It is only in the work of Shepherd and Peria, and the theoretical work of Modinos (39), that surface state emission has been seriously considered. Other workers have associated surface states with contamination rather than considering their role in the emission process as a major contributor. Surface states have to some extent been treated as artefacts and not as an intrinsic property of a semiconductor surface that can significantly participate in the emission. It is difficult to see how valence, or conduction, band emission could be expected to produce energy distributions greatly different in halfwidth from those of metallic distributions, when in thermal equilibrium, as the barrier will be of roughly the same shape and hence the tunnelling probabilities will reduce exponentially with decreasing energy. With surface states, however, the situation is slightly more complex as the localisation of the state can affect the emission current as well as the density of states and barrier thickness. It is conceivable that wide distributions could be obtained from surface states of uniform density with a triangular barrier, if the localisation of the states increases with decreasing energy, conversely

wide distributions could be produced from uniformly localised states if their density increased at lower energies; any intermediate situation would also produce broad distributions. It is quite possible that for large band gap materials the surface state density, although potentially uniform, will only be partly filled at higher energies with the majority of the electrons residing towards the bottom of the band gap, thus producing wide energy distributions.

In the works cited above where critical bias measurements have been possible the emission has always been found below the Fermi level, this led Arthur (35) to conclude he was seeing emission from a degenerate conduction band, but as identical results were obtained for (111) and (100) oriented crystals, this is extremely unlikely as in the (100) orientation conduction band emission is greatly reduced by virtue of the high transverse momenta of the conduction band electrons. Hughes and White (36) found emission from well below the Fermi level and concluded valence band emission, however, their result is not incompatible with surface state emission although they do not report any shift of the distribution with applied field, and detected no broadening with field.

6.5 SUGGESTIONS FOR FUTURE WORK

6.5 a EXPERIMENTAL TECHNIQUES

The operation of the Van Oostrum type analyser used for the majority of this work could be improved by the use of a modulated ramp with synchronous detection of the a.c. component of the collected current after the method of Russel (83). This technique would greatly improve the signal to noise ratio of the analyser and would facilitate the direct plotting of the energy distribution by detecting the signal at the second

harmonic frequency of the modulation. This system, whilst not improving the ultimate resolution of the analyser would make the instrument easier to use as the direct presentation of the energy distribution makes interpretation much simpler and information is not lost by manual differentiation. The method was not used in the present work as it had never been used in this laboratory, as physical constraints of the previous analysers made its use impossible, and time did not allow the development of such a system.

The inclusion of a gas line to the vacuum system to allow the controlled introduction of known gases to the chamber would be desirable. This would make cleaning of the tips possible by hydrogen promoted field evaporation after the method of Arthur (35) or by bombardment with inert gas ions. The emission characteristics could then be studied for field evaporated, sputtered and annealed surfaces to investigate the effect of order and disorder of the last few atomic layers of a clean emitter.

The use of an electrostatic deflection analyser, similar to that used by Plummer (10), would reveal even more structure in the energy distribution than the improvements to the present analyser described above. This type of analyser measures the energy distribution directly without recourse to differentiation; it has a resolution far superior to retarding potential analysers with much improved signal to noise characteristics as its mode of operation enables the use of an electron multiplier. With this type of instrument it should be possible to see conduction band emission even if it is orders of magnitude less than the surface state emission and to resolve surface state and valence band

emission. The use of a superior pumping system, with such an analyser, with an ultimate pressure in the 10^{-11} torr range or better would be desirable as this would allow a reasonable time to perform experiments on clean surfaces and possibly to note the effects of the slow contamination of the specimen. Facilities for gas handling should certainly be included in such a system.

6.5 b MATERIALS

The tentative suggestion put forward earlier in this chapter that surface state effects dominate the field emission process from semiconductors and that it is the surface states that produce the wide energy distributions can be tested by a systematic investigation of a range of materials of different band gaps. Investigation of a range of conductivities and types of each material would be worthwhile if only to show similar results as Modinos (39) predicts. Care should be taken with the high resistivity materials as it is difficult to locate the distribution with respect to the Fermi level if too high an emission current is drawn.

The prediction by Modinos (39) that the energy distribution should shift to lower energies with increase of applied field is a difficult effect to investigate experimentally as the field required to observe any shift could be sufficient to destroy the emitter by drawing too high an emission current. Higher fields could be applied safely if the specimens were cooled first but this may be counter-productive as it could limit the rate of generation of carriers in the bands and the supply to the surface states. Arthur (35) reports energy distributions measured at 20° K so this

problem is obviously not serious for germanium. Experiments at low temperatures would be worthwhile as higher fields can be applied without destruction of the tip and the electronic structure of the specimen should be sharpened.

REFERENCES

1. W.P. Dyke and W.W. Dolan : Adv. Electron. Electron Physics. 8,89 (1959)
2. J.W. Gadzuk and E.W. Plummer : Rev. Mod. Phys. 45, 487 (1973)
3. R.H. Fowler and L. Nordheim : Proc. Roy. Soc. Lond., Ser. A 119, 173 (1928)
4. L. Nordheim : Proc. Roy. Soc. Lond., Ser. A 121, 626 (1928)
5. E.W. Müller : Z. Physik. 106, 541 (1937)
6. R.D. Young and E.W. Müller : Phys. Rev. 113, 115 (1959)
7. R.D. Young : Phys. Rev. 113, 110 (1959)
8. J.E. Henderson and R.E. Badgley : Phys. Rev. 38, 590 (1931)
9. E.W. Müller : Z. Physik. 120, 261 (1943)
10. E.W. Plummer and C.E. Kuyatt : Rev. Sci. Instrum. 43, 108 (1972)
11. L. Apker and E. Taft : Phys. Rev. 88, 1037 (1952)
12. R. Stratton : Proc. Phys. Soc. (London). B68, 746 (1955)
13. R.L. Perry : Office of Naval Research Final Report, Project N8ONR - 72401, Authority NR072-171 (May 1957) p. 13.
14. M.I. Elison and G.F. Vasiliev : Radiotekh. i Electron. 4, 728 (1959)
15. R.L. Perry : J. Appl. Phys. 32, 128 (1961)
16. F.G. Allen : J. Phys. Chem. Solids 8, 119 (1959)
17. A.I. Klimin, B.N. Sedykh and I.L. Sokol'skaya : Sov. Phys. Solid State 2, 1673 (1961)
18. R. Stratton : Phys. Rev. 125, 67 (1962)
19. F.G. Allen : (unpublished)
20. W.R. Savage : J. Appl. Phys. 34, 732 (1963)
21. J.R. Arthur : J. Phys. Chem. Solids 25, 583 (1964)
22. J.R. Arthur : J. Appl. Phys. 36, 3221 (1965)
23. L. Ernst : Phys. Stat. Sol. 24, 177 (1967)
24. J. Marien and J. Loosveldt : Phys. Stat. Sol. (a) 8, 213 (1971)

25. J. Marien, R. Leysen and H. van Hove : Phys. Stat. Sol. (a) 5,121 (1971)

26. R. Leysen, H. van Hove, J. Marien and J. Loosveldt : Phys. Stat. Sol. (a) 11, 539 (1972)

27. L.M. Baskin, O.I. Lvov and G.N. Fursei : Phys. Stat. Sol. (b) 47, 49 (1971)

28. A.M. Russel : Phys. Rev. Letters 9, 417 (1962)

29. A.M. Russel and E. Litov : Appl. Phys. Letters 2, 64 (1963)

30. G.P. Shcherbakov and I.L. Skol'skaya : Sov. Phys. Solid State 4, 2581 (1963)

31. M.S. Kagan, T.M. Lifshits, A.L. Musatov and A.A. Sheronov : Sov. Phys. Solid State 6, 563 (1964)

32. R. Stratton : Phys. Rev. 135, A794 (1964)

33. R. Fischer : Phys. Stat. Sol. 2, 1088 (1962)

34. R. Fischer : Phys. Stat. Sol. 2, 1466 (1962)

35. J.R. Arthur : Surf. Sci. 2, 389 (1964)

36. O.H. Hughes and P.M. White : Phys. Stat. Sol. 33, 309 (1969)

37. L.T.J. Salmon and E. Braun : Phys. Stat. Sol. (a) 16, 527 (1973)

38. W.B. Shepherd and W.T. Peria : Surf. Sci. 38, 461 (1973)

39. A. Modinos : Surf. Sci. 42, 205 (1974)

40. W.B. Shepherd : Ph.D. Thesis, University of Minnesota (1969)

41. R.H. Good and E.W. Muller : Handbuch der Physik, Springer - Verlag, Berlin, 1956 Vol. 21 p. 181

42. W.A. Hamson : Phys. Rev. 123, 85 (1961)

43. E.L. Murphy and R.H. Good : Phys. Rev. 102, 1464 (1956)

44. R.E. Burgess, H. Kroemer and J.M. Houston : Phys. Rev., 90, 515 (1953)

45. P. Handler : J. Phys. Chem. Solids 14, 1 (1960)

46. R.H. Kingston and S.F. Neustadter : J. Appl. Phys. 26, 718 (1955)

47. A. Modinos : Private Communication.

48. M. Aven and J.S. Prener : Physics and Chemistry of II VI Compounds, North Holland 1967.

49. S.M. Sze : Physics of Semiconductor Devices, Wiley 1969.

50. V.E. Lashkarev, E.A. Salkov and M.K. Sheinkman : Physics of Semiconductors, proc. 7th int. conf. p. 973, Paris 1964.

51. L.T.J. Salmon : Ph.D. Thesis, University of Aston, 1972.

52. A.V. Crewe, M. Isaacson, and D. Johnson : Rev.Sci.Inst. 40, 241 (1969).

53. D.C. Joy, J.M. Titchmarsh, R.J. Woolfe and G.R. Booker : Proc 5th European Congress on Electron Microscopy, Manchester Sept. 1972 p. 16 (1972).

54. J.R.A. Cleaver and K.C.A. Smith : Proc 5th European Congress on Electron Microscopy, Manchester Sept. 1972, p. 18 (1972).

55. A.E. Standage and R. Prescott : Nature 211, 169 (1966).

56. S. Otani, K. Yamada, T. Koitabashi and A. Yokoyama : Carbon 4, 425 (1966)

57. R. Bacon and A.F. Silvaggi : Carbon 9, 321 (1971)

58. R. Moreton, W. Watt and W. Johnson : Nature 213, 690 (1967)

59. W. Johnson and W. Watt : Nature 215, 384 (1967)

60. D.V. Badami, J.C. Joiner and G.A. Jones : Nature 215, 386 (1967)

61. D.J. Johnson and C.W. Tyson : J. Phys. D, 2, 787 (1969)

62. B.J. Wicks : J. Mater. Sci, 6, 173 (1971)

63. F. Tunistra and J.L. Koenig : J. Compos. Mater. 4, 492 (1970)

64. C.N. Owston : J. Phys. D 3, 1615 (1970)

65. G. Montet, M. Hoch and G. Hennig : U.S.A.E.C. Rep. ANL-6804 (1964)

66. W.S. Williams : J. Appl. Phys. 39, 2131 (1968)

67. I.D. Hughes and H.M. Montague-Pollock : J.Phys. D 3, 228 (1970)

68. F.S. Baker, A.R. Osborn and J. Williams : Nature 239, 96 (1972)

69. J. Smith : Undergraduate project report, University of Aston (1972)

70. T.H. English, C. Lea and M.T. Lilburne : Scanning Electron Microscopy : Systems and Applications, Newcastle 1973 p. 12 (1973).

71. C. Lea : J. Phys. D 6, 1105 (1973)

72. E. Braun, R.G. Forbes, J. Smith and D.E. Sykes : To be published

73. F. Okuyama : Surf. Sci. 27, 635 (1971)

74. T. Utsumi and G.C. Dalvern : App. Phys. Lett. 11, 397 (1967)

75. A.J.G. van Costrom : Philips Research Report Supplement No. 1 (1966)

76. M.K. Norr : J. Electrochem. Soc. (USA) 109, 433 (1962)

77. J.J. Harris and B.K. Ridley : J. Phys. C 5, 2746 (1972)

78. R. Dalvern : Infra red Physics 9, 141 (1970)

79. W.E. Spicer and G.J. Lapeyre : Phys. Rev. 139, A565 (1965)

80. R.F. Egerton and C. Juhanz : J. Phys. D 2, 975 (1969)

81. A.J. Wright and E. Braun : Unpublished

82. G.N. Fursei, N.V. Egorov and S.P. Manokhin : Sov. Phys. Solid State 14, 1453 (1972)

83. A.M. Russel : Rev. Sci. Instrum. 33, 1324 (1962).

ACKNOWLEDGEMENTS

I would like to thank my supervisor, Professor E. Braun, for suggesting the project and for his encouragement during the course of the work. In addition I would like to thank Mr. F. Lane and the workshop staff for their assistance in making the analyser, Mr. B. Singh who supplied the analyser drawings, my colleagues for their advice and criticism, and Miss J. Snell for typing the manuscript.